Lawrence Berkeley National Laboratory

LBL Publications

Title

Retrospective on Recent DOE-Funded Studies Concerning the Extraction of Rare Earth Elements & Lithium from Geothermal Brines

Permalink

https://escholarship.org/uc/item/2j7688zb

Authors

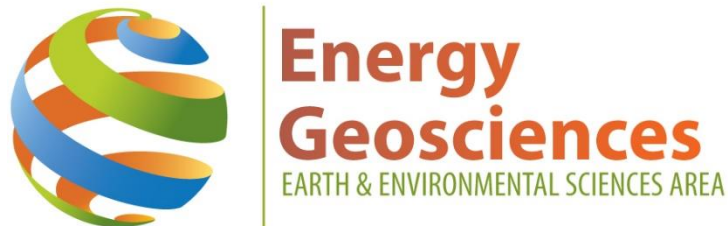Stringfellow, William
Dobson, Patrick

Publication Date

2020-09-24

DOI

10.5072/FK2KS6SS2Z

Peer reviewed

Retrospective on Recent DOE-Funded Studies Concerning the Extraction of Rare Earth Elements & Lithium from Geothermal Brines LBNL-2001359 (Final Report)

William T. Stringfellow & Patrick F. Dobson
Lawrence Berkeley National Laboratory
Energy Geosciences Division

September 23, 2020

Contents

Executive Summary

Rare earth elements (REE) and lithium are non-toxic metals that are considered critical materials due to their use in electronics, magnets, batteries, and a wide variety of industrial processes important for the economy and military preparedness. Demand for REE and lithium is increasing and these critical materials are imported, so identifying and exploiting domestic sources of REE and lithium is a national priority.

The U.S. Department of Energy (DOE) Geothermal Technologies Office (GTO) has been in the forefront of sponsoring research investigating the potential recovery of REE, lithium, and other critical minerals from geothermal brines. It has been proposed that the future of geothermal energy should include "hybrid systems" that combine electricity generation with other revenue-generating activities, such as recovery of valuable and critical minerals, including REE and lithium.

Two recent GTO funding opportunities have focused on the recovery of REE and other valuable minerals from geothermal brines. The research supported by the GTO's mineral recovery program is focused on three areas: resource characterization, technology for the extraction of REE, and technology for the extraction of lithium (Tables 1 and 2). This report is a retrospective study examining the outcome of GTO's two recent mineral recovery programs (DE-FOA-0001016 in FY 2014 and DE-FOA-0001376 in FY 2016). In this report, the knowledge, technology, and techniques that were developed by researchers funded by GTO are summarized and discussed.

Four projects were funded to assess the concentrations and amounts of REE found in geothermal brines and oil field produced waters. The GTO-funded studies compiled publically available data on REE concentrations from brines and produced water from all over the USA. In addition, new samples were collected and characterized from major geothermal and hydrocarbon basins in the Western USA. The studies examined the relationship between lithology and REE concentrations and developed models examining the influence of geology on REE concentrations in produced brines. It was determined that REE are frequently found at higher concentrations in oil field produced water than geothermal brines, but that some geothermal areas had significant REE resources.

Significant reservoirs of REE were identified in the Western USA. In some cases, concentrations of REE were more than 1000 times the concentrations found in seawater. Collectively, these studies represent a comprehensive picture of REE resources associated with geothermal and hydrocarbon systems in the USA. The studies did not examine lithium resources, but in some cases, lithium concentration data was collected. Data from these studies are housed in the Geothermal Data Repository (GDR) and represent a significant information resource and it is recommended that these data be further analyzed in a future study.

Eight projects were funded to develop new technology for REE extraction from geothermal fluids. These projects investigated sorption as an approach for removal and recovery of REE from geothermal brines. The projects investigated cutting-edge technology for selective sorption of ions from complex solutions, including the application of metal-organic frameworks and biosorbent proteins. The REE sorption studies tested different combinations of metal-binding ligands and solid supports. The most promising metal-binding ligands for REE included phosphonic acid, thiol, and carboxylic acid functional groups. Ligands were attached or incorporated into a wide variety of solid supports. In most cases, attachment was via covalent bonding to organic resins, polymers, or silica-based supports. Most of the REE projects were conducted at a low technology readiness

level (TRL) and showed promise, but direct comparison between technologies was not possible based on the available information. It is recommended that testing and reporting be standardized to the extent possible to facilitate comparisons between technologies.

Two projects were directed at novel lithium extraction technology. Both projects investigated the use of inorganic sorbents, including manganese oxides. One study also examined the use of metal-ion imprinted polymers as selective ion-exchange resins for the separation of lithium and manganese from brines. Both approaches showed promise for the selective extraction of lithium from brines, including potentially geothermal brines. Results from these GTO studies indicated that selective REE and lithium extraction is possible, but interference from co-occurring solutes, such as calcium, magnesium, or heavy metals, will interfere with process efficiency and negatively impact process economics.

Techno-economic analysis conducted as part of the resource and technology studies suggest extraction of REE from geothermal brines is unlikely to be economically viable, especially since non-geothermal produced waters frequently have higher REE concentrations. It is recommended that benchmarks for techno-economic analysis be established to the extent possible for future studies, to facilitate direct comparison of various technologies. Based on the collective results of this program, it appears that hybrid geothermal power would benefit more from recovery of lithium and other metals, rather than REE. It is recommended that future studies be conducted at a higher-TRL and that sorbents be tested against actual geothermal fluid samples. Prior higher-TRL efforts to extract metals from geothermal brines should be further evaluated for lessons learned.

Introduction

Geothermal energy production is an important clean energy source, but the economics of geothermal energy production are difficult. It has been proposed that the future of geothermal energy should include "hybrid systems" that combine electricity generation with other revenue generating activities (Wendt *et al*., 2018). Economic activities, such as mineral recovery or co-generation of heat for direct use, could provide additional revenue streams and increase the competitiveness of geothermal electricity. Hybrid geothermal energy plants are predicted to become standard in the future (Wendt *et al*., 2018). Mineral recovery is an especially attractive hybrid option, since some geothermal brines are rich in minerals, and may contain rare earth elements (REE), which have both economic and strategic value (White, 1968; Gallup, 1998; Haxel *et al*., 2002; Bourcier *et al*., 2005; Bloomquist and Povarov, 2008; Van Gosen *et al*., 2017; Department of the Interior, 2018).

The U.S. Department of Energy (DOE) Geothermal Technologies Office (GTO) has been in the forefront of supporting research investigating the potential recovery of REE and other valuable minerals from geothermal brines. Two recent funding opportunities have focused on the recovery of REE and lithium from geothermal power plant brines. Geothermal brines can include both produced brine from the geothermal reservoir, which is at high-pressure and temperature well above boiling, and "post-flash" brines, which typically are at temperatures less than 100°C and have higher total dissolved solids (TDS) than the original well fluid, after flashed steam has been separated from the feed water. The research supported by the GTO's mineral recovery program is focused on three areas: resource characterization, technology for the extraction of REE, and technology for the extraction of other valuable or strategic minerals, particularly lithium (Tables 1 and 2). Techno-economic assessments (TEA) were conducted as part of many of these studies.

The objective of this report is to provide a summary of knowledge, technology, and techniques that were developed by researchers funded by GTO and other programs in DOE. This report is retrospective study examining the outcome of GTO's two recent mineral recovery FOAs (DE-FOA-0001016 in FY 2014 and DE-FOA-0001376 in FY 2016).

The objective of this report is to bring forward technical information from scientific studies sponsored by DOE related to economic mineral recovery from geothermal brines. This report synthesizes complex and disparate information from final project reports and supporting information in a format that will assist engineers and policy makers in understanding the state of the science and how individual studies complement or contrast with each other. The report includes a description of key results and findings that are useful for future process development and provides a guide for scientists, engineers, technologists, and planners. This report provides conclusions and recommendations for future action in the context of DOE programs.

Background

REE are a group of seventeen non-toxic metals (Table 3) that are considered critical materials due to their importance to industrial manufacturing and military preparedness (Haxel *et al*., 2002; Gholz, 2014; van Gosen *et al*., 2017; Department of the Interior, 2018; Pramanik *et al*., 2020). The REE possess varying ionic radii, which produce different properties, and therefore have been broadly classified into two groups: Heavy Rare Earth Elements (HREE) and Light Rare Earth Elements (LREE) (Table 3, van Gosen *et al*., 2017). HREE typically have higher economic value relative to LREE (Zion Market Research, 2019; King, 2020; Kitco Metals Inc., 2020).

In the last twenty years, REE demand has increased due to their use in modern materials and devices, including televisions, computers, rechargeable batteries, cell phones, catalytic converters, magnets, and fluorescent lighting. Major uses for REE in the United States include chemical catalysts (55% of demand), ceramics and glass making (15%), metallurgy and alloys (10%), and glass polishing (5%). REE are also strategic minerals and are critical for national defense (Gholz, 2014; Department of the Interior, 2018; Pramanik *et al*., 2020). REE are used in critical military equipment including night-vision goggles, precision-guided weapons, and communications equipment (Haxel *et al*., 2002; Van Gosen *et al*., 2017). Although other substances can be substituted for rare earth elements in their most important uses, these substitutes are usually less effective and more costly (Haxel *et al*., 2002; Van Gosen *et al*., 2017; King, 2020; U.S. Geological Survey, 2020). Geothermal brines are identified as a potential domestic source of REE (Van Gosen *et al*., 2017).

Lithium is also an element on the critical minerals list that can be found in geothermal brines (Bradley *et al*., 2017; Department of the Interior, 2018). Lithium has a wide variety of industrial uses, including manufacture of glass and ceramics, and it is a critical battery material (Bradley *et al*., 2017). Rechargeable lithium-ion batteries are particularly important in efforts to power cars and trucks from renewable sources of electricity, instead of fossil fuels (Bradley *et al*., 2017). Lithium supplies for the USA are mostly imported from Chile and Australia. There are significant domestic lithium resources, including geothermal brines in the Western USA, but domestic lithium production is not yet a significant supplier to markets (Bradley *et al*., 2017).

Methods

The primary references for this report were the final reports for projects funded by GTO (Tables 1 and 2). These resource assessment and technology development projects were supported by recent mineral recovery funding opportunity announcements DE-FOA-0001016 in 2014 (Table 1) and DE-FOA-0001376 in 2016 (Table 2). Final reports were reviewed and analyzed for content related to process engineering, process optimization, and strategic or policy-level decision making. Information from the final reports were supplemented by a review of interim reports, patents, journal articles, and other published literature as required to support or understand technical results from the final reports. Patent searches were made by principal investigator and institution. The Geothermal Data Repository (U.S. Department of Energy, 2020) was searched for each project and for principal investigator name. In many cases projects had archived data and supplemental reports, which were examined in the context of the objectives of this document and results of that analysis are included in this report, if relevant to the report objectives.

Resource Assessments

Four projects were funded by GTO to assess the concentrations and amounts of REE found in geothermal brines (Tables 1 and 2). The potential of brines from geothermal power plants and associated geothermal systems to serve as a source of REE and other strategic or valuable minerals was evaluated. Two resource studies were conducted under the 2014 Phase I FOA and two studies were funded under the 2016 Phase II program (Tables 1 and 2).

The Phase I study by Zierenberg and Fowler (2018) at the University of California Davis (Project DE-EE-0006748) was completed in December 2018. Zierenberg and Fowler (2018) compiled published REE data on 288 thermal fluid samples from the United States. In addition, they obtained and analyzed more than 40 geothermal brine samples from 7 different geothermal systems and 4 seafloor hydrothermal systems. Three of the geothermal systems were in the USA (Don A. Campbell, NV; Puna, HI; Surprise Valley, CA) and four were in Iceland. Both the compiled data from publications and their original REE data have been uploaded to the Geothermal Data Repository (GDR). The major objective of the project was to refine geochemical models (Zierenberg and Fowler, 2018).

Because the compiled brine chemistry data were available in the GDR, the data were downloaded and examined. From the public literature, Zierenberg and Fowler (2018) compiled REE and supporting geochemical analysis from seafloor vents (152 samples), surface hot springs (158), and geothermal wells (118). Lithium was not included as an analyte in this study. An analysis of the compiled literature values showed that REE concentrations increased as pH decreased (Figure 1 and Appendix A). This data set contains compiled data from over 40 publications and is a valuable resource for future studies (Appendix A).

Zierenberg and Fowler (2018) summarized the results from the three domestic geothermal systems and evaluated REE resources in the context of potential geothermal power production. They found that geothermal well samples from Surprise Valley, CA, a proposed location for a geothermal power plant, had higher average REE concentrations than wells feeding the Don A. Campbell, NV or Puna, HI power plants. The results of the Zierenberg and Fowler (2018) study are consistent with other literature being evaluated as part of this study that show California geothermal systems

tend to be high in REE and other potentially valuable minerals (Neupane and Wendt, 2017; Nye *et al*., 2017; Wendt *et al*., 2018).

As part of their deliverables for the DE-EE-0006748 project, Zierenberg and Fowler (2018) also uploaded geospatial information on the GDR related to the REE concentration values they compiled from the literature. The combination of compiled literature values and geospatial information are valuable for the development of geospatial mapping of valuable minerals associated with geothermal resources. However, geospatial analysis of this information will require editing the existing data sets to a useable format (e.g., separating character and numeric entries, etc.) and putting the data in a relational database.

The objectives of Phase I project DE-EE-0006750 were to develop protocols for sampling and analyzing REE and other minerals in complex, high-temperature geothermal fluids and then apply those methods to analyze samples collected from operating geothermal fields in Western States (US Department of Energy, 2017). The data were intended to be used for the purpose of developing a database of REE concentrations of U.S. geothermal waters (US Department of Energy, 2017), an objective similar to other resource assessment projects under this program. After the resource assessment, the technical feasibility of extracting REE from geothermal fluids was to be assessed and laboratory testing of potential REE extraction techniques (ion exchange, solvent extraction and precipitation) were to be conducted. Finally, the economic feasibility of REE mineral extraction was to be evaluated (US Department of Energy, 2017).

The Project DE-EE-0006750 was started in 2014, but ended in the first quarter of 2015 (US Department of Energy, 2017). First and second quarter reports describe the development of methods for the analysis of geothermal brines (Harrison, 2015; Thomas, 2015), which was the first project objective. Methods of analysis for REE were developed for both high salinity and low salinity brines using ion chromatography (Harrison, 2015; Thomas, 2015). In addition, preliminary protocols for sampling geothermal and other brines were developed (US Department of Energy, 2017). After the first two quarters, the project experienced logistical problems concerning access to critical analytical equipment and no further progress was reported. The recipient of the grant, Simbol Materials, ceased significant operations in 2015. The project final report was written by DOE GTO staff (US Department of Energy, 2017).

Quillinan *et al*. (2018) measured REE in 224 "geothermal produced water" samples and 101 corresponding rock samples as part of Phase II Project DE-EE-0007603. The samples analyzed were collected from major oil and gas producing basins including the Williston Basin, ND; Permian Basin, TX; Kevin Dome Area, MT; Appalachian Basin, OH-PA; and Wind River, Powder River, and Green River Basins, WY (Figure 2). Samples from the Snake River Plain geothermal region of Idaho were also analyzed as part of this study. Rock samples were used in an effort to develop predictive chemistry for the occurrence of REE, a major research objective of this project. Data were retrieved from the GDR by searching project investigators and project number. Data included brine or water chemistry results from Wyoming and Soda Geyser, Idaho and mineral analysis (rock) data from various locations were also available. A table of all the data collected during the study was included in the appendix of the final report (Quillinan *et al*., 2018).

The available data were examined in the context of REE recovery from geothermal power plant brines (Quillinan *et al*., 2018). The electronic data for Wyoming included REE results for samples from a variety of sources, including industrial impoundments. Where sample temperatures were reported in the electronic data, all temperatures were less than 70°C, so the data may not be directly

applicable to operational geothermal power plants. For example, the Soda Geyser data reported sample temperatures < 35°C. The appendix includes results from other geothermal samples, but those data were not found in an electronic format. Since more data are available in the appendix than are currently in electronic format, these data could be extracted and compiled for future studies, particularly studies that included the evaluation of oil and gas produced waters as well as geothermal waters.

Quillinan *et al*. (2018) found measurable concentrations of REE in all analyzed samples and in some cases concentrations of REE were more than 1000 times the concentrations found in seawater. The study included a predictive mapping model (Chapter 6) that showed a within-basin correlation of REE concentrations in produced water, yielding a map identifying higher and lower value basins (Quillinan *et al*., 2018). Both the geochemical evaluation (Chapter 3 and 4) and the predictive mapping exercise supported the conclusion that the geographical distribution of higher concentration REE-containing brines was "spatially–dependent" rather than correlated or predicted by geological parameters such as formation lithology, reservoir temperature, or salinity. Although the spatial dependency was not fully defined, the results suggest a basin to basin dependency.

Quillinan *et al*. (2018) did not expressly discuss pH as a determining factor for REE concentrations. We conducted a preliminary analysis of their data from the GDR and did not find a strong relationship between pH and REE concentration (Appendix B). The pH range for the Quillinan data and the number of samples was less than the Zierenberg data (Appendix A), which may in part account for the discrepancy between these two studies concerning the observed relationship between pH and REE concentration. Further analysis using these data is warranted and Quillinan *et al*. (2018) suggested that further geospatial analysis be conducted with these data as well.

The Simmons (2019) study (Phase II Project DE-EE-0007604) investigated produced waters from geothermal fields and hydrocarbon reservoirs in Idaho, Nevada, New Mexico, Oregon, and Utah (Table 4 and Figure 3). Simmons (2019) collected and analyzed water samples from 47 production wells in 12 geothermal fields. Samples were also collected from hot springs and 25 oil and gas wells. Water sample temperatures ranged from 50-250°C at the time of collection. Concentrations of strategic, critical and valuable materials, including lithium, helium, metalloids, and REE, were measured along with a complete suite of water chemistry. Geothermal produced waters were mostly classified as chloride, sulfate, or hybrid chloride-sulfate waters (Figures 4 and 5), with salinities of between 1,000 and 10,000 mg/kg total dissolved solids. REE concentrations were low, typically at or below detection limits (0.01 µg/kg), and lithium concentrations were moderate to low (< 26 mg/kg) (Simmons, 2019). It should be noted that lanthanum, cerium, and europium concentrations were higher in oil and gas produced waters than in geothermal produced waters (Simmons, 2019).

Simmons (2019) measured REE in rock samples from geothermal reservoirs and investigated if chemistry and lithology of the rock could be used to predict or explain the observed differences between REE and lithium concentrations in produced waters. As did Quillinan *et al*. (2018), Simmons (2019) did not find lithology and other rock characteristics to be predictive of REE concentrations (or lithium concentrations) in produced brines. Simmons (2019) found only a poor correlation between REE concentration and temperature and total dissolved solids. As was found in previous studies, REE concentrations varied between basins.

Simmons (2019) made direct calculations to estimate mineral resources in geothermal reservoirs. Inventories were calculated by multiplying the average concentrations in produced fluids by the reservoir volume, assuming a porosity of 15%. The reservoir thickness was assumed to be 1 km, if specific information on the reservoir was not available. Using this method, Simmons (2019) estimated each geothermal field had to up to 25,000 kg of gallium, but the Uinta Basin hydrocarbon reservoir had greater than 100,000 kg of gallium. Of the geothermal reservoirs examined, Roosevelt Hot Spring was estimated to have the largest inventories of germanium and lithium (7 million kg); the Patua reservoir the most gallium (25,000 kg), selenium (47,000 kg), and tellurium (2,500 kg). The Raft River reservoir has the most scandium (700 kg).

Simmons (2019) included a comprehensive record of data from their project in the GDR. The records include descriptive metadata and background on sampling locations, including maps, and other supporting information that would allow for detailed geospatial analysis. The records include a complete suite of water chemistry that makes the data useful for geochemical modeling of potential extraction technologies. This data set would be very valuable for any follow-up or meta-data study concerning this region or the national inventory of REE or lithium.

New Technology

In Phase I, six projects were funded by GTO to develop new technology for REE extraction from geothermal brines and two projects focused on lithium extraction (Table 1). In Phase II, three additional projects were funded to develop technology for REE (Table 2). All of the technology projects investigated the application of sorption as an approach for removal and recovery of REE and other valuable minerals from geothermal brines. The project DE-SC0013698 examined ion-imprinted polymers for REE separation and may be a continuation of Phase I project DE-EE-0006749 (Karamalidis, 2016), but information from the Phase II project is embargoed and was not included in this analysis (Table 2). Phase II project AOP.2.5.1.14 is an investigation of magnetic separation processes (Table 2), which was also the subject of a Phase I project (McGrail *et al.*, 2017). Reports for this Phase II project were not available or were not found and are not included in this analysis.

New Technology for REE Recovery

Functionalized Resins & Silica (DE-EE-0006749)

Karamalidis (2016) investigated the use of chelating resins for the separation and recovery of REE. Chelating resins were developed by grafting ligands with chelating groups (e.g., carboxylic acids) to solid supports, including silica and polyacrylic or polystyrenic resins. Ligands with known affinity for REE that were evaluated in this study included diethylenetriaminepentaacetic dianhydride (DTPADA), 1,4,7,10-tetraazacyclododecane-1,4,7,10-tetraacetic acid (DOTA) N,N-bis(phosphonomethyl)glycine (BPG), diethylenetriaminepentaacetic acid (DTPA), and phosphonoacetic acid (PAA) (Figure 6). BPG, DTPA and PAA were selected as the most interesting candidates for REE sorption in the context of geothermal fluids (Karamalidis, 2016).

Karamalidis (2016) synthesized the sorbents via a "bottom-up" scheme, where supports were pre-aminated and then functionalized with active sites, or a "top-down" method, where chelating ligands were first functionalized with a silane, which was subsequently attached to the silica support. Synthesized resins were characterized by X-ray photoelectron spectroscopy (XPS), attenuated total reflectance-Fourier Transform Infrared Spectroscopy (ATR-FTIR),

thermogravimetric analysis (TGA), and other methods to determine active site concentration, grafting efficiency, organic content, amine conversion rates, ligand loading, electrophoretic mobility, and other characteristics (Karamalidis, 2016).

The REE sorption properties for BPG, DTPA and PAA were evaluated in both batch and continuous-flow experiments (Karamalidis, 2016). Contact time varied from three hours to three days, depending on the experimental objectives. Batch experiments were mostly conducted at 100 µg/L REE concentrations. Batch experiments used a mixture of three REE, neodymium, gadolinium, and holmium, which were selected as being representative of light-, middle-, and heavy-REE, respectively. In addition to using laboratory solutions, some equilibrium experiments were conducted with saline waters from the Great Salt Lake (UT). Experiments were conducted with materials of varying, but unspecified, particle size (e.g., fine and coarse materials).

Adsorption of REE was found to be pH-dependent, with different ligands having different optimum pH ranges (Karamalidis, 2016). DTPA performed better under acidic pH (< pH 4), BPG at near-neutral pH, and PAA under basic conditions (optimal ~ pH 8). Linear, poly-dentate carboxyl ligands showed the most promise for gadolinium uptake, however, phosphonate-based ligands were also considered as good sorbents for REE generally. Differences were observed for the sorption kinetics of the three REE studied, with DTPA absorbing the LREE neodymium faster than gadolinium and holmium at pH $\geq$ 4. PAA-functionalized adsorbents show a tendency to complex heavy lanthanides more than their light counterparts (Karamalidis, 2016).

REE were recovered from the various sorbents using nitric acid (Karamalidis, 2016). Elution was performed with 5% HNO_3, and extraction efficiencies were between 85% and 90% of the adsorbed REE mass recovered. Recycled materials, which had been extracted with nitric acid and then used again in batch sorption experiments, were reported to show higher total uptake than those that were freshly synthesized (Karamalidis, 2016). The authors theorized that the PAA or DTPA may have reactions between neighboring ligands during synthesis and the process of acid elution may free hindered ligands and increase overall adsorption efficiency.

Karamalidis (2016) tested the effects of temperature, ionic strength, and interfering ions on REE sorption. Sodium chloride had little effect on sorption between approximately 30,000 and 175,000 mg/L (0.5 M and 3 M NaCl). These sorbents were reported as being temperature tolerant up to 150ºC (Karamalidis, 2016). Experiments carried out in aqueous fluid at 20ºC, 60ºC, and 100ºC reported no negative effect on performance as determined by percent sorption. Competitive adsorption tests were conducted and results showed no distinguishable decrease in REE sorption in the presence of either calcium or magnesium at concentrations up to 1000 mg/L. However, iron, zinc, and aluminum were found to interfere and reduce the REE sorption capacity. In the case of PAA, which was tested at higher pH, the investigators suspected that metal interference may have been due to metal precipitation on the sorbent media (Karamalidis, 2016).

Karamalidis (2016) was one of the few research projects to analyze their sorbents using a standard engineering sorption model that allow comparison of sorbents more easily and rigorously between experimental conditions. Karamalidis and collaborators applied one of the commonly used standard engineering adsorption models, the Freundlich adsorption isotherm. The Freundlich isotherm model describes surface concentration of the adsorbent in relation to the absorbent solution equilibrium concentration (Kolodynska, 2013; Awad *et al.*, 2019). Although values for Freundlich constants were reported to be calculated, the constants were not included in the report and project data was not found in the GDR (Karamalidis, 2016). DTPA isotherms were conducted

at pH values close to 2 and PAA isotherms were conducted at near-neutral pH. Results for BPG were not given. The graphic presentation suggests DTPA is the most efficient absorbent with the highest capacity, but final sorption capacity values were not reported for any of the sorbents. However, since DTPA is optimized for use at pH 2, it is unclear from these tests which sorbent might perform best under conditions found in geothermal power plants.

Impregnated Granular Activated Carbon (DE-EE-0006751)

Stull (2016) and associates conducted a proof-of-concept study on the use of modified Tusaar Media for extracting REE from geothermal brines. Tusaar Media was not described in the report, but an examination of the patent literature suggests that this sorbent is granular activated carbon impregnated with carboxylic acid and heterocyclic nitrogen containing ligands, possibly including variants with carboxy-, butyl-, nitrated- or other alkylated derivatives of benzothiazoles and benzotriazoles or similar functional groups (Hernandez *et al*., 2018). The grantee tested a sorbent that is at a higher technology readiness level (TRL) than most of the other Phase I projects, and the approach taken was somewhat different than other Phase I studies. Since the Tusaar Media had already been used for other purposes at commercial scale, Stull (2016) and collaborators conducted experiments and tests to establish technical criteria for application of Tusaar Media to geothermal power systems.

Stull (2016) conducted sorption experiments using a variety of synthetic brines (Table 5). Synthetic brine formulation was based on a proposed composition of an actual geothermal brine (Brine 1 in Table 5); however, problems with initial experiments led the researchers to exclude silicon oxides and lead from their formulations (Table 5). All of the brine formulas used in batch and column experiments contained 45,700 mg/L sodium, 20,300 mg/L potassium, and 14,300 mg/L calcium, presumably as chloride salts, and lanthanum, cerium, praseodymium, neodymium, europium, terbium, and dysprosium at 2 mg/L each. Variants of the brine formula contained metals and other cations and anions, including iron, barium, lithium, and magnesium (Table 5). The pH of the brine was varied by experiment, with many experiments carried out at pH 5.5. Synthetic brine 1C, which contained iron at 660 mg/L and boron at 180 mg/L, formed precipitates that interfered with sorption tests, so the 1C formulation was not used in subsequent testing (Table 5). A brine without iron and boron was formulated (Brine 1CF) and used in subsequent testing, including column testing (Stull, 2016). These results suggest significant interference with sorption by these chemicals.

The benchmark sorption capacity of 1.5% for REE on Tusaar Media was established using europium at 500 mg/L in a 90-minute batch test at 22°C (Stull, 2016). Although not specified, the test was presumably conducted at pH 5.5. Europium had a reported linear K_d of between 49 and 59 mL/g, which corresponds to an adsorption capacity of between 1.4% and 1.8% weight to weight (Stull, 2016). Sorption of europium was the benchmark parameter for the media throughout the project. Experiments with flow-through columns, conducted at 22°C and a pH between 5 and 6, supported the use of a 1.0% total REE sorption capacity as a reasonable design estimate.

Stull and collaborators (Stull, 2016) conducted experiments examining extraction and recovery of REE sorbed on the Tusaar Media. Extractions were conducted with 1.5 M and 3M nitric acid. The amount and concentration of acid and the contact time in the column (e.g., flow rate) were found to be important variables. The optimal nitric acid concentration was reported to be 1.5 M, but the contact time variable was not reported as an engineering constant or optimal range. After stripping,

the pH was brought back to the operating pH of 5 to 6 with caustic. The authors reported metal recovery to be quantitative, but the actual amount recovered was not reported (Stull, 2016).

It was noted that sorption and stripping reactions were temperature sensitive. At 90°C, gas production, presumably a nitrous oxide, was observed during acid stripping. The process stripping temperature was therefore reduced to 40°C for safety reasons (Stull, 2016). It was also found that the impregnated chelating compound bled out of the granular activated carbon at a temperature of 90°C. The media performed as expected at temperatures of 70°C and below (Stull, 2016).

Stull (2016) proposed a final process model based on the outcome of the experiments that included new elements not proposed in the original conceptual model of an REE extraction plant. For the final process design, Stull and coworkers (Stull, 2016) proposed to include a "catch column" to collect potential ligand bleed. It was proposed that the ligand could be recovered from the catch column and used to reload the sorption column, but the recovery process was not described. Additionally, the load/strip/regenerate procedure was revised to include chemical addition to replace ligand lost to bleed-out. The final design includes the use of two equivalent column sets and associated process tanks to allow continuous operation during alternating load/strip/regenerate cycles (Stull, 2016). These design changes impacted the outcome of the techno-economic analysis, as described below.

Metal Binding Biosorbents (AOP 2.5.1.4 & AOP 2.5.1.12)

The Phase I project AOP 2.5.1.4 tested the use of genetically modified bacteria for the sorption of REE from solution (Ajo-Franklin, 2015; Ajo-Franklin *et al*., 2017). The objective of the project was to modify bacteria to over-express S-layer proteins (a class of proteins found on bacterial surfaces) that were previously known for the binding of gadolinium and zinc (Figure 7) (Ajo-Franklin, 2015; Ajo-Franklin *et al*., 2017). Plasmids were designed and constructed to contain metal-binding regions of the thermophilic S-layer protein SbsB from the thermophilic, salt-tolerant bacteria *Geobacillus stearothermophilus*. The plasmid was introduced to both *G. stearothermophilus* and *Escherichia coli* with the intention of causing overexpression of the metal-binding regions of the SbsB protein on the surface of the bacteria, thereby increasing the specific metal-binding activity of the cells (Ajo-Franklin *et al*., 2017). Transformed bacteria were tested for absorption of gadolinium and zinc. In addition, SbsB protein was isolated and purified and tested for sorption of metals (Ajo-Franklin *et al*., 2017).

Ajo-Franklin *et al*. (2017) were not able to transform *G. stearothermophilus* and get surface expression of genetically engineered SbsB S-layer, but they were able to transform *E. coli* successfully. They then used conjugation with *E. coli* carrying the plasmids to produce *G. stearothermophilus* isolates with the SbsB plasmid, however the plasmid was not stable in this organism and was not maintained after continued culturing. The design and construction of the plasmid with the engineered SbsB S-layer proteins and methods for transformation of *E. coli* with the SbsB plasmid are described in detail by the investigators (Ajo-Franklin, 2015; Ajo-Franklin *et al*., 2017).

E. coli variants with modified genes for expression of the metal-binding S-layer were grown and the SbsB S-Layer protein was extracted and purified (Ajo-Franklin, 2015; Ajo-Franklin *et al*., 2017). Methods for the extraction and purification of the SbsB protein are described and discussed (Ajo-Franklin *et al*., 2017). Purified proteins from the genetically engineered S-layer were formed into sheets (nanosheets) and tested for zinc (as Zn^{2+}) binding in comparison to native (wild-type)

SbsB S-layer nanosheets. S-layer nanosheets were incubated with fixed concentrations of zinc (1,000 nM) for 20 min at 40°C. At lower concentrations (0.05 nM), the S-layer nanosheets bearing a zinc-binding domain and the native S-layers bound similar amounts of zinc. At higher zinc concentrations (0.2 nM), the engineered variant bound all of the available zinc, whereas the native S-layer only bound approximately 75% of the available zinc, demonstrating that the engineered SbsB S-layer had more metal-binding regions that the native or wild-type S-layer (Ajo-Franklin *et al.*, 2017).

Similar experiments were conducted to examine the ability of genetically engineered S-layer protein to bind gadolinium (as Gd^{3+}). Two engineered S-layers containing different binding domains were compared to the gadolinium-binding abilities of the native SbsB S-layer. Varying concentrations of S-layer were contacted with 1,000 nM gadolinium for 20 min at 40°C or room temperature. At the lowest S-layer concentration tested, all the variants bound up to approximately 20% of the available gadolinium. At higher concentrations of S-layers, the native protein only showed marginally increased gadolinium-binding, however the genetically engineered protein demonstrated increased binding of gadolinium. This data suggested that the engineered S-layer protein more tightly bound gadolinium than the native protein (Ajo-Franklin *et al.*, 2017).

The Phase II project AOP 2.5.1.12 investigated the development of an ion-exchange biosorbent made of whole bacterial cells that had been genetically modified to express surface proteins containing lanthanide binding tags (LBT) (Jiao, 2020). LBT are regions of bacterial S-layer proteins that have been demonstrated to preferentially bind REE (Brewer *et al.*, 2019a). The objectives of the project were to genetically modify *E. coli* to express LBT on cell surfaces and demonstrate that LBT-modified cells could bind REE. LBT-modified bacteria were then imbedded in a solid support resin and used in flow-through ion-exchange columns to demonstrate the use of REE-binding bacteria as ion-exchange sorbents (Brewer *et al.*, 2019b; Jiao, 2020). In addition, the project developed a simple cell surface complexation model to simulate REE separation under column flow (Chang *et al.*, 2020; Jiao, 2020).

Jiao and collaborators engineered *E. coli* to express an LBT having a short peptide sequences that bind terbium (as Tb^{+3}) with high affinity (Brewer *et al.*, 2019a; Jiao, 2020). The surface properties (protonation behavior) of the native *E. coli* was compared to LBT-engineered *E. coli* by modeling acid-base titration and terbium sorption data. Surface complexation was modeled using terbium binding at discrete sites, assuming constant capacitance surface complexation (Chang *et al.*, 2020; Jiao, 2020). Acid titration and terbium binding by native bacteria could be described using a one-site carboxyl model (Figure 8). In contrast, modeling terbium sorption by LBT-engineered *E. coli* required the inclusion of phosphoryl and LBT peptide sites, as well as carboxyl sites (Figure 8). The investigators concluded that incorporation of LBT peptides into *E. coli* S-layers benefited whole-cell sorptive properties by the presence of high-affinity, low-capacity LBT sites for selective terbium-binding, but also allowed binding by lower-specificity native carboxyl and phosphoryl groups. The result was an engineered bacterium with overall increased sorption capacity at higher aqueous REE concentrations (Brewer *et al.*, 2019a; Chang *et al.*, 2020; Jiao, 2020).

Batch adsorption of REE by bacteria were carried out using a sample of fluid from the Blue Mountain geothermal field in Nevada, USA (Jiao, 2020). This brine had a pH of approximately 6, but was low in REE and was therefore supplemented with 10 ppb of terbium (Jiao, 2020). Batch sorption experiments were conducted at a cell density of approximately $1x10^8$ cells/mL,

presumably at room temperature. Batch tests included a single adsorption/desorption cycle, using 5 mM citrate for metal recovery. LBT-displayed *E. coli* cells extracted approximately 76% of the available terbium under these conditions (Jiao, 2020). The LBT-modified *E. coli* appeared to be selective for terbium. Eluents from the desorption cycle contained less than <1% of the sodium, lithium, and rubidium found in solution and concentrations of potassium, calcium, arsenic, cesium, barium, or tungsten were below the instrumental detection limits (Jiao, 2020). Other metals were partially extracted by the bacteria: iron (~29% extracted from solution), magnesium (~5%), manganese (~9%), and strontium (~2%) (Jiao, 2020). Compared to the feedstock prior to adsorption, the concentration of metal relative to the total concentration of major cations increased 100-fold for terbium. Terbium was enriched approximately 40-fold in relation to iron, 10-fold over magnesium and manganese, and 3-fold over strontium (Jiao, 2020).

LBT-engineered *E. coli* were encapsulated in beads and tested for REE sorption on both batch and flow-through experiments (Chang *et al.*, 2020; Jiao, 2020). Bacteria were encapsulated within a permeable polyethylene glycol diacrylate (PEGDA) hydrogel at high cell density, using an emulsion process (Brewer *et al.*, 2019b; Jiao, 2020). Cell densities and PEGDA concentrations were varied to determine the optimal microbe bead formulation (Jiao, 2020). REE sorption by microbeads increased proportionally to cell concentration in the beads between cell densities of approximately $1.5x10^{10}$ to $9.6x10^{10}$ cells/mL. With a cell density above $4.3x10^{10}$ cells/mL, a higher PEGDA content (>15 vol%) was required to maintain the physical integrity of the microbe beads, however, PEGDA content up to 25 vol% had little effect on bead REE sorption (Jiao, 2020). The optimal microbead formulation was chosen to be 10^{11} cells/mL in 25 vol% PEGDA (Jiao, 2020). Jiao and collaborators used a variety of microscopic imaging techniques to characterize the beads (Figure 9) (Jiao, 2020). The microbe-impregnated PEGDA beads were shown to be approximately spherical or aggregates of spherical particles with an average bead diameter of 59 ± 24 μm. Both confocal microscopy and TEM with thin-sectioned microbe beads showed that the *E. coli* cells were homogenously distributed within the microbe beads (Figure 9) (Jiao, 2020).

The REE adsorption capacity of the microbe beads was determined in batch using equilibrium adsorption experiments in a buffered solution (pH 6) containing neodymium (Jiao, 2020). Adsorption data were fit with a Langmuir isotherm model (Figure 10), which revealed a maximum neodymium adsorption capacity of 2.64 mg Nd/g dry weight of bead. The adsorption capacity of control PEGDA beads lacking bacteria was negligible (Figure 10). Microscopic analysis also showed that neodymium sorption was associated with bacterial cells, not PEGDA, and that in addition to surface sorption, some precipitation of a neodymium phosphate may also be occurring (Figure 9) (Jiao, 2020). Precipitation reactions between metals and phosphate at cell surfaces have been observed previously and can be an important mechanism for metals removal in microbial systems (Kovacova and Sturdik, 2002). Other experiments showed gadolinium penetrated PEGDA beads and associated with LBT-displayed cells (Jiao, 2020).

The sorption capacity of cells alone was approximately 26 mg Nd/g dry cells and since the beads are approximately 87% PEGDA, the results suggest that the majority of the cells in the beads are available for ion-exchange reactions (Jiao, 2020). The kinetics of the sorption/desorption exchange was investigated and a measurable effect on sorption-desorption ion-exchange kinetics was observed (Figure 10). When encapsulated, bacterial neodymium adsorption capacity was observed to be stable for a period of one month. Based on these results, flow-through ion-exchange columns were made with the LBT-engineered microbial PEGDA beads (Jiao, 2020).

Column experiments were conducted to measure breakthrough curves and develop a 1-dimensional (1-D) flow model for biosorbent treatment of REE mixtures (Jiao, 2020). Column breakthrough curve experiments are experiments in which an influent solution is flowed through a column until the effluent concentration is equal to the influent concentration. Column break-through is an important measurement or parameter for the development and scale-up of ion-exchange absorbent technology.

In order to develop a 1-D model for flow-through columns, the cell surface complexation model (described above) was modified to include advective-reaction-dispersion equations and to account for both inter-bead porosity (e.g., pore space between the hydrogel bead encapsulated bacteria) and intra-bead porosity (e.g., porosity within the beads themselves) (Chang *et al*., 2020; Jiao, 2020). The model established two explicit transport regions: inter-bead and intra-bead. Advective and dispersive transport occur in the inter-bead region, while dispersive transport and chemical reactions take place in the intra-bead region (Chang *et al*., 2020; Jiao, 2020). The model predicts outlet lanthanide concentration as a function of inlet metal concentrations and key variables, such as pH, biomass density, bioreactor column length, and flow rate (Jiao, 2020).

The 1-D model for simulation of lanthanide separation was initially calibrated using experimental data from the batch sorption of neodymium (described above) and then to experimentally generated neodymium breakthrough curves in 20 cm columns. The model was fitted to experimental data by calibration of dispersivity and the intra-particle diffusion coefficients, which could not be directly measured (Chang *et al*., 2020; Jiao, 2020). All other surface complexation model parameters were adopted from the batch adsorption isotherm model calibrations. The model was found to accurately reproduce the breakthrough time and column dispersivity (e.g., the width or sharpness of the breakthrough curve) for neodymium in columns packed with LBT-engineered biosorbent (Jiao, 2020).

The calibrated column was further tested in 100 cm columns for the prediction of the breakthrough of lanthanide mixtures (Chang *et al*., 2020; Jiao, 2020). In these experiments, a mixture of all of the lanthanides was pumped through a 100 cm column and the breakthrough of the REE was measured (Figure 11). The 1-D model included competition for carboxyl and LBT surface sites by each REE based on each lanthanide's unique affinity to those functional groups (Jiao, 2020). As can be seen in Figure 11, the model showed good agreement with the experimental data. The investigators noted that the LBT-engineered biosorbent showed selectivity for different REE, and could therefore be used to enrich or separate different lanthanides in the mixture (Jiao, 2020). For example, lanthanum was observed to have lower selectivity compared to metals such as europium and samarium. It was proposed that the biosorbent could be used to separate LREE and HREE (Jiao, 2020).

Functionalized Metal Organic Frameworks & Silica (AOP 2.5.1.5)

McGrail *et al*. (2017) investigated the use of a functionalized metal organic framework (MOF) material and silica particles as sorbents for REE from acidic solutions. Silica and MOF were functionalized for sorption with chelating ligands thought to be selective for REE (e.g., Figure 12). The media were tested for sorption of REE in batch conditions in low temperature laboratory experiments at low salinity. Sorbents were evaluated in the context of a plan to coat the sorbents on magnetic iron oxide nanoparticles, which could be added to geothermal fluids, and subsequently separate the sorbent from the fluid with a magnet, thereby recovering REE (Figure 13) (McGrail *et al*., 2017).

The final report does not include a full description of the MOF material used, but supporting material from the GDR and related publications suggest the MOF is similar or identical to MIL-101, a chromium terephthalate metal–organic framework (Bhattacharjee *et al*., 2014; Elsaidi *et al*., 2016; De *et al*., 2017; Elsaidi *et al*., 2017; McGrail, 2017). MIL-101, named for the Institut Lavoisier (France), is comprised of trimeric chromium(III) octahedral clusters interconnected by 1,4-benzenedicarboxylates, resulting in a highly porous 3-dimensional structure. MOF have reported surface areas of over 3000 m^2/g (Bhattacharjee *et al*., 2014; Elsaidi *et al*., 2018), which is equivalent to the surface area of activated carbon.

McGrail *et al*. (2017) modified MOFs with anionic functional groups (-COO^-, -CO^{2-}, -SO^{3-}, -PO_3^{2-}) but details of the functionalization were not provided. The MOF used in this project were fine powders on the order of 50 μm diameter, not nanoparticles. Batch experiments for functionalized MOF were performed by contacting synthesized MOFs with 70 or 700 mg/L (0.0005 M and 0.005 M) solutions of individual REE at pH 3 to 4, for 5 minutes. Loads and linear sorption coefficients (K_d) were calculated from these experiments.

Different MOF (designated MOF-1, -1a, -2, and -3) had variable sorption characteristics, with reported K_d for europium varying between 190 mL/g and >5000000 mL/g (McGrail *et al*., 2017). In some cases, sorption was reported to be 100%, which could affect K_d calculations. Loads varied between approximately 50 to 120 mg Eu/g MOF. The authors concluded that MOF-1a was the best sorbent for REE extraction based on a quantitative removal of > 99% REE after 5 minutes of exposure. MOF-2 was also rated as a good sorbent, having the highest observed load (122 mg Eu/g MOF), which was higher than the proposed target of 50 mg/g for the MOF-based sorbents (McGrail *et al*., 2017). It was not reported which functional groups were on which MOF number, so it is difficult to generalize these results. It was indicated that MOF-2 and MOF-3 sorbent were functionalized with the same anionic group and MOF-1 had a different functional group.

The experiments with functionalized silica particles were described in more detail (McGrail *et al*., 2017). Silica sorbents were functionalized with either propylcarboxylic acid, ethyl/butyl phosphonic acid, 3-propylsulfonic acid, or 3-(ethylenediamino)propyl, which provided carboxylic acid, phosphonic acid, sulfonic acid, and amino reactive sites, respectively. McGrail *et al*. (2017) also tested silica derivatized with amidoxime-based polymeric materials designated PNNL-1, PNNL-2, PNNL-3, and PNNL-4 (Figure 12). Amidoxime-based polymeric materials were developed at Pacific Northwest National Laboratory for sorption of uranium and other actinides (e.g., Gill *et al*., 2016).

Batch experiments were conducted as described for MOF, in that functionalized silica was mixed with 10 mL of 0.005 M acidic REE solutions for 5 min and then filtered through a 0.2-micron filter (McGrail *et al*., 2017). The residual concentration of rare earth metal ions in the supernatant was determined by inductively coupled plasma - optical emission spectrometry (ICP-OES). McGrail *et al*. (2017) did not report K_d for these sorbents, but loading for europium were reported to vary between approximately 50 and 70 mg/g, with the phosphonic acid and amino reactive groups being higher than the carboxylic acid and sulfonic acid functionalized silica. Silica functionalized with PNNL 1 through 4 had sorption of less than 40 mg Eu/g from a 0.005 M acidic REE solution. Silica functionalized with amino groups displayed an approximately 11% removal of europium from a 0.005 M solution. All other sorbents and REE showed a less than 10% removal after 5 minutes of contact time (McGrail *et al*., 2017).

Based on the results of the sorption experiments, McGrail *et al*. (2017) envisioned a final process consisting of functionalized MOF coated on iron-oxide nanoparticles. The process would consist of the addition of coated nanoparticles to the flowing geothermal fluid at the geothermal power plant, recovery of the nanoparticles with a magnet, and extraction of the sorbed REE of the nanoparticles (Figure 13).

Functionalized Organic Polymer (AOP 2.5.1.6)

Addleman and collaborators examined the utility of commercially available sorbents and proprietary sorbents developed at PNNL for the sorption of REE and precious metals from geothermal brines (Addleman *et al*., 2015; Addleman *et al*., 2016b). The patented PNNL sorbents were not described in detail in the technical reports and patents were not cited (Addleman *et al*., 2015; Addleman *et al*., 2016b). However, a patent search found only one patent and one patent application, both which described a functionalized organic polymer that could be applied to a variety of supports to make selective sorbents (Addleman *et al*., 2010; Addleman *et al*., 2016a), suggesting this is the patented sorbent referred to in the report. Technical details concerning the functional groups on the organic polymer sorbents and the application of thin films to solid supports suggests that publications concerning "self assembled monolayers on mesoporous supports" may also be relevant (Figure 14) (Busche *et al*., 2009; Johnson *et al*., 2011). Commercial sorbents tested in this study include a variety of ion-exchange resins and manganese dioxide resin from Eichrom Technologies; strong anionic exchange resins and an iminodiacetate from Biorad; activated carbon (Darco®KB-B), manganese dioxide particles (<5μm and 63-250 μm), and weak anionic exchange resins from Sigma-Aldrich; and an amidoxime resin (Purolite® S910) from Purolite (Addleman *et al*., 2016b).

Proprietary organic polymer sorbents that were tested include sorbents functionalized with diphosphonic acid, phosphonic acid, and thiol groups on a silica support (Figures 15 and 16) (Addleman *et al*., 2016b). Inorganic sorbents included manganese doped on iron oxide (Fe_3O_4) supports and manganese dioxide (MnO_2) on silica supports (Figure 17) (Addleman *et al*., 2015). Standard batch sorption tests included equilibration times over 2 hours at approximately pH 8, but some tests were conducted under acidic conditions (pH < 5). The sorbents were tested for sorption of REE, silver, copper, and zinc at concentrations of approximately 40, 19, 50, and 80 μg/L, respectively. As with other studies, europium was used as a representative REE and was added at 45 μg/L. Sorbents were tested for temperature tolerance to 95°C. REE were recovered from sorbents by acid stripping and the sorbents were tested for the ability to be reused after REE recovery. The type of acid used in the stripping process was not specified and the number of times the media could be reused was not reported (Addleman *et al*., 2015; Addleman *et al*., 2016b).

Sorption tests were carried out in both laboratory solutions and water samples from a variety of environments (Addleman *et al*., 2015; Addleman *et al*., 2016b). Test were conducted in river water, seawater, desalination brine, hot springs water, and diluted and undiluted samples from the Great Salt Lake. Synthetic brines included the "synthetic GTO simple brine," which is composed of sodium (19,000 mg/L), calcium (200 mg/L), magnesium (100 mg/L), potassium (700 mg/L), barium (20 mg/L), and chloride (30,600 mg/L), for a total dissolved solids of 50,600 mg/L. Salinities of these solutions ranged from approximately 300 m/L to over 200,000 mg/L (Addleman *et al*., 2016b). Results of the sorption tests were reported as percent removal. Sorption capacity and sorption coefficient (Kd) were discussed in the annual and final reports, but specific values were not reported (Addleman *et al*., 2015; Addleman *et al*., 2016b).

The authors concluded that phosphonic acid-based sorbents, including commercial phosphonic acid resins, showed the best overall performance for the collection of europium in all geothermal brines, including very high ionic strength solutions (Addleman *et al*., 2015; Addleman *et al*., 2016b). Metal oxides showed similar results for europium (Addleman *et al*., 2016b). Sorbents with both thiol and diphosphonic acid functional groups exhibited high silver and copper removal, even in high salinity solutions. Metal oxide sorbents showed good uptake of Cu and Ag, however, their performances were reduced when the ionic strength of brines increased (Addleman *et al*., 2016b).

Since the proprietary organic polymer sorbents could be coated on silica and iron oxide solids, Addleman *et al*. (2016b) tested a variety of supports in the context of the most likely reactor configurations for an REE removal process in a geothermal plant: a packed bed column, a fluidized bed, or a moving slurry bed. In addition, they examined the potential of using thin film coatings on fixed surfaces as an alternative to sorbent particles in contact beds.

Support structures evaluated included nano-fiber silica, nano-porous silica, nano-structured silica, and packed column silica (Addleman *et al*., 2016b). The authors recommended nano-fiber silica as the most appropriate support for applications in fluidized beds and thin films, because of its fine, submicron size structure. Mn- Fe_3O_4 magnetic nano-particles (e.g., Warner *et al*., 2010) were recommended for moving slurry beds applications. The authors proposed Mn- Fe_3O_4 magnetic nano-particles (8 nm) in a magnetic separation process. Mn-F_3O_4 was also proposed for application in thin sorbent films (Addleman *et al*., 2015; Addleman *et al*., 2016b).

Addleman *et al*. (2015) also tested the use of sorbent thin films on support surfaces. In thin films, sorbents are integrated into polymers and as a result have desired properties, such as high surface area, affinity, selectivity, permeability, water adsorption, thermal stability, mechanical strength, and anti-biofouling (Addleman *et al*., 2016a; Addleman *et al*., 2016b). The functionalized polymers can be applied as thin coats to support media, such as small silica beads, or on larger objects, such as ceramics (Addleman *et al*.,2016a). The authors proposed that thin films would be easy to incorporate into mineral extraction processes and would be resistant to fouling (Addleman *et al*., 2016a). It was proposed that thin films could be coated on basic filtration and separation media and used for industrial processing (Addleman *et al*., 2016b). Thin films of 54% (wt/wt) sorbent in a Nafion polymer binder were deposited on a stainless steel disc and tested for REE sorption in hot spring water at room temperature. The thin films sorbed dissolved REE and other valuable trace metals in a manner consistent with previous results. It was demonstrated that thin films could be made with both organic and inorganic sorbents. For the TEA (see discussion below) it was not specified which plant configuration was chosen (e.g., a packed bed column, a fluidized bed, or a moving slurry bed).

New Technology for Lithium Recovery

Manganese Oxide in a Hybrid TEG Power Plant (DE-EE-0006746)

In project DE-EE-0006746, Renew and Hansen (2017) investigated the potential to combine a series of modular technologies to extract lithium from geothermal waters and at the same time produce electricity via a thermoelectric energy generation (TEG) power plant. The modules tested included silica removal by precipitation with iron, brine concentration with membrane distillation (MD), nano-filtration to remove divalent cations, and manganese oxide absorbents to extract and recover lithium. These technologies or treatment steps were investigated in the context of integration into a hybrid geothermal TEG power plant. The research partnership for this project

consisted of a consortium of a water-treatment chemical provider (Carus Corporation), a membrane manufacturer (Applied Membrane Technology, Inc.), and Southern Research Institute, a 501(c)(3) nonprofit, scientific research organization. Each technology module was tested independently and the integration of the modules was considered in a techno-economic analysis (discussed in next section).

Experiments investigating silica removal were conducted using a high-strength brine and a low-strength brine that was approximately a 10 times dilution of the high-strength brine (Renew and Hansen, 2017). The high-strength brine was composed of silica (~ 100 mg/L), sodium (~ 3,000 mg/L), potassium (~ 680 mg/L), magnesium (~ 150 mg/L), and calcium (~ 440 mg/L). Silica removal was tested using pH adjustment with sodium hydroxide and ferric chloride addition at different temperatures, followed by filtration. Optimal silica removal was achieved at iron/silica molar ratios above 5.5 and pH > 9. Tests were run at 50°C and 80°C, and the higher temperature provides better silica removal. Most favorable silica precipitation conditions for the low-strength brine were defined as a pH of 9.0, a temperature of 80°C, and an iron/silica molar ratio of 5.65. For the high-strength brine, Renew and Hansen (2017) recommended the same temperature, but silica removal could be accomplished by pH adjustment alone, without ferric chloride addition.

Experiments for nano-filtration used synthetic brines with calcium (460 mg/L), chloride (14,220 mg/L), lithium (22 mg/L), magnesium (230 mg/L), sodium (7,050 mg/L), silica (12 mg/L) and sulfate (400 mg/L). Corresponding low-strength brines were diluted 10 or 20-fold for individual ions. They also tested a high-strength brine without silica (Renew and Hansen, 2017). The low-strength and high-strength brine had unadjusted initial pH values in the neutral pH range. The high-strength brine with silica added was adjusted to pH 5 prior to the experiment. The rationale for brine formulations and differences between brine formulation between experiments was not explained (Renew and Hansen, 2017).

Renew and Hansen (2017) reported that at 200 psi, the average flux through the nano-filter for the batch-scale experiments varied from $2.3 \times 10^{-2} - 4.1 \times 10^{-2}$ gallons per minute (gpm)/ft^2, $2.4 \times 10^{-2} - 3.2 \times 10^{-2}$ gpm/ft^2, and $1.5 \times 10^{-2} - 3.1 \times 10^{-2}$ gpm/ft^2 for the low-strength brine, high-strength brine, and high-strength brine with silica, respectively. Batch experiments were conducted until approximately 70% of the fluid had permeated the membrane on a closed-loop recycle. Using the synthetic brines, optimal separation of divalent cations from lithium was achieved with a Snyder NFX polyamide membrane with a molecular weight cutoff (MWCO) of ~150-300, although other membranes with lower and higher MWCO were also at least partially effective at separating calcium and magnesium from lithium.

Membrane distillation (MD) was investigated using high, medium, and low-strength brines (Renew and Hansen, 2017). The rationale for applying MD was to distill water and increase the lithium concentration in the remaining brine, with the objective of enhancing the efficiency of the sorption process. The MD column contained a microporous, hydrophobic, polypropylene fiber membrane with a thin hydrophobic microporous coating of a silicone-fluoropolymer to prevent pore wetting. Hot brine (46-74°C) was recirculated through the column at a constant rate of 1 gpm and the MD pilot unit was run a minimum of six (6) hours on each brine solution. In addition, a longer-term test (~ 87 hours) was conducted. Average flux rates were 5.33×10^{-3} gpm/ft^2 for the longer-term test (Renew and Hansen, 2017). Not surprisingly, distillation served to concentrate lithium in the residual brine.

Renew and Hansen (2017) conducted experiments testing potential Mn-oxide absorbents based on work by Shi *et al*. (2011). Using a Mn-oxide absorbent to recover lithium from solution has been proposed since at least the 1980s (Ooi *et al*., 1986; Miyai *et al*., 1988). Shi *et al*. (2011) prepared $Li_{1.6}Mn_{1.6}O_4$ sorbents with a pickling process that Renew and Hanson believed gave improved stability to the sorbent. Renew and Hansen (2017) compared sorption of lithium by commercially available $LiMn_2O_4$ with nano-hydrous manganese oxide (nano-HMO) and "hydrothermally synthesized" $LiMn_2O_4$. Hydrothermally synthesized $LiMn_2O_4$ has a spinel form (spinel-$LiMn_2O_4$) and was prepared by Carus. Southern Research synthesized the $Li_{1.6}Mn_{1.6}O_4$ sorbent. The sorbents were tested in batch equilibrium studies using a solution of 100 to 300 mg/L lithium in distilled water. The form of the lithium added was not specified (Renew and Hansen, 2017).

Overall, lithium absorption to Mn-oxide sorbents was pH-dependent, with sorption being higher at increasing pH (Renew and Hansen, 2017). With nano-HMO, lithium sorption was measurable above pH 8 and reached a maximum at approximately pH 12. Commercially available $LiMn_2O_4$ had minimal absorption below pH 10 and also seemed to reach a maximum at about pH 12. The hydrothermally prepared spinel-$LiMn_2O_4$ showed similar results to the commercially purchased $LiMn_2O_4$, with absorption measurable above pH 10 with a linear increase in sorption capacity until pH 12. Although it is not apparent from the results presented, which plotted as percent-removed from solution as a function of pH, the hydrothermally prepared spinel-$LiMn_2O_4$ was judged to be superior to the other preparations (Renew and Hansen, 2017).

In the case of $Li_{1.6}Mn_{1.6}O_4$ prepared by Southern Research, the sorbent was tested for lithium absorption in synthetic brines with varying sodium chloride concentrations up to 250,000 mg/L. The brines contained lithium between 40 and 456 mg/L, magnesium concentration up to 215 mg/L, and calcium concentrations up to 824 mg/L. Sorption experiments were conducted at a pH of 11 or 12. The equilibrium sorption capacity increased with brine salinity from approximately 7 mg lithium/g sorbent to be between 11.6 -12.1 mg lithium/g sorbent in the presence of high salts. In comparison, equilibrium sorption capacity for nano-HMO in distilled water at a pH between 11 and 12 was reported to be approximately 37 mg lithium/g sorbent; however the data were not analyzed using Langmuir's adsorption model or another method (Kolodynska, 2013; Awad *et al*., 2019), so it is not possible to directly compare the sorbents (Renew and Hansen, 2017).

A significant part of the effort by Renew and Hansen (2017) was not directly related to strategic mineral recovery from geothermal brines. Renew and Hanson tested Bi_2Te_3-based TEG thermoelectric materials from Novus Energy Technologies, made by mechanical alloying and hot pressing, against commercially available polycrystalline materials manufactured by unidirectional crystal growth techniques. Materials were cut and assembled and tested by an independent contract laboratory (Custom Thermoelectric). Testing indicated that Novus' nano-structured materials had lower thermal conductivity than the polycrystalline materials, which indicates that for a given heat availability, conversion efficiency will be higher. However, the authors concluded that "the overall performance" of the Novus material was not better than the commercially available materials (Renew and Hansen, 2017). The study also examined integrating membrane distillation and TEG to evaluate the viability of utilizing the TEG unit and temperature differential driven by the cold side heat exchanger to both generate electric power and to drive the temperature-driven membrane distillation process. The authors concluded that the concept of producing distillate while producing electric power was feasible (Renew and Hansen, 2017).

In the study by Renew and Hansen (2017), all of the modular treatment process components (silica removal, nano-filtration, membrane distillation and lithium absorption) were tested independently and under non-uniform conditions. The authors did not integrate the various modules, except in the techno-economic analysis, discussed below. Most of the individual treatment modules were "off-the-shelf" and the testing defined specific conditions that were used in the TEA. Renew and Hansen (2017) concluded that the silica removal goal (>80%) could be achieved by increasing the pH of the brine and, in some cases, without adding ferric chloride. As has been found in other studies, nano-filtration was shown to remove the divalent cations calcium and magnesium while allowing most lithium to pass (Renew and Hansen, 2017). Membrane distillation was shown to concentrate synthetic brines with negligible fouling under the conditions tested.

Metal-Ion Imprinted Polymers (DE-EE-0006747)

Ventura *et al*. (2016) investigated the use of metal-ion imprinted polymers as selective ion-exchange resins for the separation of lithium and manganese from brines in the context of geothermal power production. Ventura *et al*. (2016) manufactured polymers by chelating the metal target (lithium or manganese), polymerizing the metal chelate monomer, and, with or without a co-monomer, applying ethylene glycol dimethacrylate as a crosslinking agent. The metal ion is then extracted from the polymer to leave pores and ion exchange sites specific to the imprinted metal (Figure 18). The resulting product consists of resin beads approximately 100 to 150 microns in diameter, which could form larger agglomerates with a size of 300 microns or more (Figure 19). Variations on lithium-imprinted polymers included varying the amount of crosslinking and substituting copolymers. Manganese-imprinted polymers were prepared by varying the relative amount of functional monomer and crosslinking agent. In one experiment, manganese-imprinted polymers were grafted onto silica particles (Ventura *et al*., 2016).

The resins were found to be thermally stable to approximately 240°C in air and were tested at three fluid temperatures: 45°C, 75°C, and 100°C (Ventura *et al*., 2016). All experiments were conducted with synthetic brines. Tests were performed in aqueous solutions with a pH of about 7 and in pH 9 buffer solutions of 0.1 M NH_4Cl/NH_4OH, which corresponds to more than 5,300 mg/L of NH^{4+}. For batch sorption experiments, initial lithium concentrations were approximately 400 mg/L and manganese concentrations were 1,500 mg/L. Flow-through column experiments were also conducted. The resins were reported to be reusable after seven sorption/acid extraction cycles (Ventura *et al*., 2016).

The lithium uptake capacity of the ion-imprinted polymer varied as a function of the composition and degree of crosslinking. Lithium uptake as high as 2.8 mg lithium/g polymer was found for the best-performing lithium-imprinted polymers when tested in an aqueous solution containing 390 mg/L lithium at 45°C (Ventura *et al*., 2016). The solution pH 7 and pH 9 buffers did not measurably change the lithium capacity of the polymer. Lithium uptake was also reasonably temperature-independent, with a slight decrease in sorption capacity found at 100°C, compared to 45°C and 75°C. The authors recommended further study to determine if the reduced capacity at 100°C was due to lower binding constant or polymer instability (Ventura *et al*., 2016).

Comparable batch experiments conducted for manganese-imprinted polymer found the highest sorption capacity measured was 19.3 mg manganese/g polymer from a brine containing 1,500 mg/L manganese and 2,800 mg/L sodium in 4.65 pH buffer at 45°C. A representative manganese-imprinted copolymer was tested in a packed-bed column and regenerated four times at 75ºC. The

manganese uptake capacity did not change significantly for the four cycles with an average capacity of 23.1 mg manganese/g polymer in flow-through tests.

Lithium-imprinted polymers were tested for their lithium uptake capacity in the presence of other, potentially interfering ions. Batch tests were conducted at 45°C in a synthetic brine containing 412 mg/L lithium, 405 mg/L sodium, and 435 mg/L potassium, prepared from chloride salts, at pH 9. Monovalent cations did not reduce imprinted polymer lithium sorption capacity significantly (~10%). Polymers showed lithium selectivity (lithium absorbed/cation absorbed) between 2.3-3.7 for sodium and 3.2-4.5 for potassium, depending on the polymer composition (Ventura *et al*., 2016).

Ventura *et al*. (2016) did find that calcium and magnesium interfered with lithium sorption. When tested in a solution containing 400 mg/L lithium, 400 mg/L magnesium, and 265 mg/L calcium, lithium sorption capacity was reduced by approximately one-third. Selectivity for lithium varied between approximately 0.1 to 0.5. The authors concluded that calcium and magnesium interference is significant and calcium and magnesium will need to be removed before the sorption step in any application (Ventura *et al*., 2016).

As part of the TEA (discussed below), it was noted that the volumetric sorption capacity for a functioning filter bed needed to be equivalent to 2 g lithium/L bed volume to be economical. Using the current polymer formulation, the polymer packing density was calculated to be approximately 300 g/L, which provides a sorption capacity of about 0.6 g lithium/L bed volume (Ventura *et al*., 2016). The authors suggested that a functioning filter could reach the 2g lithium/L objective if it was filled with a mixture of hydrous manganese oxide (HMO) or aluminum hydroxide and the lithium-imprinted polymer in the form of porous macro-beads (Ventura *et al*., 2016).

Techno-Economic Analysis

Technologies for the extraction of REE and other strategic minerals from geothermal brines need to be economical if they are to provide additional revenue sources to geothermal operators in hybrid energy-mineral-recovery operations (Wendt *et al*., 2018; Meng *et al*., 2019). Two of the four resource assessment projects included an assessment of the economics of REE recovery from a resource availability perspective (Tables 1 and 2). In addition, TEAs were conducted for all of the Phase I technology projects (Table 1). The major assumptions and final outcomes of those economic analysis are presented here. Dollar amounts reported here are given as found in the reports, with rounding, and therefore represent dollar values approximate to the year the reports were published.

Economic Assessments Based on Resource Analysis

The resource assessment by Zierenberg and Fowler (2018) (DE-EE-0006748) included a quantitative analysis to evaluate the economic potential of REE in geothermal brines from the Don A. Campbell plant in Nevada and the Puna facility in Hawaii. Zierenberg and Fowler (2018) used average REE concentrations found in geothermal fluids multiplied by the total fluid production per year to calculate total potential production of REE, assuming a technology with 100% recovery efficiency. In addition to an assumption of 100% recovery of REE, they assumed a zero capital cost for a processing plant, no interest on capital investment, and no operation and maintenance costs. The total mass of REE produced was multiplied by published commodity prices from 2014 to determine the upper limit of revenue that could conceivably come from harvesting REE at these

facilities. They calculated that revenues from REE would be negligible, with an economic potential of only 0.05% of the estimated value of electricity produced at the Don A. Campbell geothermal plant. The total economic value of REE from fluid from the Don A. Campbell plant was calculated to be less than $2000 per year and even lower at the Puna facility (Zierenberg and Fowler, 2018). Even with the optimistic estimate of 100% efficiency and zero costs, Zierenberg and Fowler (2018) concluded that REE was not a viable economic target for these facilities.

Quillinan *et al*. (2018) started their economic analysis of emerging technologies with the assumption that recovery of REE was not profitable, based on the conclusion of a prior study by Smith *et al*. (2017). Smith *et al*. (2017) concluded that extraction of REE was not economical, but held out hope that a new technology or combining REE recovery with the extraction of other more valuable materials could improve the economics of recovery of strategic and valuable minerals from geothermal brines. Quillinan *et al*. (2018) followed up on this analysis using their own data and contemporary mineral commodity prices.

A major factor affecting the unfavorable economics of REE extraction from geothermal brines included the very low concentrations (nano-gram to microgram per liter) of REE in brines. Using "emergent self-organizing mapping" (Chapter 6), Quillinan *et al*. (2018) predicted many produced waters to be enriched in REE by 1000 times relative to seawater. Although Quillinan *et al*. (2018) used seawater as a benchmark for comparison of geothermal brines, it was recognized that even brines with a thousand times higher REE concentrations than seawater might not be economical to process. The extraction of REE from brines with such low concentrations is complicated by complexation reactions between the REE and other materials in the brine solution (Quillinan *et al*., 2018). The TEA included the observation that there are significant knowledge gaps concerning the actual costs of proposed REE separation processes that add uncertainty (Quillinan *et al*., 2018). The authors observed that the "lack of economic data of REE separation processes represents perhaps the most significant gap in the literature and the greatest need in terms of future research" (Quillinan *et al*., 2018).

Quillinan *et al*. (2018) also recognized a trade-off between process economics and the selectivity of any proposed REE process. They proposed that higher selectivity lowers the number of stages, and hence capital and chemical inventory costs. They used the example of chemical requirements for neutral and anionic ion-exchangers in comparison to cation exchangers to argue that the more specific the initial sorption, the lower the overall process costs will be (Quillinan *et al*., 2018). It is clear that the more stages required for extraction of REE, the higher the costs are likely to be.

Quillinan *et al*. (2018) ultimately concurred with the finding of Smith *et al*. (2017) concerning the economics of REE extraction. They used mineral commodity values published by the USGS (U.S. Geological Survey, 2018) to estimate prices of $180-$190 per kg for Dy_2O_3 and $470-$480 per kg for Tb_2O_3. Even assuming 100% removal of both dysprosium and terbium from produced or geothermal water samples, revenues were calculated to be less than a $0.01/barrel of produced water (1 barrel = 42 gallons). The authors observed that disposal costs for brines within the United States generally span the range of roughly $0.10 to more than $4.00 per barrel (Quillinan *et al*., 2018). The authors concluded that the economic worth of the two most valuable REE, dysprosium and terbium, would be significantly less than typical costs required to dispose of any waste brines from an REE extraction process (Quillinan *et al*., 2018).

Even though Simmons (2019) did not conduct a formal TEA, they did compare their estimated REE and lithium inventories from geothermal plants in Idaho, Nevada, New Mexico, Oregon, and

Utah with other sources of these strategic materials. In this analysis, they compared geothermal sources of REE to mineral deposits in the same region (the Basin and Range). They found numerous mineral deposits in the Basin and Range region that could potentially be mined for REE (Simmons, 2019). In addition, Simmons (2019) noted that geothermal brines from the Salton Sea have estimated inventories of lithium of about 3 x 10^9 kg, which is 40 times larger than their estimate for the lithium resource in the Roosevelt Hot Springs reservoir. From this analysis, Simmons (2019) concluded that, due to the very low REE concentrations in geothermal waters, extraction technology would need to be "very efficient" to be viable.

Economic Assessments Based on Technological Processes

Economics of REE Extraction Processes

Stull (2016) did not include a full TEA in the final report, but identified the greatest process cost variables as the REE concentration within the geothermal water; the contact time between the media and the geothermal water (e.g., plant size requirements); and the method for media stripping and regeneration. Tusaar is an established water treatment company and the initial expectation of the investigators was that the process of extracting REE from geothermal produced water would be the same as treating other waters. The initial process design was that the REE-laden water would be passed through a fixed bed column until the sorption media was saturated (fully loaded) and then the REE would be stripped out of the loaded media by a chemical process, such as acid treatment (Stull, 2016). Experimental results, described above, showed that a more complex process was needed to extract REE from geothermal fluids and costs increased as process changes were made. Factors increasing costs included the addition of "catch" columns, to recover sorbent ligands, and parallel systems to allow continuous operation (Stull, 2016). Additionally, poor reactor kinetics required larger reactor sizes than initially expected from prior experience in water treatment applications (Stull, 2016).

With these changes, Stull (2016) calculated capital costs for construction of a commercial plant to be between $2.8M and $4.3M in 2016 dollars. Media startup costs were estimated to be $4.6M. It was calculated that, in order to be economical, at the expected REE concentrations, the value of the REE recovered would have to be $90/kg. The actual blended 2016 market value of REE was calculated by Stull (2016) to be only $16/kg, almost six time lower than needed (Stull, 2016). Stull (2016) concluded that the process would not be financially viable at current market prices for REE, but noted that the world market price for REE has been turbulent over the past several years and was currently near historical lows. Stull held out hope that improvement in plant efficiencies and rising REE prices might improve profitability (Stull, 2016).

McGrail *et al*. (2017) considered the use of derivatized MOF and silica particle sorbents in a full-scale system that included a design feature of having a magnetic separation process. The concept proposed was to coat iron-oxide nano-particles with MOF or silica sorbents, add the coated nano-particle to geothermal fluids in a power plant and then use a magnet to capture the iron particles and recover the sorbed mineral, including REE. The TEA consisted of an estimate of the costs of producing the magnetic nano-particle adsorbents, the design and operation of a proposed magnetic separation system, and the current prices of REE and other minerals (McGrail *et al*., 2017).

McGrail *et al*. (2017) used average concentrations of REE in geothermal brines to establish the "typical geothermal brine conditions" used in the TEA. For the TEA, the brine was assumed to contain 500 μg/L cerium, 30 μg/L dysprosium, 15 μg/L europium, 200 μg/L neodymium and 300

µg/L yttrium and the flow rate was 6,000 gpm. Assuming 90% of metal ions will be removed and using 2017 market prices, maximum potential annual revenue from REE was estimated at $0.8M per year.

To estimate the costs of producing magnetic nano-particle cores, McGrail *et al.* (2017) assumed that an unidentified procedure could be scaled up to synthesize iron oxide (Fe_3O_4) nano-particle cores with sizes of 13-20 nm^3. Including materials, energy, equipment, processing, and labor, the estimated manufacturing cost for the core was estimated to be $34/kg in 2017. The core preparation cost was estimated to be 20% of the magnetic nano-particles cost. Cost of the final magnetic sorbents were based on estimated manufacturing costs for the four best sorbents from the laboratory tests (described above): MOF-1a, MOF-3, ethyl phosphonic acid-silica, and SiO_2-PNNL-2 were priced at approximately $2,000, $900, $600, and $900 per kg, respectively. In calculating sorbent requirements, a scaling factor of 200X was applied to laboratory sorption results to account for increased surface area on 50 nm nano-particles, compared to the larger particles used in the laboratory studies. A 6,000-hour lifetime was assumed for all the adsorbents. Based on the laboratory sorption studies and the expected amounts of REE in the geothermal fluid, the mass of sorbent needed for a full-scale process treating 6,000 gpm was estimated to be approximately 4 kg MOF-3, 6 kg MOF-1a, 40 kg ethyl phosphonic acid-silica, or 40 kg SiO_2-PNNL-2 per year. Sorbent costs varied between a low of $600/kg for ethyl phosphonic acid-silica and $2,000/kg for MOF-1a. Estimated annual cost for sorbent varied between approximately $5,000 to $50,000 per year, depending on which magnetic sorbent was used (McGrail *et al.*, 2017).

The REE extraction assumed by McGrail *et al.* (2017) is a fairly simple process: magnetic sorbent is mixed with the feed brine, the flow in the pipes provides the mixing and contact time, and at the end of the plant, the fluid-sorbent mixture is passed through a separator that removes the sorbent using electromagnetic force (McGrail, 2017; McGrail *et al.*, 2017). Two magnetic separators are used to make the separation a continuous process. An unspecified stripping agent will be used to desorb the REE and regenerate the magnetic nano-particles. The capital costs for the REE extraction process was estimated using the method of Guthrie (McGrail *et al.*, 2017). The equipment for the "magnetic nano-fluid extraction process" installed cost was estimated to be $480,000. Including supporting infrastructure total capital costs were priced at a little over $960,000. Annual operating costs, not including the cost of the sorbent, were approximately $500,000 per year (McGrail *et al.*, 2017).

The annual total production of REE was expected to be approximately 12,000 kg, which was assigned an average value of approximately $70/kg (McGrail *et al.*, 2017). The plant operation time was assumed to be 30 years with a 10-year debt payment period. The internal rate of return (IRR) was calculated to be 20% for the MOF-3 absorbent. The IRRs for other adsorbents were estimated to be between 15% and 19%. From this analysis the authors concluded that an REE extraction process based on sorbents bound to iron-oxide nano-particles would be economically viable (McGrail *et al.*, 2017). This conclusion assumes the cost of an unproven magnetic separation process and an REE price that may be optimistic (Bogner, 2015; Argus Media Group, 2020; Kitco Metals Inc., 2020). Phase II project AOP.2.5.1.14 is continuing to investigate the sorption and magnetic separation process (Table 2).

Addleman *et al.* (2016b) looked at two scenarios in their TEA for a process based on a functionalized organic polymer. In one case, an average REE and precious metal brine concentrations used, and in the alternative case, the geothermal brine was based on values from

the Salton Sea, which has a higher concentration of valuable minerals. The authors considered three flow regimes (3,000, 6,000, and 12,000 gpm) and specified a 72% mineral recovery. The type or configuration of process was not described, but the estimated "sorbent plant" capital costs ranged from approximately $25M to $66M, increasing with the amount of flow (Addleman *et al.*, 2016b).

The TEA included costs for sorption, stripping, and concentrating of minerals at the geothermal site (Addleman *et al.*, 2016b). Refining of the recovered metals was accounted for by assuming that recovered mineral concentrates could be shipped to an off-site location for further refining and smelting (Addleman *et al.*, 2016b). Off-site refining costs were assumed to have a fixed "toll" cost of $2.1 million per 1000 gpm plant capacity, plus a handling charge of 20%. The net 72% recovery of REE is estimated based on the calculation that mineral recovery from the brines will be 80% and tool refining will recover 90%. Shipping costs are based on a 90% by weight solids with 45% of the solids being valuable metals and was assigned a flat rate of $85 per wet ton. Present prices (in 2016) were assigned as $480 per dry ton of REE oxide, $120 per dry ton of precious metal, $240 per dry ton of base metal, and assumes all of the metal is saleable. The plant was assumed to have a 10-year operational life. Brine treatment was estimated to cost of $0.88/1000 gallons, which includes sorbent cost, stripping acid, and neutralizing caustic for neutralizing (Addleman *et al.*, 2016b).

Using this approach, the capital cost for the 6,000 gpm plant treating the average geothermal brine was almost $45M with operational costs of approximately $17M per year. Gross annual revenue from metals was calculated as slightly over $7M with a net revenue of over $11M after refining, which yields a Net Revenue/Capex ration (ROI) of 23%, which suggests a plant with this configuration would be profitable (Addleman *et al.*, 2016b). The plant treating the Salton Sea brine was proportionally better. The authors concluded that both scenarios showed positive economics for the mineral recovery process associated with a geothermal plant. It should be noted that even though Addleman *et al.* (2016b) calculated a potential profit for mineral recovery from geothermal power plants, the profit was not from REE recovery. Addleman assumes that 75% of the metals recovered will be gold, palladium, platinum, silver, manganese, copper, and zinc, which will account for the majority of the revenue (Addleman *et al.*, 2016b). Lithium was not considered nor included in this analysis.

Economics of Lithium Extraction Processes

Renew and Hansen (2017) conducted a TEA on a hypothetical geothermal plant that integrated nano-filtration, membrane distillation and lithium adsorption with TEG power generation. They used an unspecified DOE cost estimate tool and incorporated costs from NETL for construction of electric power plants (Renew and Hansen, 2017). The TEA was based on a hybrid plant treating 500 gpm of brine flow with lithium content of 150 mg/L and an incoming brine temperature of 150°C. The TEG efficiency was assumed to be 5.24%. The brine treatment system consisted of a silica removal/filtration step, followed by nano-filtration, two membrane distillation stages, and then the lithium recovery adsorbers. In contrast to the experimental work, discussed above, the plant does not include a large settling tank for silica removal, and chemical costs are based on the system operating at pH 9. The equipment capital costs for the nano-filtration step were estimated to be approximately half the amount of a similar-sized reverse osmosis desalination plant produced by Dow. Electrical prices for both generation and consumption were assumed to be $0.055/kWh and the selling price of lithium carbonate was fixed at $20,000 per ton (Renew and Hansen, 2017).

Renew and Hansen (2017) determined that the profitability of the hybrid TEG plant was highly dependent on the concentration of lithium in the brine and the market price of lithium. They estimated that plants with lithium concentrations above 150 mg/L could overcome the startup barrier imposed by the initial capital cost because they could capture more lithium while utilizing the same sized equipment. Renew and Hansen (2017) calculated that the required investment would not net a viable return unless the price of lithium carbonate was $28,000/metric ton. If capital costs could be reduced by ~27% then a breakeven point could be reached with lithium prices of $20,000 /metric ton (Renew and Hansen, 2017). The spot price for lithium carbonate is currently less than $9,000 per metric ton (The London Metal Exchange, 2020). The authors conclude that the economics are unfavorable for a hybrid geothermal TEG lithium recovery process (Renew and Hansen, 2017).

Ventura *et al*. (2016) conducted a techno-economic assessment of their ion-imprinted polymers. Capital costs were estimated using known methods and costs were based on established protocols and references. One variation of note: the process they modeled included a stage where the sorbent is regenerated with CO_2, instead of the more conventional acid regeneration with HCl. They assert that the feasibility of the CO_2 regeneration has been demonstrated to be effective and economical in their laboratories and that the process could be used for the direct production of Li_2CO_3 (Ventura *et al*., 2016). References for the CO_2 regeneration process were not provided. As discussed above, the authors also proposed filling the lithium exchanger with a mixture of HMO or aluminum hydroxide and the lithium-imprinted polymer, to meet volumetric sorption capacity.

The cost calculations included microfiltration to separate solids, followed by membrane nano-filtration to separate divalent cations before the lithium sorption process (Ventura *et al*., 2016). Their calculations were based on a brine flow rate of 6,000 gpm; a recovery efficiency of 90%; lithium concentrations of 400 mg/L in the brine; and a sorbent capacity of 2g lithium/L sorbent, which would yield a lithium production rate of almost 50 kg/min. The total capital costs of the lithium extraction plant were estimated as approximately $21M, with a total annual operating cost of $11M. Revenues from the sale of lithium carbonate (Li_2CO_3) were expected to exceed $40M at a production rate of almost 50 kg/min and sale price of $2,000/ton for Li_2CO_3 (Ventura *et al*., 2016). This analysis, although it included several optimistic assumptions, including high brine lithium concentrations, offers some promise that geothermal lithium extraction could be profitable.

Summary & Conclusions

The objective of this report is to provide a retrospective analysis of the projects associated with two GTO FOAs that focused on the extraction of REE and lithium from geothermal brines (Tables 1 and 2). Four projects focused on understanding the occurrence of REE in geothermal brines and produced waters. Eleven projects focused on the development and testing of sorption systems and recovery of REE and other valuable metals from geothermal brines. Most of the sorption technology projects were focused on development of low-TRL technology (Tables 1 and 2). One project focused on the application of a higher-TRL sorbent for REE extraction from geothermal brines (Stull, 2016). One project examined the potential for a hybrid geothermal system, based on TEG electrical generation combined with production of clean water and lithium carbonate (Renew and Hansen, 2017).

GTO projects evaluated the occurrence and concertation of REE in geothermal brines and produced water from the oil and gas industry. It was found that REE were generally higher in

produced waters than in geothermal fluids (Quillinan *et al*., 2018). Two studies examined the relation between reservoir lithology and fluid REE concentrations and found that lithology did not predict REE concentrations in produced waters or brines (Quillinan *et al*., 2018; Zierenberg and Fowler, 2018). These two studies noted that there was discernable basin to basin variation in REE concentrations, but why REE concentrations were higher in one basin over another was not determined. This program generated valuable data, archived on the GDR, that could be used in for geospatial analysis and evaluation of mineral resources.

All of the technology development projects investigated the use of sorption as a mechanism by which to harvest REE from geothermal fluids (Tables 1 and 2). In most studies, various kinds of support media were functionalized with carboxylic acid, phosphonic acid, amide, sulfur oxide, or similar chelating ligand. Most studies concluded that phosphonic acid gave the best results for selective or preferential sorption of REE (Addleman *et al*., 2015; Karamalidis, 2016; McGrail *et al*., 2017). Most studies found that divalent cations and metals interfere with REE sorption processes, but salinity from simple salts (NaCl, KCl) did not interfere, even at high salt concentrations. Temperature limited the usefulness of impregnated media (Stull, 2016), which in combination with results from other studies, suggests that covalently bound functional groups are more appropriate for high temperature geothermal fluids. The projects conducted by researchers in the National Laboratories suggest that MOF and organic polymers continue to be of interest and show potential for the recovery of metals from geothermal fluids (Addleman *et al*., 2016b; McGrail *et al*., 2017). Since MOF and organic polymers are able to be functionalized in a variety of ways, they have potential application in the absorption of lithium and other valuable metals as well as REE.

Many studies used synthetic brines, some of which did not include metals or divalent cations likely to interfere with sorption processes. All studies used percent removal as a metric for sorption testing. Although useful for within laboratory comparisons of sorption tests, percent removal is not a good metric for comparison between media, especially between different laboratories, since the result is entirely dependent on the test conditions. Fitting data to engineering sorption models (Langmuir, Freundlich, or linear) and reporting sorption constants for specific test conditions, would allow a more through and accurate comparison between sorption media (Kolodynska, 2013; Awad *et al*., 2019). Some studies apparently applied the Freundlich solid-water distribution model, but results of that analysis were not reported. Some studies reported linear sorption coefficients, which may be adequate for low REE concentrations, but may be inaccurate if applied to higher concentration solutions. Reporting Langmuir or Freundlich adsorption models would allow an engineering design comparison between sorbents from different studies (Kolodynska, 2013; Awad *et al*., 2019).

The results of these studies show that the technology for extraction of REE has now been developed to the approximate TRL 4 level. There appears to be little more to be gained by testing sorbents in simple synthetic brines. Studies that investigated REE sorption in more complex synthetic brines provided insight on the importance of competing ions for extraction of REE. Future programs should include more studies at TRL 5 and above that offer opportunities to test technology against real geothermal brines.

Most of the projects had a component of economic evaluation and analysis. All of the projects that investigated the recovery of REE from geothermal waters concluded that the recovery of REE from geothermal brines was unlikely to be profitable. Several different approaches were taken to

evaluating the potential profit from REE extraction. One convincing analysis calculated economic potential for two geothermal power plants in Nevada and Hawaii, and concluded that even if all of the REE were collected, at no cost, the profit would be a small percentage of the revenue from electrical generation and would therefore not represent a significant change in the profitability of geothermal power production. An analysis of REE in brines in the western USA (Figure 3) concluded that ore deposits in the region, some of which were associated with active mines, were a more likely alternative source of REE if demand for these mineral increased.

Projects that evaluated the scale-up of sorption technology as part of a hybrid geothermal plant also concluded that REE were not a profitable target, despite significant technological advances that were accomplished as part of these projects. Major limitations to profitability were the low concentration of REE in geothermal brines and the low and volatile market price of REE. The potential costs of REE extraction process were important, but not the main driver for economic sustainability. The conclusive outcome of the GTO program is that REE recovery from fluids at geothermal power plants is unlikely to prove profitable.

Studies from this program showed lithium, precious metals, and base metals could be profitably recovered from geothermal fluids and are therefore better economic targets. The project that projected a profitable outcome for a hybrid system achieved a profitable projection based on the recovery of valuable metals other than REE. The studies that examined extraction of lithium and manganese from geothermal fluids suggest that recovery of these metals could be economically sustainable. This result suggests that future programs concerning the development of mineral recovery processes for application in hybrid geothermal power systems should focus on the recovery of lithium and other metals, rather than REE.

Recommendations

- **Mineral recovery research that is funded to benefit hybrid geothermal power economic objectives should focus on recovery of lithium and other metals, rather than REE.** The GTO program has conclusively proven REE extraction will not be economical unless there is a significant disruption in the market. REE recovery may benefit national security objectives, but REE recovery is unlikely to improve the economic competitiveness of geothermal power production.
- **Reporting of results from technology development projects should be standardized to the extent possible.** Reporting of sorption media test results should include fitting standard engineering sorption models (Langmuir, Freundlich, or linear) to better allow comparison between media and enable preliminary engineering design.
- **Benchmark conditions for technology testing should be established to the extent possible.** Recommended formulations for synthetic brines, representative of major geothermal areas should be established. Temperatures at which technology should be tested should be specified. Benchmark conditions should include testing against interference from common geothermal fluid components, such as iron, calcium, and magnesium. Testing of technology against fluids consisting mostly of sodium chloride or other simple salts no longer address the major challenges associated with mineral recovery from more complex geothermal fluids.
- **Benchmarks for techno-economic analysis should be established to the extent possible.** Establishing reference benchmarks for the price of metals and specifying average metal concentrations for geothermal brines would allow better comparison between

projects. Benchmarks could include recommending standard sources for pricing capital costs and recommending methods or sources for data (e.g., Chemical Engineering Plant Cost Index). Using common benchmarks for non-variable items would simplify interpretation of economic analysis.

- **Future research should include testing against actual geothermal fluid samples.** Technology for metals extraction from geothermal brines has reached TRL level 4 or above. The next step is to challenge new technology against more realistic conditions. A method for supplying researchers with geothermal fluid samples should be established. Developing cooperating industrial partners and establishing testbed facilities are needed as the interim step between laboratory testing and full-scale application. Testing against geothermal fluids under realistic conditions will reduce the economic risk associated with implementing hybrid geothermal electric power production.

- **Data collected and compiled during resource assessment studies should be further analyzed to answer important questions concerning strategic mineral resources in the USA.** Data collected and compiled in resource assessment studies sponsored under GTO programs are a valuable resource that should be further compiled, edited, standardized, and integrated into a relational database or similar format. This data can be used to answer outstanding questions concerning the geospatial distribution of strategic minerals in the USA and the total resources available. A meta-analysis of this data could provide more in-depth understanding of the geochemistry of REE in brines and the factors controlling relationships between solid and fluid REE concentrations in the subsurface.

- **Prior industrial-scale efforts to extract metals from geothermal brines should be further evaluated for lessons learned.** For example, a commercial-scale plant was installed by CalEnergy for the recovery of zinc from geothermal brines at the Salton Sea geothermal field (Clutter, 2000), but was discontinued after only a few years of operation due to a lack of profitability (Geothermal Resources Council, 2004). Understanding the factors affecting economic success, such as recovery efficiency and production levels, plant installation and operations costs, and the impact of changing commodity prices, will help with future mineral recovery projects.

Acknowledgments

References

Addleman, R.S., Bays, J.T., Carter, T.G., Fontenot, S.A., Fryxell, G.E., Johnson, D.W., 2010. Renewable sorbent material and method of use (US 2010/0147768 A1). US 2010/0147768 A1.

Addleman, R.S., Chouyyok, W., Li, X.S., Cinson, A.D., Gerasimenko, A.A., 2016a. Porous multi-component material for the capture and separation of species of interest. United States Patent 9,370,749.

Addleman, R.S., Chouyyok, W., Palo, D., Dunn, B.M., Billingsley, G., Johnson, D., Nell, K.M., 2015. Recovery of Rare Earths, Precious Metals and other Critical Materials from

Geothermal Waters with Advanced Sorbent Structures. AOP 2.5.1.6. (FY 2015 Annual Report). Pacific Northwest National Laboratory, Richland, Washington.

Addleman, R.S., Chouyyok, W., Palo, D., Dunn, B.M., Brann, M., Billingsley, G., Johnson, D., Nell, K.M., 2016b. Evaluation of Advanced Sorbent Structures for Recovery of Rare Earths, Precious Metals and other Critical Materials from Geothermal Waters –Preliminary Results (AOP 2.5.1.6 Final Report). Pacific Northwest National Laboratory, Richland, WA, p. 31.

Ajo-Franklin, C.M., 2015. Quarterly Research Performance Progress Report: Engineering Thermophilic Microorganisms to Selectively Extract Strategic Minerals from Low Temperature Geothermal Brines (2.5.1.4). p. 7.

Ajo-Franklin, C.M., Ajo-Franklin, J.B., Viani, B., Charrier, M., Borgin, S., Yang, L., Murray, G., 2017. Engineering Thermophilic Microorganisms to Selectively Extract Strategic Metals from Low Temperature Geothermal Brines. (Final Report AOP 2.5.1.4). Lawrence Berkeley National Laboratory, Berkeley, CA.

Argus Media Group, 2020. Argus Rare Earths Monthly Outlook. Argus Media Group, London.

Awad, A.M., Shaikh, S.M.R., Jalab, R., Gulied, M.H., Nasser, M.S., Benamor, A., Adham, S., 2019. Adsorption of organic pollutants by natural and modified clays: A comprehensive review. Separation and Purification Technology 228.

Bhattacharjee, S., Chen, C., Ahn, W.S., 2014. Chromium terephthalate metal-organic framework MIL-101: synthesis, functionalization, and applications for adsorption and catalysis. Rsc Advances 4, 52500-52525.

Bloomquist, G.R., Povarov, K.O., 2008. Mineral Extraction—Result Studies of World Bank. Geothermal Resources Council Transactions, pp. 375-378.

Bogner, S., 2015. The 'REE Basket Price' Deception And The Clarity Of Opex. Rockstone Research Ltd., London.

Bourcier, W.L., Lin, M., Nix, G., 2005. Recovery of Minerals and Metals from Geothermal Fluids. Lawrence Livermore National Laboratory Report UCRL-CONF-215135.

Bradley, D.C., Stillings, L.L., Jaskula, B.W., Munk, L., McCauley, A.D., 2017. Lithium, Chapter K of Critical Mineral Resources of the United States—Economic and Environmental Geology and Prospects for Future Supply, Professional Paper 1802–K. in: Schulz, K.J., Jr., J.H.D., II, R.R.S., Bradley, D.C. (Eds.). Critical Mineral Resources of the United States—Economic and Environmental Geology and Prospects for Future Supply. U.S. Department of the Interior, U.S. Geological Survey, Reston, Virginia.

Brewer, A., Chang, E., Park, D.M., Kou, T., Li, Y., Lammers, L.N., Jiao, Y., 2019a. Recovery of rare earth elements from geothermal fluids through bacterial cell surface adsorption. Environmental Science & Technology 53, 7714-7723.

Brewer, A., Dohnalkova, A., Shutthanandan, V., Kovarik, L., Chang, E., Sawvel, A.M., Mason, H.E., Reed, D., Ye, C.W., Hynes, W.F., Lammers, L.N., Park, D.M., Jiao, Y.Q., 2019b. Microbe Encapsulation for Selective Rare-Earth Recovery from Electronic Waste Leachates. Environmental Science & Technology 53, 13888-13897.

Busche, B., Wiacek, R., Davidson, J., Koonsiripaiboon, V., Yantasee, W., Addleman, R.S., Fryxell, G.E., 2009. Synthesis of nanoporous iminodiacetic acid sorbents for binding transition metals. Inorganic Chemistry Communications 12, 312-315.

Chang, E., Brewer, A.W., Park, D.M., Jiao, Y., Lammers, L.N., 2020. Surface complexation model of rare earth element adsorption onto bacterial surfaces with lanthanide binding tags. Applied Geochemistry 112, 104478.

Clutter, T.J., 2000. Mining economic benefits from geothermal brine. Geo-Heat Center Bulletin, June 2000, 1-3.

De, S., Nandasiri, M.I., Schaef, H.T., McGrail, B.P., Nune, S.K., Lutkenhaus, J.L., 2017. Water-Based Assembly of Polymer-Metal Organic Framework (MOF) Functional Coatings. Advanced Materials Interfaces 4.

Department of the Interior, 2018. Final List of Critical Minerals 2018, 83 Fed. Reg. 23295.

Elsaidi, S.K., Mohamed, M.H., Banerjee, D., Thallapally, P.K., 2018. Flexibility in Metal-Organic Frameworks: A fundamental understanding. Coordination Chemistry Reviews 358, 125-152.

Elsaidi, S.K., Mohamed, M.H., Loring, J.S., McGrail, B.P., Thallapally, P.K., 2016. Coordination Covalent Frameworks: A New Route for Synthesis and Expansion of Functional Porous Materials. Acs Applied Materials & Interfaces 8, 28424-28427.

Elsaidi, S.K., Sinnwell, M.A., Banerjee, D., Devaraj, A., Kukkadapu, R.K., Droubay, T.C., Nie, Z., Kovarik, L., Vijayakumar, M., Manandhar, S., Nandasiri, M., McGrail, B.P., Thallapally, P.K., 2017. Reduced Magnetism in Core-Shell Magnetite@MOF Composites. Nano Letters 17, 6968-6973.

Gallup, D.L., 1998. Geochemistry of geothermal fluids and well scales, and potential for mineral recovery. Ore geology reviews 12, 225-236.

Geothermal Resources Council, 2004. CalEnergy cuts zinc production, lays off quarter of workforce. Geothermal Resources Council Bulletin, p. 136.

Gholz, E., 2014. Energy Report: Rare Earth Elements and National Security. Council on Foreign Relations, New York, NY, pp. 1-15.

Gill, G.A., Kuo, L.-J., Strivens, J., Wood, J., Schlafer, N., Tsouris, C., Wai, C.M., Pan, H.-B., 2016. Summary of Adsorption Capacity and Adsorption Kinetics of Uranium and Other Elements on Amidoxime-based Adsorbents from Time Series Marine Testing at the Pacific Northwest National Laboratory (PNNL-25899). Pacific Northwest National Laboratory, Richland, Washington 99352, Prepared for the U.S. Department of Energy under Contract DE-AC05-76RL01830.

Harrison, S., 2015. Quarterly Research Performance Progress Report Q1: Determination of Rare Earths in Geothermal Brines and Evaluation of Potential Extraction Techniques (DE-EE0006750).

Haxel, G.B., Hedrick, J.B., Orris, G.J., 2002. Supporting Sound Management of Our Mineral Resources: Rare Earth Elements - Critical Resources for High Technology. U.S. Geological Survey Fact Sheet 087-02.

Hernandez, M.T., Abu-Dalo, M., Khanna, G., Quick, A., 2018. Metal Removal System. US Patent 10,106,437.

Jiao, Y., 2020. Extraction of Rare Earth Metals from Geothermal Fluids using Bioengineered Microbes. Final report AOP 2.5.1.12. Lawrence Livermore National Laboratory, Livermore, CA.

Johnson, B.E., Santschi, P.H., Addleman, R.S., Douglas, M., Davidson, J., Fryxell, G.E., Schwantes, J.M., 2011. Optimization and evaluation of mixed-bed chemisorbents for extracting fission and activation products from marine and fresh waters. Analytica Chimica Acta 708, 52-60.

Karamalidis, A., 2016. Final Project Report: Chelating Resins for Selective Separation and Recovery of Rare Earth Elements from Low Temperature Geothermal Water (DOE-CMU-EE06749).

King, H.M., 2020. Rare Earth Elements and their Uses: The demand for rare earth elements has grown rapidly, but their occurrence in minable deposits is limited. Geology.com, Lemont Furnace, PA.

Kitco Metals Inc., 2020. New York Spot Price. Kitco Metals Inc., Montreal, Quebec.

Kolodynska, D., 2013. Application of a new generation of complexing agents in removal of heavy metal ions from different wastes. Environ. Sci. Pollu. Res. 20, 5939-5949.

Kovacova, S., Sturdik, E., 2002. Interactions between microorganisms and heavy metals including radionuclides. Biologia 57, 651-663.

McGrail, B.P., 2017. Demonstrating a Magnetic Nanofluid Separation Process for Rare Earth Extraction from Geothermal Fluids. (Geothermal Technologies Program Peer Review of AOP 2.5.1.5). Pacific Northwest National Laboratory, Richland, WA.

McGrail, B.P., Liu, J., Thallapally, P.K., Nune, S.K., 2017. Magnetic Partitioning Nanofluid for Rare Earth Extraction from Geothermal Fluids (PNNL-26721). Pacific Northwest National Laboratory, Richland, WA.

Meng, F., McNeice, J., Zadeh, S.S., Ghahreman, A., 2019. Review of Lithium Production and Recovery from Minerals, Brines, and Lithium-Ion Batteries. Mineral Processing and Extractive Metallurgy Review DOI: 10.1080/08827508.2019.1668387.

Miyai, Y., Ooi, K., Katoh, S., 1988. Recovery of lithium from seawater using a new type of ion-sieve adsorbent based on $MgMn_2O_4$. Separation Science and Technology 23, 179-191.

Neupane, G., Wendt, D.S., 2017. Assessment of mineral resources in geothermal brines in the US. 42nd Workshop on Geothermal Reservoir Engineering, Stanford University, Stanford, CA, USA.

Nye, C.W., Quillinan, S.A., Neupane, G., McLing, T., 2017. Aqueous Rare Earth Element Patterns and Concentration in Thermal Brines Associated With Oil and Gas Production. 42nd Workshop on Geothermal Reservoir Engineering, Stanford University, Stanford, California.

Ooi, K., Miyai, Y., Katoh, S., 1986. Recovery of lithium from seawater by manganese oxide adsorbent. Separation Science and Technology 21, 755-766.

Pramanik, B.K., Nghiem, L.D., Hai, F.I., 2020. Extraction of strategically important elements from brines: Constraints and opportunities. Water Research 168.

Quillinan, S., Nye, C., Engle, M., Bartos, T., Neupane, G., Brant, J., Bagdonas, D., McLing, T., McLaughlin, J.F., 2018. Assessing rare earth element concentrations in geothermal and oil and gas produced waters: A potential domestic source of strategic mineral commodities (DE-EE0007603).

Renew, J., Hansen, T., 2017. Geothermal thermoelectric generation (G-TEG) with integrated temperature driven membrane distillation and novel manganese oxide for lithium extraction (DE-EE0006746). Southern Research Inst., Birmingham, AL (United States).

Shi, X.C., Zhou, D.F., Zhang, Z.B., Yu, L.L., Xu, H., Chen, B.Z., Yang, X.Y., 2011. Synthesis and properties of $Li_{1.6}Mn_{1.6}O_4$ and its adsorption application. Hydrometallurgy 110, 99-106.

Simmons, S., 2019. Final Report-Draft: Western USA Assessment of High Value Materials in Geothermal Fluids and Produced Fluids (DE-EE-0007604).

Smith, Y.R., Kumar, P., McLennan, J.D., 2017. On the extraction of rare earth elements from geothermal brines. Resources 6, 39.

Stull, D.P., 2016. Final Report: Environmentally Friendly Economical Sequestration of Rare Earth Metals from Geothermal Waters (DE-EE0006751).

The London Metal Exchange, 2020. LME Offical Prices. The London Metal Exchange, London.

Thomas, H., 2015. Quarterly assessment: Determination of Rare Earth Elements in Geothermal Waters and Evaluation of Potential Extraction Techniques (DE-EE0006750).

U.S. Department of Energy, 2017. Final Technical Report: Determination of Rare Earths in Geothermal Brines and Evaluation of Potential Extraction Techniques, Simbol Inc. (DBA Simbol Materials), Award Number: DE-EE0006750 Department of Energy, EERE, Geothermal Technologies Program, Washington, DC.

U.S. Department of Energy, 2020. Geothermal Data Repository. U.S. Department of Energy, Geothermal Technologies Office, Washington, DC.

U.S. Energy Information Administration, 2020. Levelized Cost and Levelized Avoided Cost of New Generation Resources in the Annual Energy Outlook 2020. U. S. Department of Energy, Washington, DC.

U.S. Geological Survey, 2018. Mineral commodities summary 2018. U.S. Geological Survey, Reston, Virginia, p. 200.

U.S. Geological Survey, 2020. Mineral commodities summary 2020. U.S. Geological Survey, Reston, Virginia, p. 204.

Van Gosen, B.S., Verplanck, P.L., Seal, R.R., II., Long, K.R., Gambogi, J., 2017. Rare-earth elements, Chap. O of Schulz, K.J., DeYoung, J.H., Jr., Seal, R.R., II, and Bradley, D.C., eds., Critical mineral resources of the United States—Economic and environmental geology and prospects for future supply: U.S. Geological Survey Professional Paper 1802, pp. O1-O31.

Ventura, S., Bhamidi, S., Hornbostel, M., Nagar, A., Perea, E., 2016. Selective Recovery of Metals from Geothermal Brines (DE-EE0006747). SRI International, Menlo Park, CA (United States).

Warner, C.L., Addleman, R.S., Cinson, A.D., Droubay, T.C., Engelhard, M.H., Nash, M.A., Yantasee, W., Warner, M.G., 2010. High-performance, superparamagnetic, nanoparticle-based heavy metal sorbents for removal of contaminants from natural waters. ChemSusChem 3, 749-757.

Wendt, D.S., Neupane, G., Davidson, C.L., Zheng, R., Bearden, M.A., 2018. GeoVision Analysis Supporting Task Force Report: Geothermal Hybrid Systems, INL/EXT-17-42891, PNNL-27386. Idaho National Laboratory, Idaho Falls, Idaho 83415.

White, D.E., 1968. Environments of generation of some base-metal ore deposits. Economic Geology 63, 301-335.

Zierenberg, R., Fowler, A., 2018. Maximizing REE Recovery in Geothermal Systems (DE-EE0006748).

Zion Market Research, 2019. Rare Earth Metals Market by Product (Cerium, Lanthanum, Neodymium, Praseodymium, and Others) and by Application (Catalyst, Magnets, Ceramics, Metallurgy, and Others): Global Industry Perspective, Comprehensive Analysis, and Forecast, 2018–2025. Zion Market Research, New York, NY.

Tables

Table 1. Summary description of GTO's Phase I mineral recovery projects. In 2014, GTO issued its first of two funding opportunity announcements (FOA) with DE-FOA-0001016 Low Temperature Geothermal Mineral Recovery Program. From this Phase I FOA, DOE made nine awards with $4 million in federal funds, with each project receiving between $200,000 and $500,000. These projects focused on Extraction Technologies, Process Economics, and Resource Assessment with emphasis on Lithium, Manganese, and Rare Earth Elements. The projects from this 2014 Phase I FOA are summarized in this table.

Project Under 2014 Funding *Project, Organization, Title*	Products & Technology
DE-EE-0006746: Southern Research – Geothermal Thermoelectric Generation (G-TEG) with Integrated Temperature Driven Membrane Distillation and Novel Manganese Oxide for Lithium Extraction Final report: (Renew and Hansen, 2017)	Target: Lithium Technology: Precipitation-nanofiltration-distillation-sorption Sorbent: Mn-oxide Brine: Synthetic TEA conclusion: Not economic Notes: Silica removal; Integrated; NF for divalent cations; Lithium as target; pH
DE-EE-0006747: SRI International – Selective Recovery of Metals from Geothermal Brines Final Report: (Ventura *et al.*, 2016)	Target: Lithium Technology: Organic polymers Sorbent: Li & Mn imprinted polymers Brine: Synthetic TEA: Economic Notes: Mn-imprinted polymers less subject to interference from Mg, Ca; CO_2 sorbent regeneration, TEA based on achieving future technology goals.
DE-EE-0006748: University of California, Davis - Maximizing REE Recovery in Geothermal Systems Final Report: (Zierenberg and Fowler, 2018)	Target: Rare earth elements Technology: Resource characterization & modeling Sorbent: Not applicable Brine: Compiled data from previous studies TEA: Not economic Notes: TEA not economic even at 100% recovery. Getting samples was a barrier to research.
DE-EE-0006749: Carnegie Mellon University – Chelating Resins for Selective Separation and Recovery of Rare Earth Elements from Low Temperature Geothermal Water Final Report: (Karamalidis, 2016)	Target: Rare earth elements Technology: Chelating sorbents Sorbent: Glycine, acetic acid, phosphate on silica Brine: Synthetic TEA: None Notes: Lanthanides; pH; good tests & data

Project Under 2014 Funding *Project, Organization, Title*	Products & Technology
DE-EE-0006750: Simbol – Determination of Rare Earths in Geothermal Brines and Evaluation of Potential Extraction Techniques Final Report: (U.S. Department of Energy, 2017)	Target: Rare earth elements Technology: Resource characterization & methods development Sorbent: Not applicable Brine: Not described TEA: None Notes: Project was not completed.
DE-EE-0006751: Tussar – Environmentally Friendly Economical Sequestration of Rare Earth Metals from Geothermal Waters Final Report: (Stull, 2016)	Target: Rare earth elements Technology: Impregnated GAC Sorbent: Tussar Media Brine: Synthetic TEA: None Notes: Media failed temperature-regeneration tests.
AOP 2.5.1.4: LBNL – Engineering Thermophilic Microorganisms to Selectively Extract Strategic Minerals from Low Temperature Geothermal Brines Final Report: (Ajo-Franklin *et al*., 2017)	Target: Rare earth elements Technology: Bacterial sorption Sorbent: S-Layers Brine: Synthetic TEA: None Notes: Biosorbent development
AOP 2.5.1.5: PNNL – Magnetic Partitioning Nanofluid for Rare Earth Extraction from Geothermal Fluids Final Report: (McGrail *et al*., 2017)	Target: Rare earth elements Technology: Magnetic separation Sorbent: Silica (derivatized) & metal organic framework (MOF) Brine: Synthetic TEA: Economic. Notes: Positive TEA dependent on achieving very optimistic technology advances.
AOP 2.5.1.6: PNNL – Evaluation of Advanced Sorbent Structures for Recovery of Rare Earths, Precious Metals and other Critical Materials from Geothermal Waters Final Report: (Addleman *et al*., 2016)	Target: Rare earth elements Technology: Sorbent development based on phosphonic acid and Mn-oxide surface chemistry Sorbent: Organic; Inorganic (MnO_2); Nafion polymer; derivatized silica Brine: Synthetic TEA: None Notes: Tested Ag, Cu, Zn, Eu; reported linear K_d & percent removal; Good technical evaluation on sorption.

Table 2. Summary description of GTO's Phase II mineral recovery projects. In 2016, GTO launched the phase II effort with the release of DE-FOA-0001376 Mineral Recovery Phase II: Geothermal Concepts and Approaches to Validate Extraction Technologies. This FOA made $3.8M of federal funds available to 4 awardees. Two awards were made on U.S. Regional or Nationwide Assessment Projects - Collaborations with USGS, while the other two awards focused their efforts on R&D for extraction technologies.

Project Under 2016 Funding *Contract: (Documents), Organization, Title*	Products & Technology[1]
DE-EE-0007603: University of Wyoming - Assessing rare earth element concentrations in geothermal and oil and gas produced waters: A potential domestic source of strategic mineral commodities Final Report: (Quillinan *et al.*, 2018)	Target: Rare earth elements Technology: Resource assessment, technology review (sorption, solvent, membrane) Sorbent: Various (reviewed) Brine: Geothermal & PW; Wyoming, Idaho, Montana, N. & S. Dakota, Ohio, Pennsylvania, Texas TEA: None Notes: Data by location, not compiled. Produced water focus. Chapter 7 is technology review. Concludes nanofiltration is best method for REE. Similar to DE-EE-0007604.
DE-EE-0007604: University of Utah - Western USA Assessment of High Value Materials in Geothermal Fluids and Produced Fluids Final Report: (Simmons, 2019)	Target: Rare earth elements Technology: Resource assessment Sorbent: Not applicable Brine: Geothermal & PW; Idaho, Nevada, New Mexico, Oregon, Utah TEA: Compared GT brines to other sources of REE and lithium (not formal TEA) Notes: Similar to DE-EE-0007603.
AOP 2.5.1.12: LLNL – Extraction of Rare Earth Metals from Geothermal Fluids using Bioengineered Microbes Final Report: (Jiao, 2020)	Target: Rare earth elements Technology: Biosorption Sorbent: S-Layer (lanthanide binding tags) Brine: Synthetic; mining leachate, geothermal TEA: Economic, but not assessed for geothermal Notes: Good technical evaluation on sorption, several publications available from study.
AOP 2.5.1.14: PNNL – Demonstrating a Magnetic Nanofluid Separation Process for Rare Earth Extraction from Geothermal Fluids Final Report: Not available	Target: Rare earth elements Technology: Metal organic framework (MOF) attached to magnetic nanoparticle Sorbent: MOF Brine: Not known TEA: Not available Notes: Information from Elsaidi *et al.* (2018)

Project Under 2016 Funding *Contract: (Documents), Organization, Title*	Products & Technology[1]
DE-SC0013698: Anactisis – Ion Imprinted Polymers for the Extraction and Recovery of Rare Earth Elements from Geothermal Fluids [FINAL REPORT EMBARGOED – OSTI # 1255948] Final Report: Not available	Target: Rare earth elements Technology: Ionic Imprinted Polymer (IIP) Sorbent: DTPA-bianhydride and other. Brine: Laboratory TEA: None Notes: No information on this project was found in GDR Data (gdr.openei.org). US Patent Publication US 2017/0101698 A1 used as source. Anactisis was formerly Karamalidis Extraction Technologies.

[1]Determined from available public information, not confirmed.

Table 3. List of rare-earth elements (REE) from Van Gosen *et al.* (2017). Promethium (Pm, atomic number = 61) is not included in this list because it is extremely rare in nature. Yttrium is included as an REE in this classification (Van Gosen *et al.*, 2017)

Element	Symbol	Atomic number	Atomic weight	Crustal abundance (part per million)
Light REE				
Lanthanum	La	57	138.91	39
Cerium	Ce	58	140.12	66.5
Praseodymium	Pr	59	140.91	9.2
Neodymium	Nd	60	144.24	41.5
Samarium	Sm	62	150.36	7.05
Europium	Eu	63	151.96	2.0
Gadolinium	Gd	64	157.25	6.2
Heavy REE				
Yttrium	Y	39	88.91	33
Terbium	Tb	65	158.92	1.2
Dysprosium	Dy	66	162.50	5.2
Holmium	Ho	67	164.93	1.3
Erbium	Er	68	167.26	3.5
Thulium	Tm	69	168.93	0.52
Ytterbium	Yb	70	173.04	3.2
Lutetium	Lu	71	174.97	0.8

Table 4. Geothermal areas sampled as part of an assessment of high value materials in geothermal fluids (Simmons, 2019).

Geothermal Areas	State	Plant Power Output (MWe)	Produced Fluid Flow (gpm)
Raft River	Idaho	10	4700
Beowawe	Nevada	18	5000
Blue Mountain	Nevada	49.5	15,000 max
Dixie Valley	Nevada	70	13,000
Patua	Nevada	30	9100
San Emidio	Nevada	11.8	4500
Soda Lake	Nevada	23	5400
Lightning Dock	New Mexico	4	1500-1600
Tularosa[1]	New Mexico	no power plant	NR[2]
Neal Hot Springs	Oregon	22	12,000
Roosevelt Hot Springs	Utah	38	3900
Thermo	Utah	10	10,000
Sevier Thermal Belt	Utah	hot springs	NR
Newcastle	Utah	direct use	NR

[1]DOE Play Fairway
[2]NR = Not reported

Table 5. Synthetic brines used by Stull (2016) to test Tusaar sorbent material. Brine 1 was the estimated chemical formula for geothermal brines. Brines 1M, 1C, and 1CF were used in experiments. Brine 1C formed a precipitate over time and was not used in successful experiments.

Elements	Original Brine 1 Calc values ppm*	Brine 1M Experimental ppm*	Brine 1C Experimental ppm*	Brine 1CF Experimental ppm*
Na	45700	43300	45700	51100
K	17400	17400	20300	17800
Ca	14300	14300	14500	14600
Mn	720	0	760	710
Ba	180	0	190	180
Sr	410	0	400	410
Zn	280	0	320	290
Li	160	0	140	150
Mg	160	0	160	150
Fe	470	0	660	0
B	180	0	180	0
Pb	50	0	0	0
Si	270	0	0	0
La	2	2	2	2
Ce	2	2	2	2
Pr	2	2	2	2
Nd	2	2	2	2
Eu	2	2	2	2
Tb	2	2	2	2
Dy	2	2	2	2
* Formula prepared to original specification as described;				
values reported as experimentally determined.				

Figures
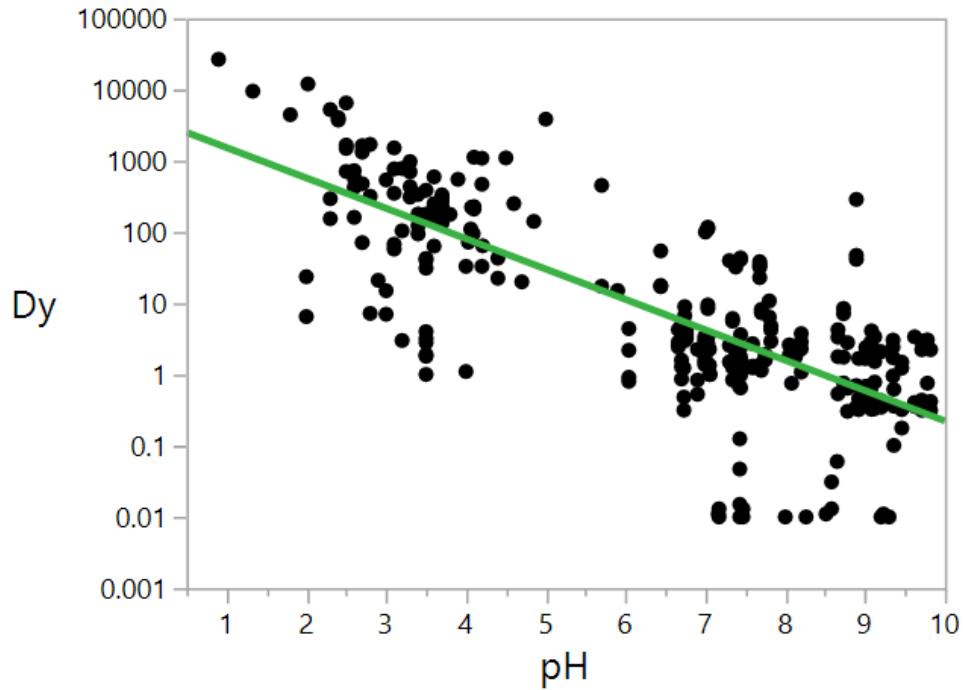
$$Log(Dy) = 8.32 - 0.982*pH$$

Figure 1. Analysis of the relationship between dysprosium (Dy) concentration and pH using data available on the Geothermal Data Repository. Compiled data from Zierenberg and Fowler (2018) is shown here. Further analysis of the relationship between pH and REE concentrations using the data from REE data from Zierenberg and Fowler (2018) can be found in Appendix A. Similar analysis for data from Quillinan *et al*. (2018) can be found in Appendix B.
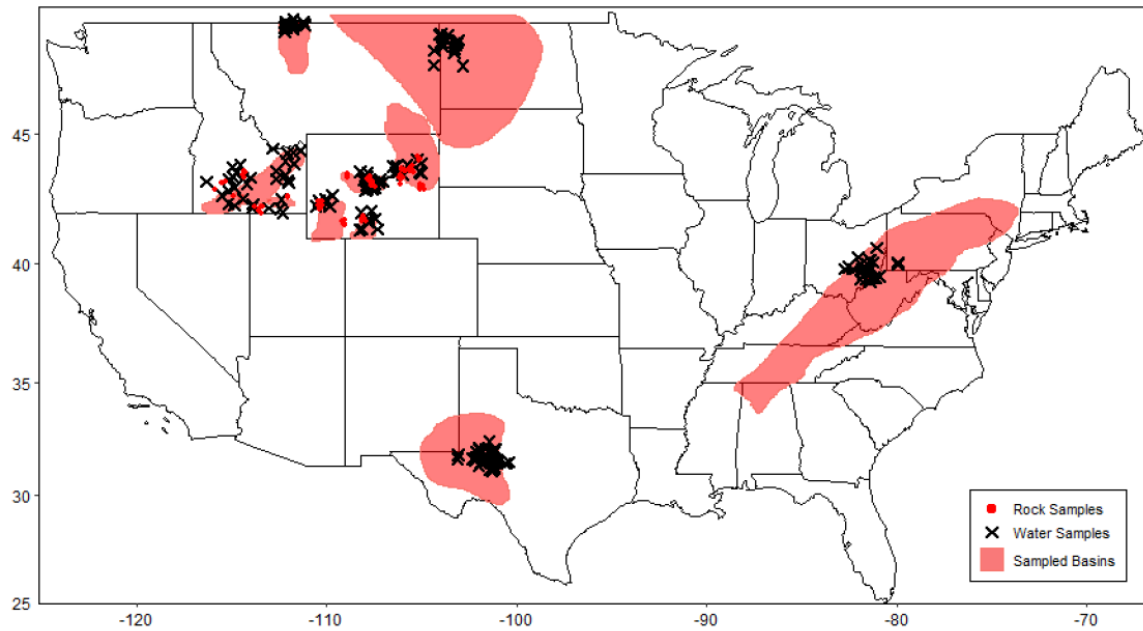
Figure 2. Basins in the United States that were analyzed for REE by Quillinan *et al*. (2018). The red points in Wyoming and Idaho are rock samples collected and analyzed for REE and geochemistry. Black Xs indicate the locations of water samples analyzed for REE. From Quillinan *et al*. (2018).
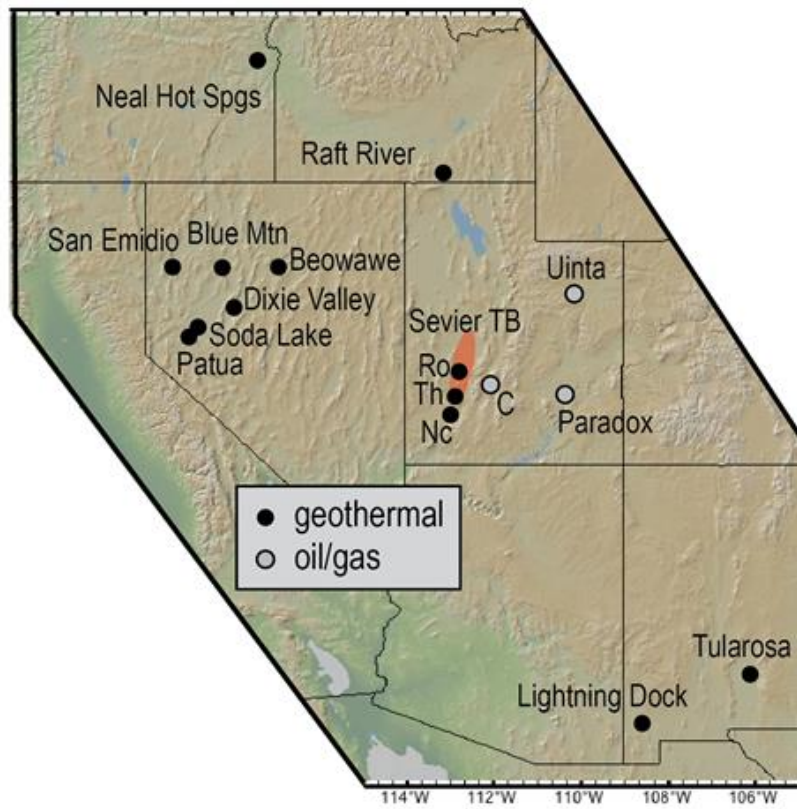
Figure 3. Production fluid sampling sites for the study by Simmons (2019). Abbreviations: C=Covenant; Nc=Newcastle; Ro=Roosevelt Hot Springs; Sevier TB=Sevier thermal belt (orange); Th=Thermo. From Simmons (2019).
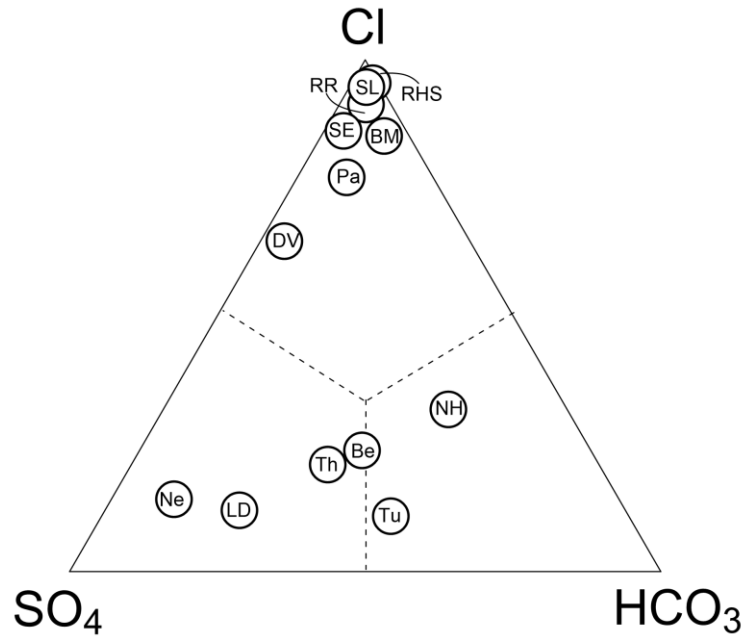
Figure 4. Relative concentrations of major dissolved anions in produced geothermal waters. Abbreviations: Be=Beowawe; BM=Blue Mountain; DV=Dixie Valley; LD=Lightning Dock; Ne=Newcastle; NH=Neal Hot Springs; Pa=Patua; RHS=Roosevelt Hot Springs; RR=Raft River; SE=San Emidio; SL=Soda Lake; Th=Thermo; Tu=Tularosa. From Simmons (2019).
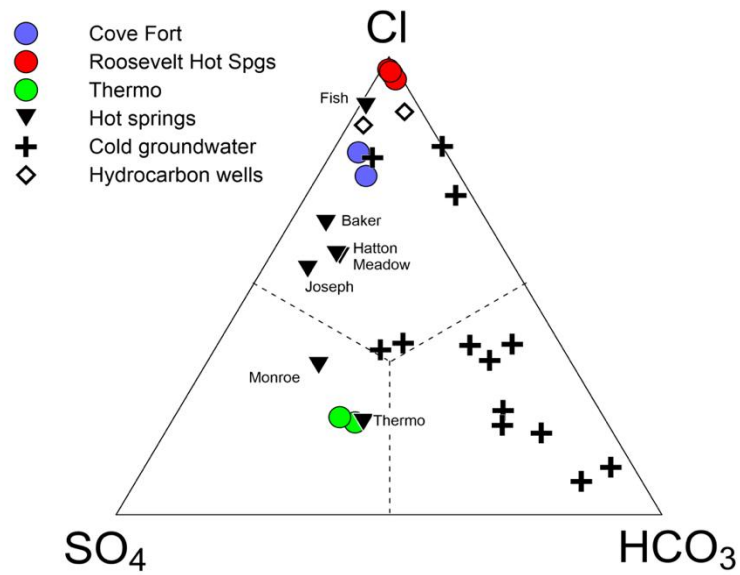
Figure 5. Relative concentrations of chloride, bicarbonate, and sulfate in water samples obtained from geothermal and oil & gas production wells, hot springs, cold springs and ground water wells. From Simmons (2019).
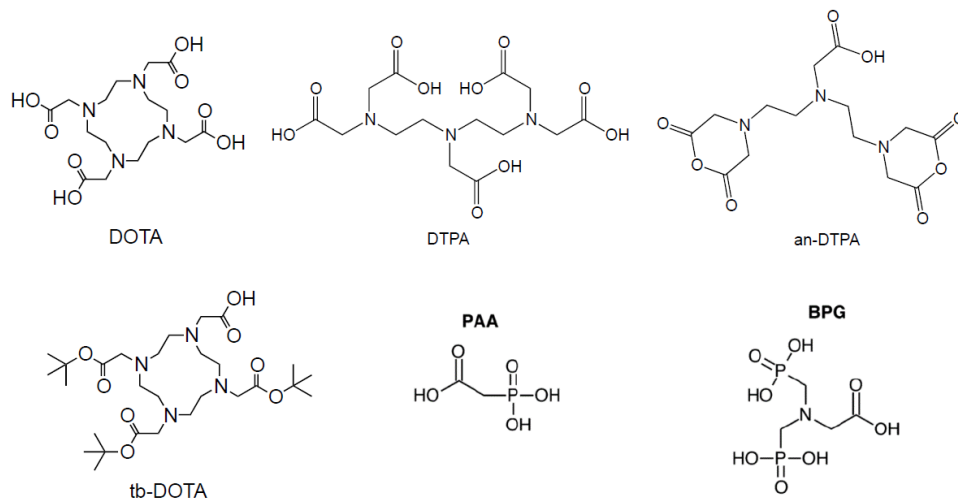
Figure 6. Structures of ligands attached to silica supports as part of Project DE-EE-0006749 From Karamalidis (2016).
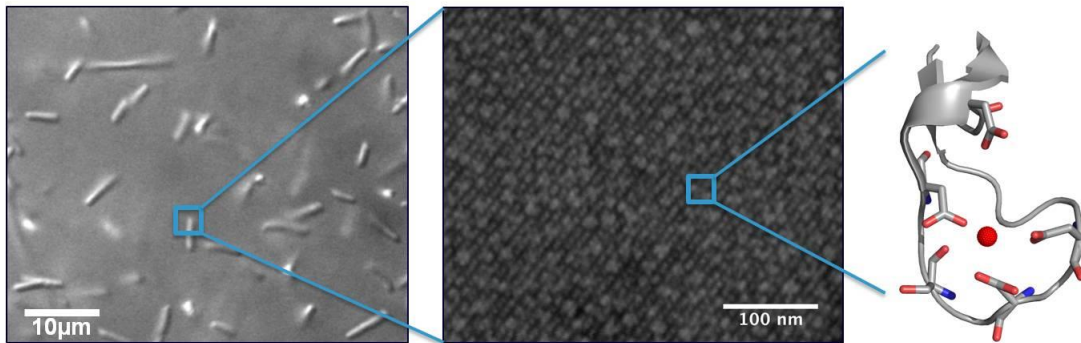
Figure 7. Conceptual approach to the genetic engineering of biosorbents. The thermophilic, salt-tolerant microorganism G. stearothermophilus (left) presents S-layer proteins at high density on its surface (middle), which in turn display selective metal-binding domains (right) to the extracellular solution. From Ajo-Franklin *et al.* (2017)
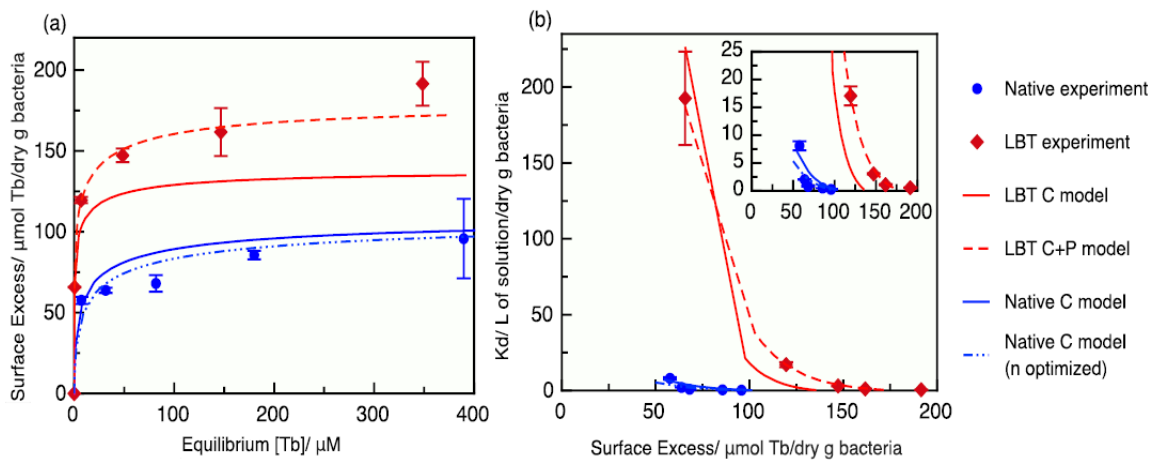
Figure 8. Sorption isotherm and distribution coefficient modeling fit at a pH of 6. Native C model refers to a 1-site carboxyl model describing the sorption of the native strain. LBT C+P model refers to a 3-site carboxyl, phosphoryl, and LBT model describing the sorption of the LBT strain. All models were fit to Kd experimental data except the Native C model (n optimized), which was fit based off surface excess, n, experimental data. From Jiao (2020) and Chang *et al.* (2020).
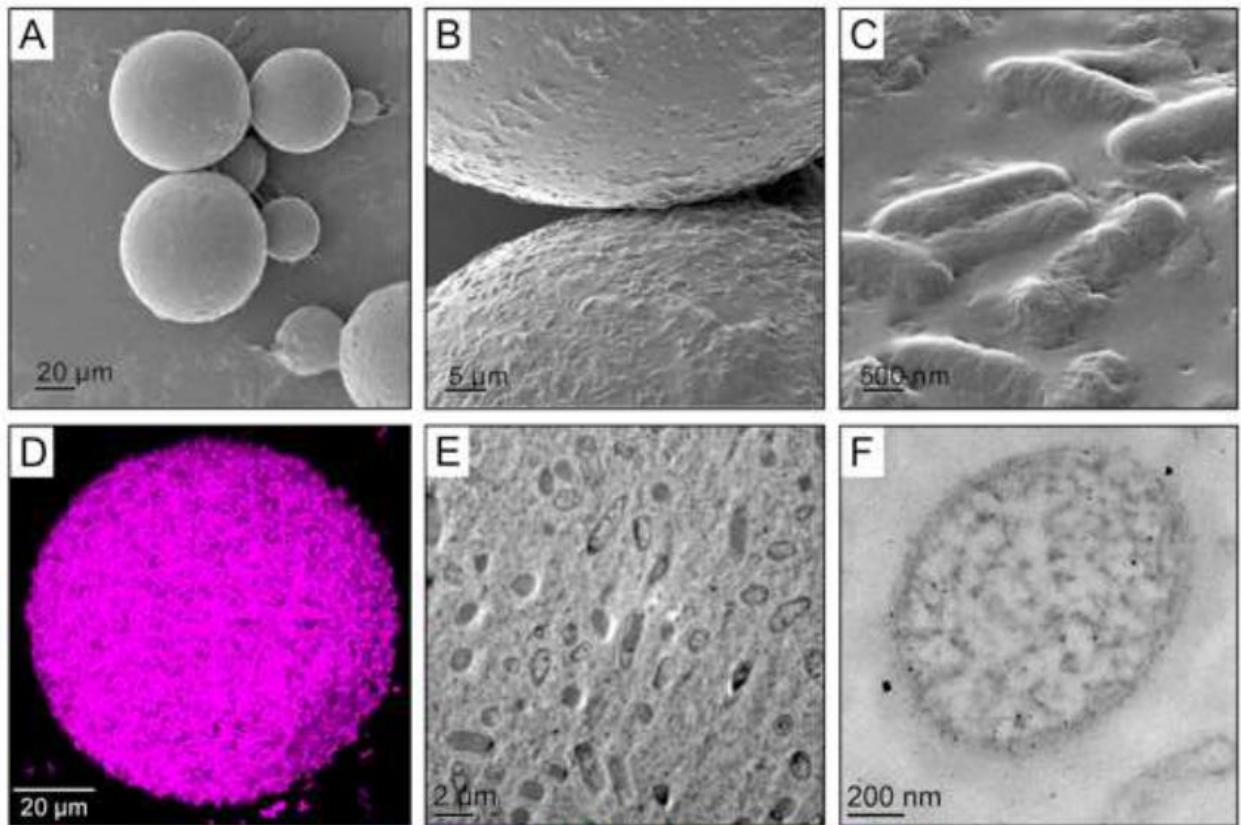
Figure 9. Microbe bead imaging. (A-C) Helium ion microscopy images of microbe beads at different magnification. At high magnification, encapsulated microbes are visible on the microbe bead surface. (D) Confocal microscope image showing a 3-D reconstruction of a representative microbe bead from Z stack images. The image depicts the homogeneous distribution of cells across the 3D surface of the microbe beads. (E) TEM image of a microbe bead cross-section showing individual cells imbedded in the PEDGA polymer. (F) TEM image of a representative cell from a neodymium-adsorbed microbe bead showing cell associated needle-like biogenic minerals. From Jiao (2020).
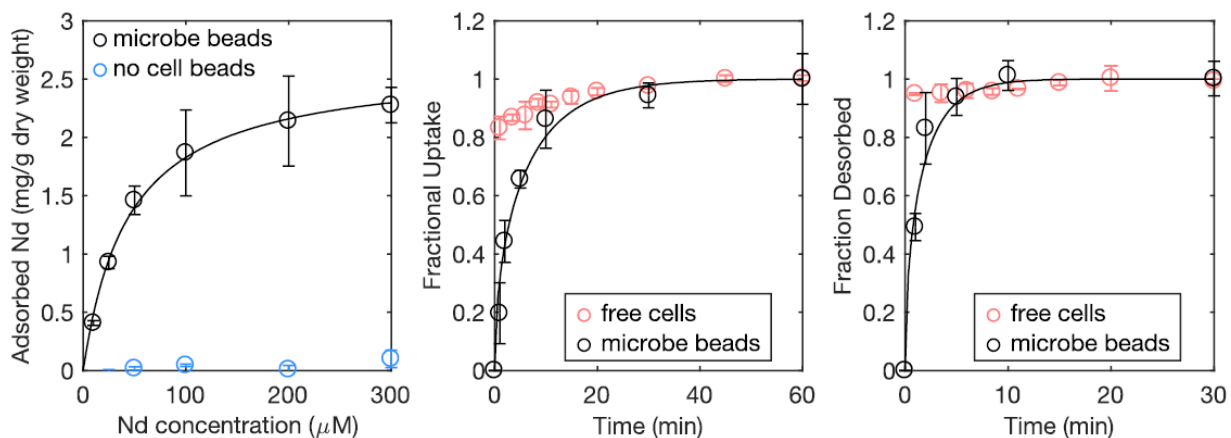
Figure 10. Neodymium adsorption isotherm and kinetics by microbe beads and comparison to free cells. (A) neodymium adsorption isotherm with microbe beads (black circles) and beads without cells (blue circles). Experimental data were fit to a Langmuir isotherm (solid line) using nonlinear regression (see Methods). (B) neodymium adsorption kinetics of microbe beads (black circles), in comparison to free-floating cells (red circles). MES solution (pH 6) containing 500 μM neodymium was used. (C) neodymium desorption kinetics using citrate solution (10 mM citrate, pH 6) with microbe beads (black circles), in comparison to free-floating cells (red circles). The kinetics data were fit with the Vermeulen model and yielded correlation coefficient r^2 values of 0.98 for both adsorption and desorption. From Jiao (2020).
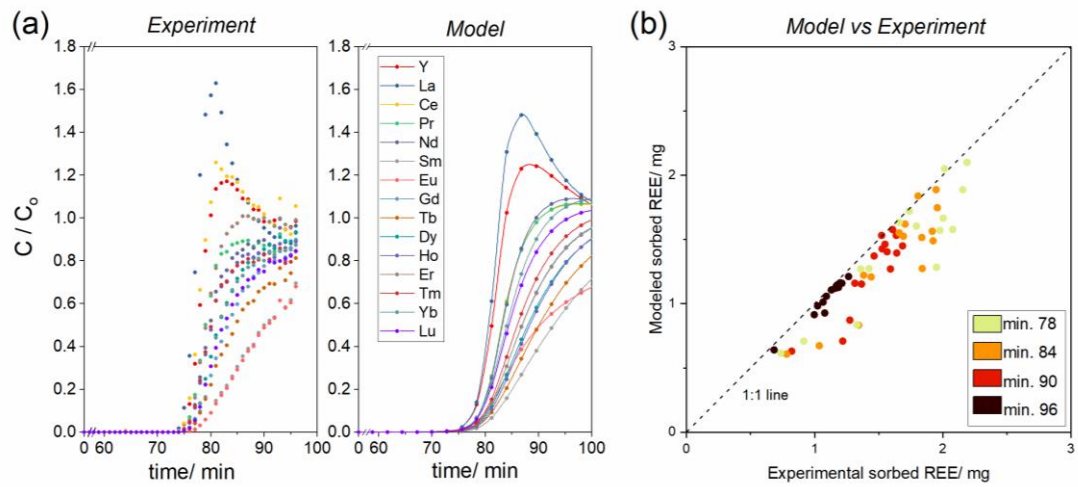
Figure 11. (a) Experimental and modeling results of breakthrough curves using a 100 x 1 cm column packed with 23 dry g/L dLBTx8 *E. coli* under 1 mL/min flow rate and a 500 µM equimolar inlet solution of rare earths, and (b) modeled vs experimental results of adsorbed REEs for the same column at the 78th, 84th, 90th and 96th min. From Jiao (2020).
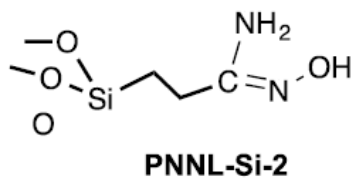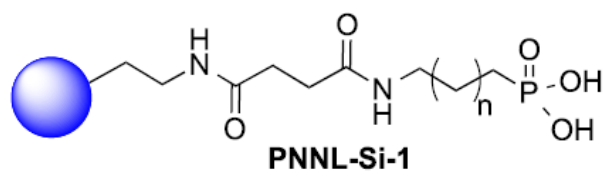
Figure 12. Functional groups used with silica sorbents for extraction of neodymium, europium, ytterbium and dysprosium. From McGrail *et al*. (2017).
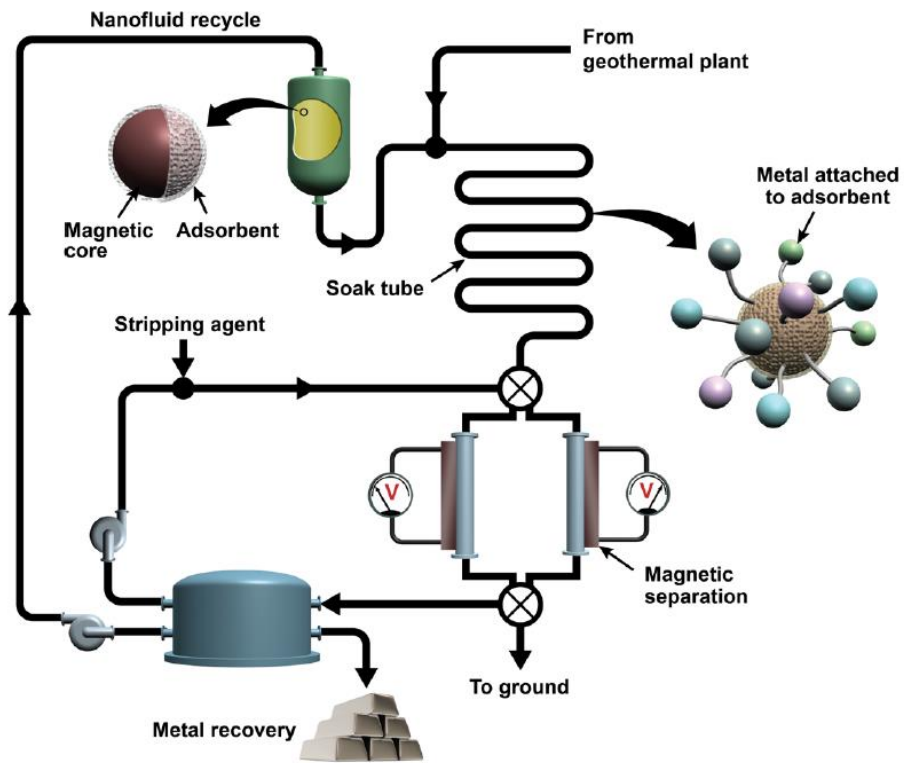
Figure 13: Conceptual plan of a magnetic partitioning nanofluid extraction system. From McGrail *et al.* (2017).
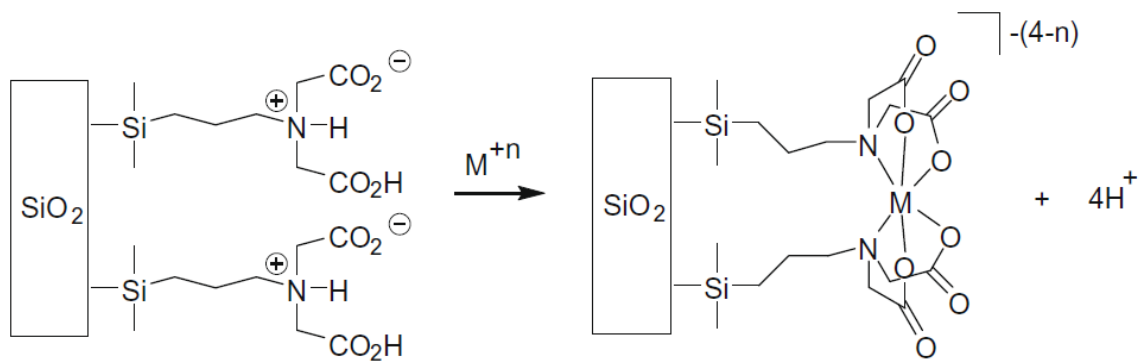
Figure 14. Iminodiacetic acid (IDAA) forms strong complexes with a wide variety of metal ions. From Busche *et al.* (2009).
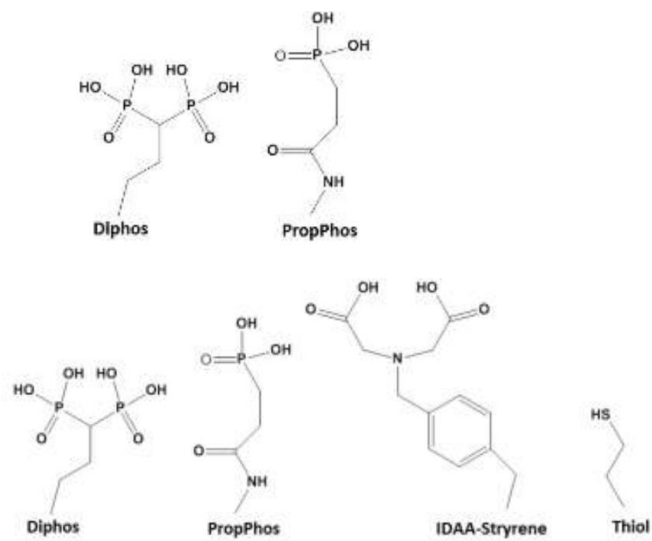
Figure 15. Chemical structures of organic ligands used for the collection of REE and other valuable minerals from geothermal waters. From Addleman *et al.* (2015).
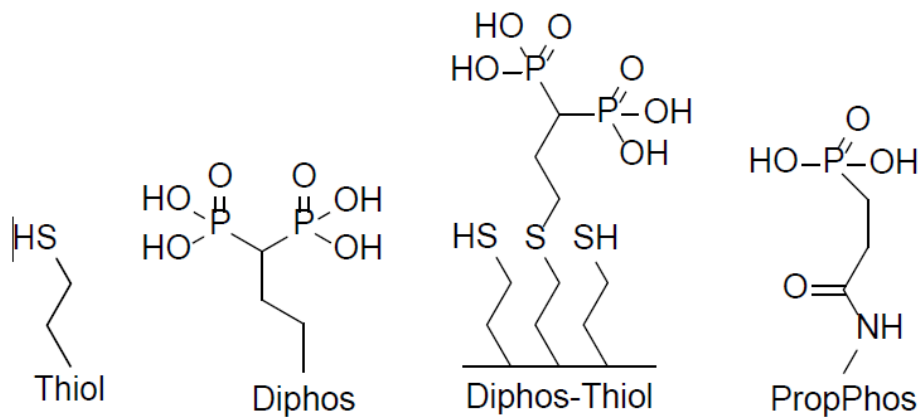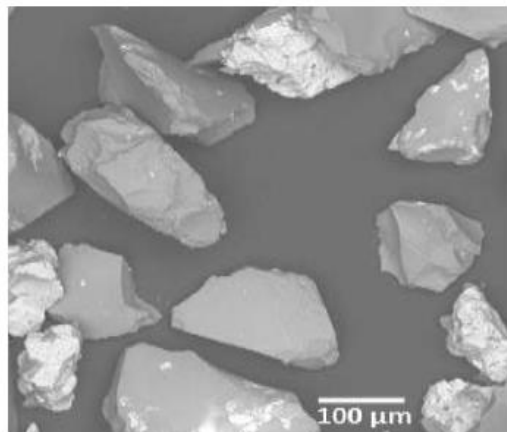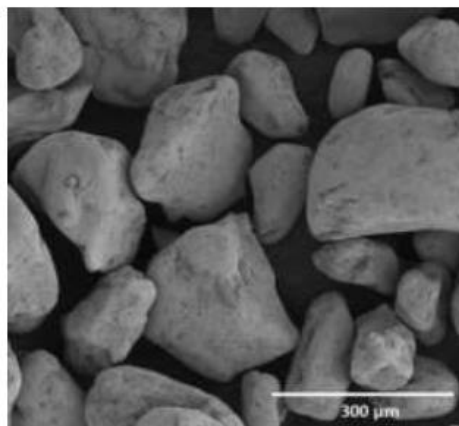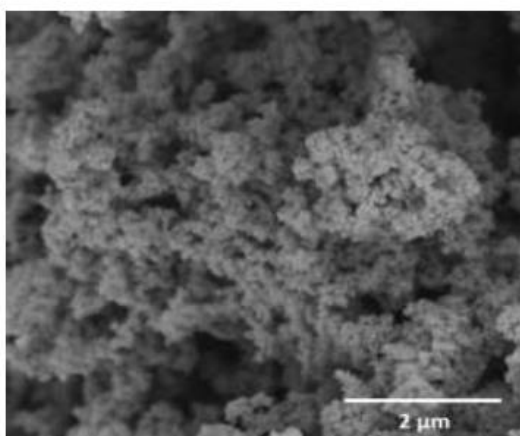
Figure 16: Chemical structures of organic ligands used for the collection of REE and other valuable minerals from geothermal waters (continued). From Addleman *et al.* (2016).
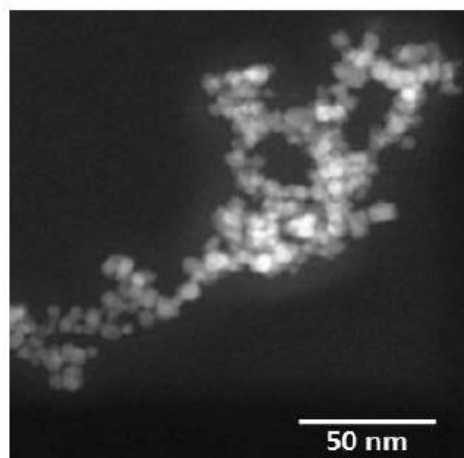
Figure 17: Electron micrograph images of selected metal oxide sorbents. SEM of Fe/MnO$_2$-SiO$_2$(A), SEM of MnO$_2$-SiO$_2$ composite (B), SEM of Mn-doped Fe$_3$O$_4$ cluster (C), and TEM of Mn-doped Fe$_3$O$_4$ nanoparticles (D). From Addleman *et al.* (2015).

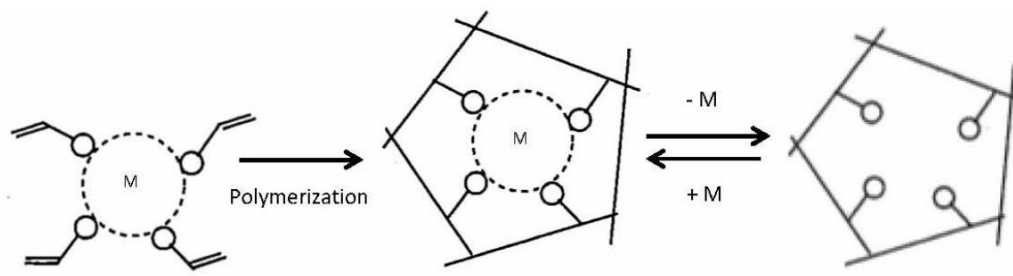Figure 18. Schematic diagram of metal ions polymer imprinting. These polymers have high selectivity because of the affinity of the ligand for the imprinted metal ion and the unique size and shape of the generated cavities. From Ventura *et al*. (2016).
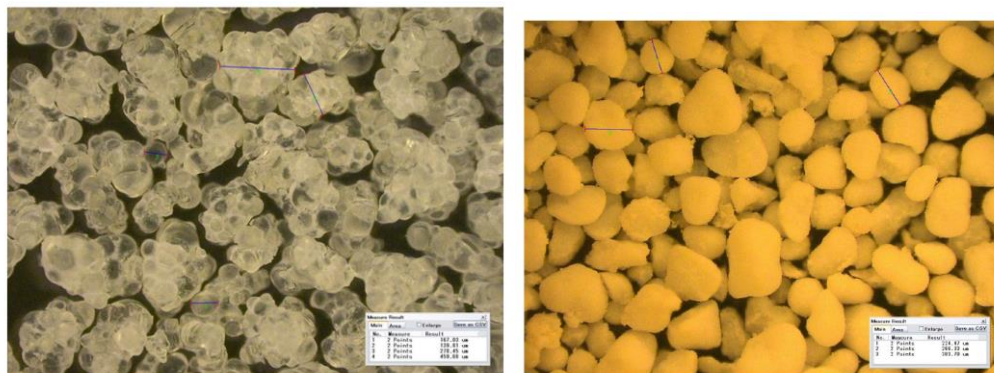
Figure 19. Optical microscope photograph of Li-imprinted polymer beads (left) and Mn-imprinted polymer beads (right). From Ventura *et al*. (2016).

Appendix A

Preliminary Analysis of Data from Zierenberg and Fowler, 2018. Maximizing REE Recovery in Geothermal Systems (DE-EE-0006748).

William Stringfellow & Patrick Dobson, Lawrence Berkeley National Laboratory

May 14, 2020

Fit Group

Bivariate Fit of Ce By pH
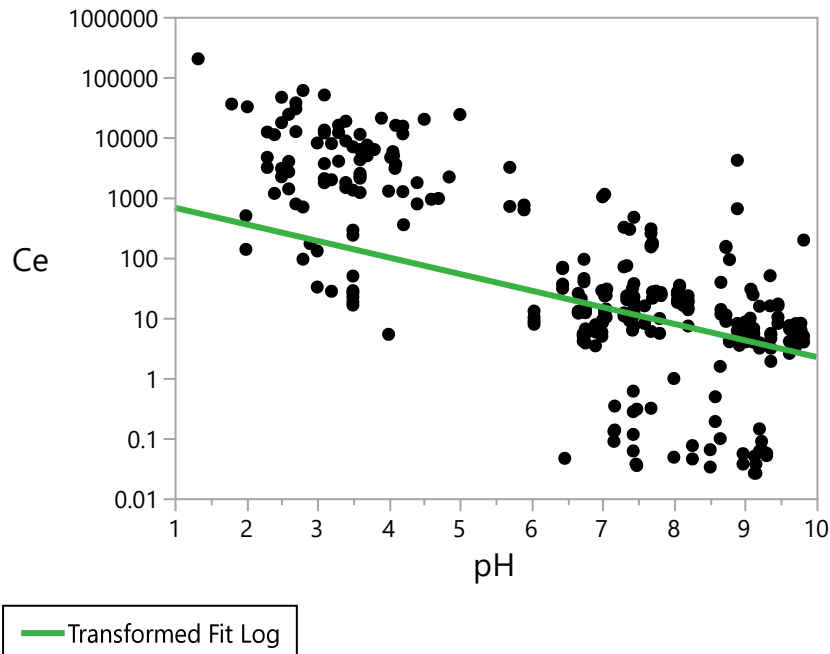
Transformed Fit Log
Log(Ce) = 7.1459419 - 0.6344046*pH

Summary of Fit

RSquare	0.179348
RSquare Adj	0.175999
Root Mean Square Error	2.308062
Mean of Response	2.310469
Observations (or Sum Wgts)	247

Analysis of Variance

Source	DF	Sum of Squares	Mean Square	F Ratio
Model	1	285.2323	285.232	53.5431
Error	245	1305.1513	5.327	
C. Total	246	1590.3836		<.0001*

Parameter Estimates

Term	Estimate	Std Error	t Ratio	Prob>|t|
Intercept	7.1459419	0.676948	10.56	<.0001*
pH	-0.634405	0.086699	-7.32	<.0001*

Fit Measured on Original Scale

Sum of Squared Error	4.29e+10
Root Mean Square Error	13232.566
RSquare	-0.002166
Sum of Residuals	290866.44

Bivariate Fit of Dy By pH
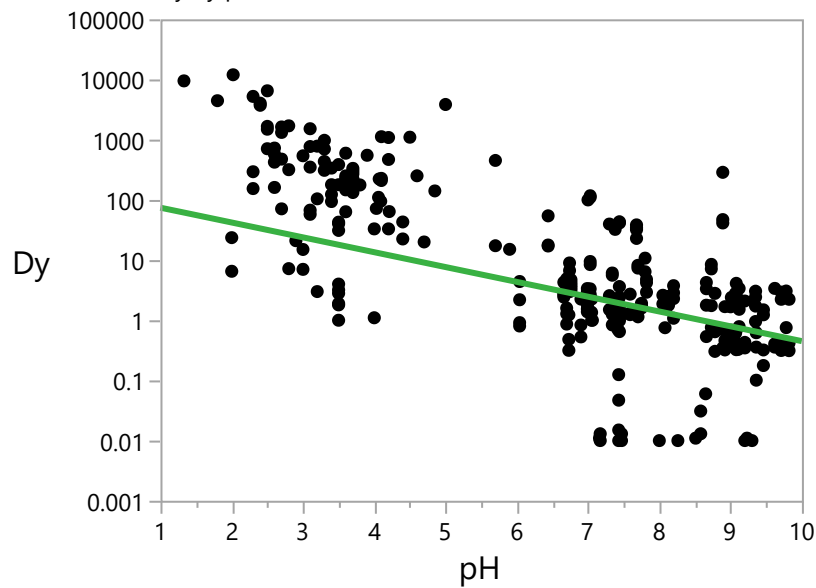
Transformed Fit Log
$Log(Dy) = 4.8728446 - 0.5673363*pH$

Summary of Fit

RSquare	0.200217
RSquare Adj	0.196548
Root Mean Square Error	1.980246

Mean of Response 0.615811
Observations (or Sum Wgts) 220

Analysis of Variance

Source	DF	Sum of Squares	Mean Square	F Ratio
Model	1	214.0046	214.005	54.5739
Error	218	854.8593	3.921	
C. Total	219	1068.8639		<.0001*

Parameter Estimates

Term	Estimate	Std Error	t Ratio	Prob>|t|
Intercept	4.8728446	0.591518	8.24	<.0001*
pH	-0.567336	0.076798	-7.39	<.0001*

Fit Measured on Original Scale
Sum of Squared Error 274083752
Root Mean Square Error 1121.2783
RSquare -0.005458
Sum of Residuals 29048.608

Bivariate Fit of Er By pH
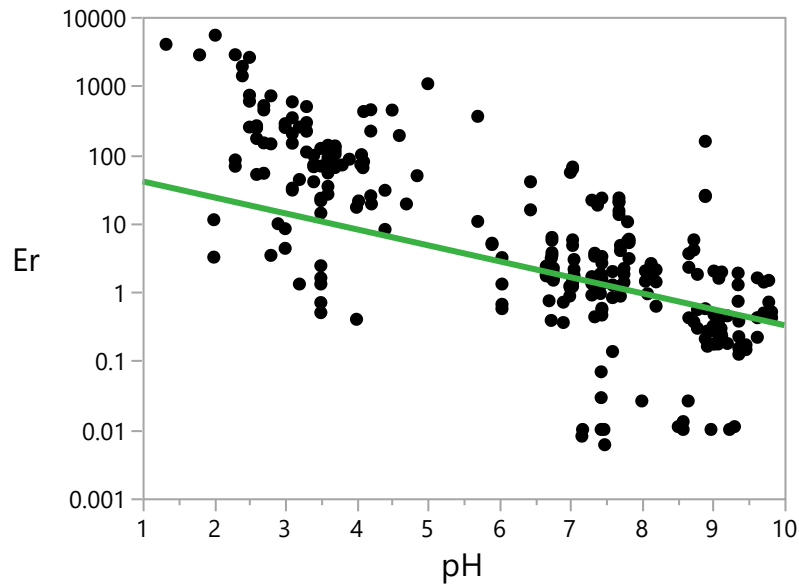
Transformed Fit Log

Transformed Fit Log

Log(Er) = 4.2362943 - 0.5349515*pH

Summary of Fit

RSquare	0.187343
RSquare Adj	0.183154
Root Mean Square Error	1.998522
Mean of Response	0.264088
Observations (or Sum Wgts)	196

Analysis of Variance

Source	DF	Sum of Squares	Mean Square	F Ratio
Model	1	178.62832	178.628	44.7232
Error	194	774.85320	3.994	
C. Total	195	953.48152		<.0001*

Parameter Estimates

Term	Estimate	Std Error	t Ratio	Prob>|t|
Intercept	4.2362943	0.610885	6.93	<.0001*
pH	-0.534952	0.079992	-6.69	<.0001*

Fit Measured on Original Scale

Sum of Squared Error	51037708
Root Mean Square Error	512.91419
RSquare	-0.004962
Sum of Residuals	12552.275

Bivariate Fit of Eu By pH
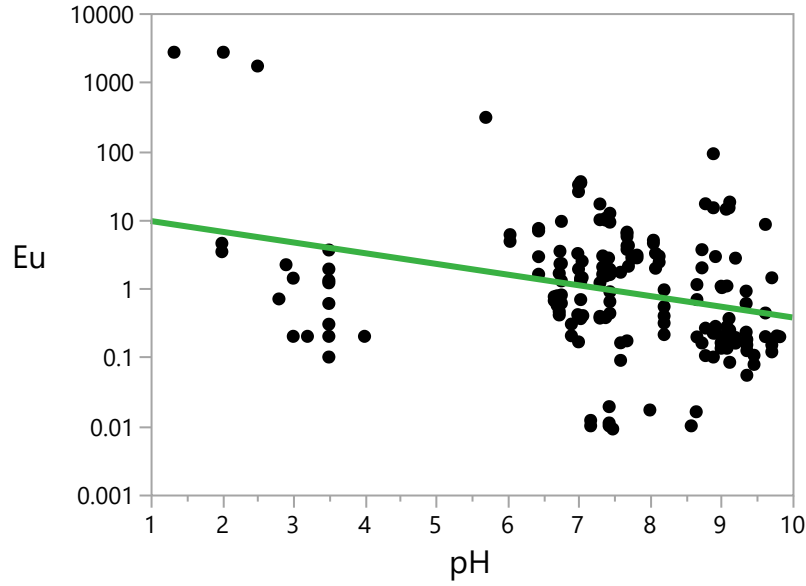
Transformed Fit Log
Log(Eu) = 2.6107775 - 0.358663*pH

Summary of Fit

RSquare	0.095274
RSquare Adj	0.090162
Root Mean Square Error	2.048318
Mean of Response	-0.04605
Observations (or Sum Wgts)	179

Analysis of Variance

Source	DF	Sum of Squares	Mean Square	F Ratio
Model	1	78.20304	78.2030	18.6393
Error	177	742.62203	4.1956	
C. Total	178	820.82507		<.0001*

Parameter Estimates

Term	Estimate	Std Error	t Ratio	Prob>|t|
Intercept	2.6107775	0.634147	4.12	<.0001*
pH	-0.358663	0.083075	-4.32	<.0001*

Fit Measured on Original Scale

Sum of Squared Error	17476742
Root Mean Square Error	314.22707
RSquare	-0.01498
Sum of Residuals	7796.5124

Bivariate Fit of Gd By pH
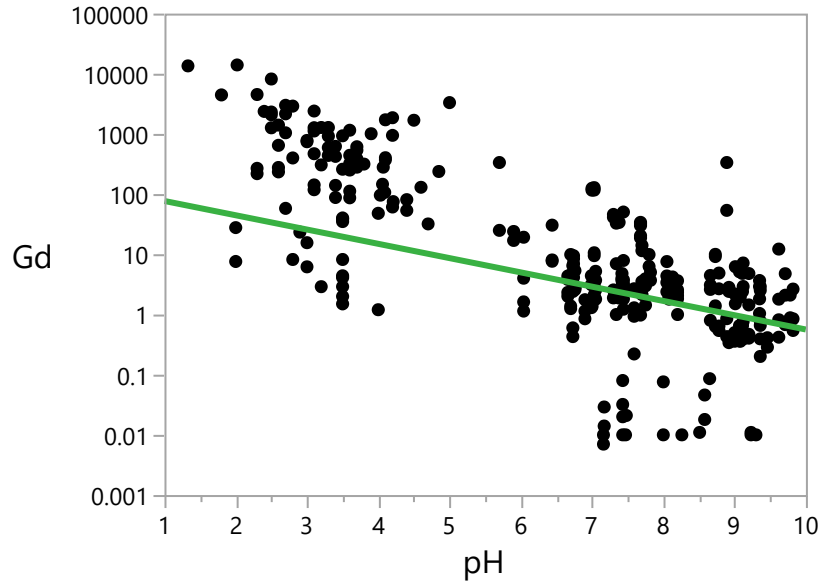
Transformed Fit Log

Transformed Fit Log
Log(Gd) = 4.8899213 - 0.5464537*pH

Summary of Fit
RSquare	0.171198
RSquare Adj	0.167671
Root Mean Square Error	2.057362
Mean of Response	0.74824
Observations (or Sum Wgts)	237

Analysis of Variance

Source	DF	Sum of Squares	Mean Square	F Ratio
Model	1	205.4643	205.464	48.5417
Error	235	994.6937	4.233	
C. Total	236	1200.1581		<.0001*

Parameter Estimates

Term	Estimate	Std Error	t Ratio	Prob>|t|
Intercept	4.8899213	0.609292	8.03	<.0001*
pH	-0.546454	0.078432	-6.97	<.0001*

Fit Measured on Original Scale

Sum of Squared Error	441678733
Root Mean Square Error	1370.9427
RSquare	-0.005747
Sum of Residuals	36885.386

Bivariate Fit of Ho By pH
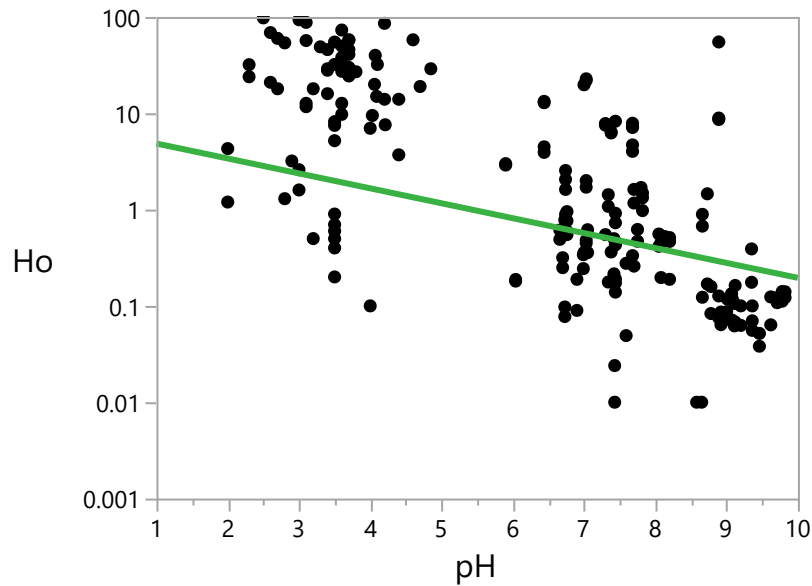
Transformed Fit Log

Log(Ho) = 1.9351141 - 0.3566302*pH

Summary of Fit

RSquare	0.136909
RSquare Adj	0.130957
Root Mean Square Error	1.634263
Mean of Response	-0.69017
Observations (or Sum Wgts)	147

Analysis of Variance

Source	DF	Sum of Squares	Mean Square	F Ratio

Model	1	61.43105	61.4310	23.0009
Error	145	387.26822	2.6708	
C. Total	146	448.69927		<.0001*

Parameter Estimates

Term	Estimate	Std Error	t Ratio	Prob>|t|
Intercept	1.9351141	0.563751	3.43	0.0008*
pH	-0.35663	0.074361	-4.80	<.0001*

Fit Measured on Original Scale

Sum of Squared Error	5772.4206
Root Mean Square Error	6.3095005
RSquare	-0.093073
Sum of Residuals	258.57953

Bivariate Fit of La By pH
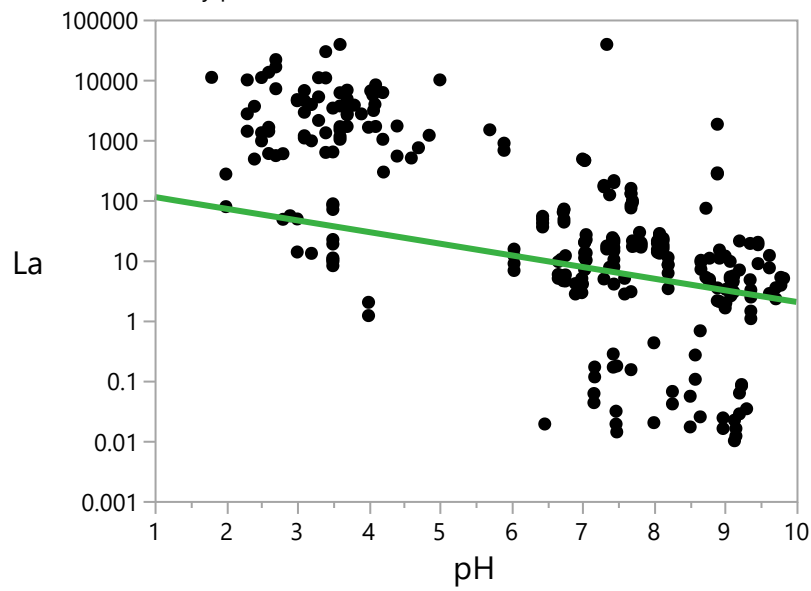
Transformed Fit Log

$Log(La) = 5.1683994 - 0.4461299 \cdot pH$

Summary of Fit

RSquare	0.081085
RSquare Adj	0.076624
Root Mean Square Error	2.474381
Mean of Response	1.780322
Observations (or Sum Wgts)	208

Analysis of Variance

Source	DF	Sum of Squares	Mean Square	F Ratio
Model	1	111.2919	111.292	18.1773
Error	206	1261.2480	6.123	
C. Total	207	1372.5400		<.0001*

Parameter Estimates

Term	Estimate	Std Error	t Ratio	Prob>|t|
Intercept	5.1683994	0.812982	6.36	<.0001*
pH	-0.44613	0.10464	-4.26	<.0001*

Fit Measured on Original Scale

Sum of Squared Error	1.4864e+9
Root Mean Square Error	2686.1352
RSquare	-0.006834
Sum of Residuals	45465.608

Bivariate Fit of Lu By pH

Transformed Fit Log
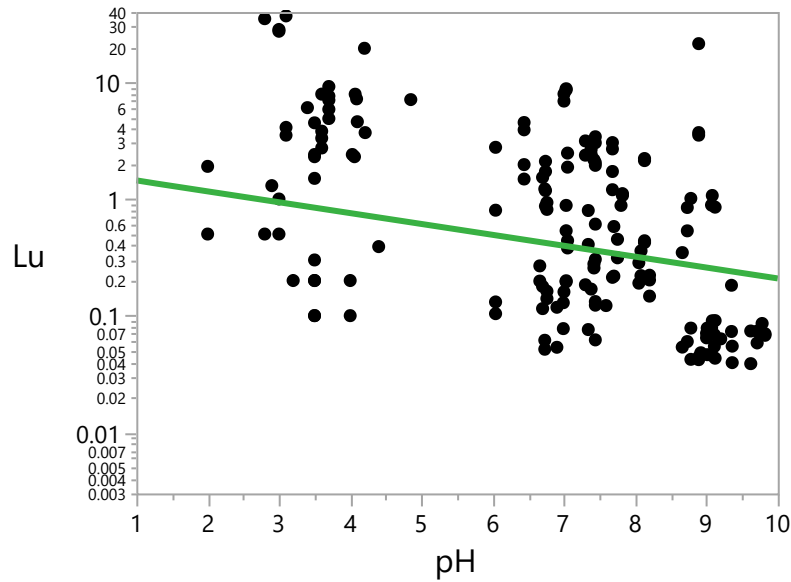
Transformed Fit Log
Log(Lu) = 0.5799527 - 0.2148201*pH

Summary of Fit

RSquare	0.064839
RSquare Adj	0.05839
Root Mean Square Error	1.471235
Mean of Response	-0.98407
Observations (or Sum Wgts)	147

Analysis of Variance

Source	DF	Sum of Squares	Mean Square	F Ratio
Model	1	21.76127	21.7613	10.0536
Error	145	313.85715	2.1645	
C. Total	146	335.61842		0.0019*

Parameter Estimates

Term	Estimate	Std Error	t Ratio	Prob>|t|
Intercept	0.5799527	0.507974	1.14	0.2555
pH	-0.21482	0.067751	-3.17	0.0019*

Fit Measured on Original Scale

Sum of Squared Error	858.17307
Root Mean Square Error	2.4327834
RSquare	-0.114806
Sum of Residuals	109.18556

Bivariate Fit of Nd By pH
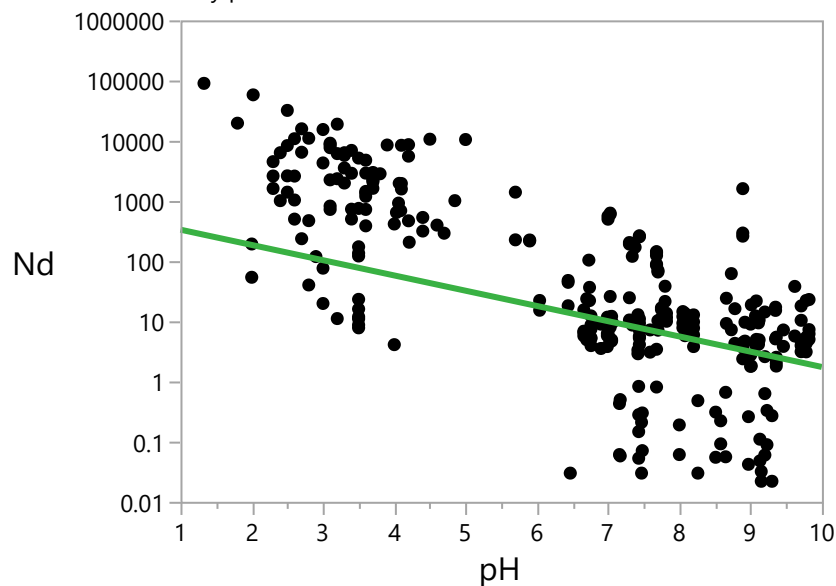
Transformed Fit Log
Log(Nd) = 6.3902796 - 0.5832385*pH

Summary of Fit

RSquare	0.175778
RSquare Adj	0.171908
Root Mean Square Error	2.233267
Mean of Response	1.974432
Observations (or Sum Wgts)	215

Analysis of Variance

Source	DF	Sum of Squares	Mean Square	F Ratio
Model	1	226.5588	226.559	45.4255
Error	213	1062.3332	4.987	
C. Total	214	1288.8920		<.0001*

Parameter Estimates

Term	Estimate	Std Error	t Ratio	Prob>|t|
Intercept	6.3902796	0.672656	9.50	<.0001*
pH	-0.583238	0.086536	-6.74	<.0001*

Fit Measured on Original Scale

Sum of Squared Error	1.241e+10
Root Mean Square Error	7633.944
RSquare	-0.007075
Sum of Residuals	185856.08

Bivariate Fit of Pr By pH
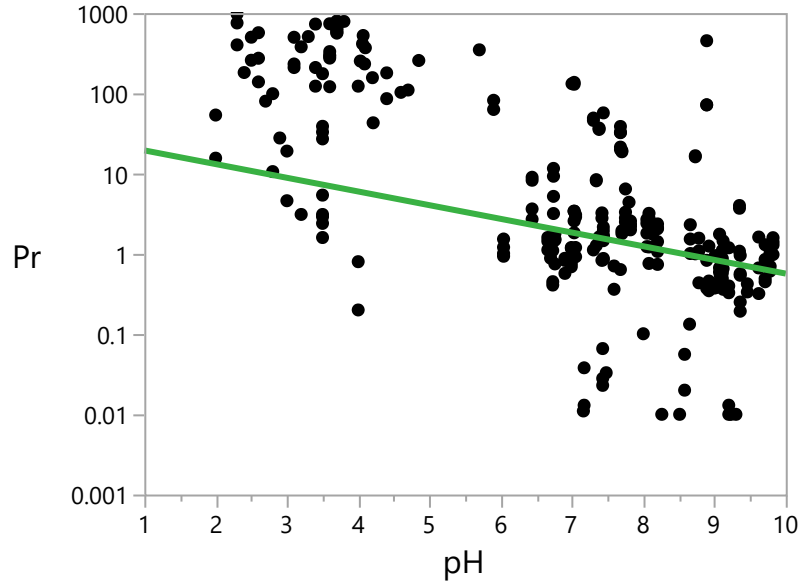
Transformed Fit Log
Log(Pr) = 3.3625437 - 0.3930703*pH

Summary of Fit

RSquare	0.109658
RSquare Adj	0.105335
Root Mean Square Error	1.873935
Mean of Response	0.373659
Observations (or Sum Wgts)	208

Analysis of Variance

Source	DF	Sum of Squares	Mean Square	F Ratio
Model	1	89.09592	89.0959	25.3716
Error	206	723.39663	3.5116	
C. Total	207	812.49255		<.0001*

Parameter Estimates

Term	Estimate	Std Error	t Ratio	Prob>|t|
Intercept	3.3625437	0.607442	5.54	<.0001*
pH	-0.39307	0.078036	-5.04	<.0001*

Fit Measured on Original Scale

Sum of Squared Error   306821.79
Root Mean Square Error   38.593084
RSquare   -0.04699
Sum of Residuals   1740.9975

Bivariate Fit of Sm By pH
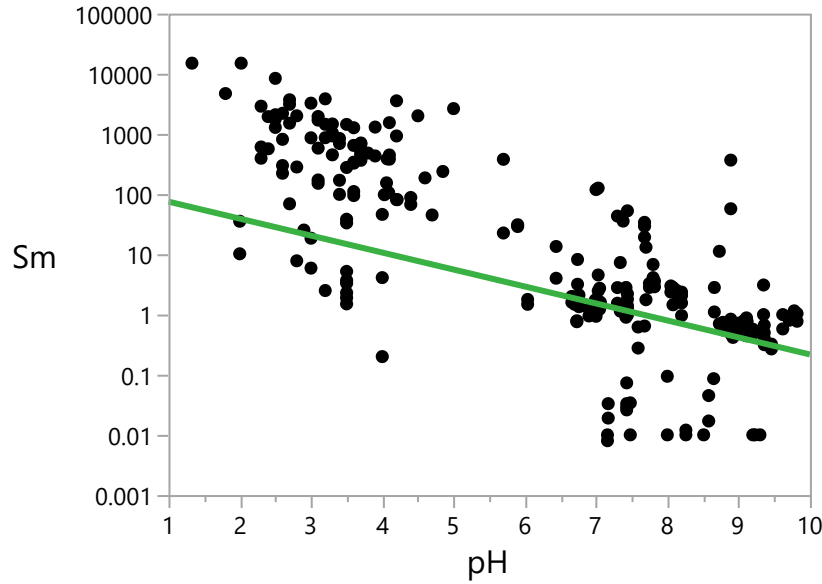
Transformed Fit Log

Transformed Fit Log
Log(Sm) = 4.9677577 - 0.6494352*pH

Summary of Fit
RSquare	0.243968
RSquare Adj	0.238994
Root Mean Square Error	2.260775
Mean of Response	0.1853
Observations (or Sum Wgts)	154

Analysis of Variance

Source	DF	Sum of Squares	Mean Square	F Ratio
Model	1	250.6976	250.698	49.0496
Error	152	776.8876	5.111	
C. Total	153	1027.5852		<.0001*

Parameter Estimates

Term	Estimate	Std Error	t Ratio	Prob>|t|
Intercept	4.9677577	0.706746	7.03	<.0001*
pH	-0.649435	0.09273	-7.00	<.0001*

Fit Measured on Original Scale

Sum of Squared Error	517291714
Root Mean Square Error	1844.7859
RSquare	-0.013311
Sum of Residuals	39136.274

Bivariate Fit of Tb By pH
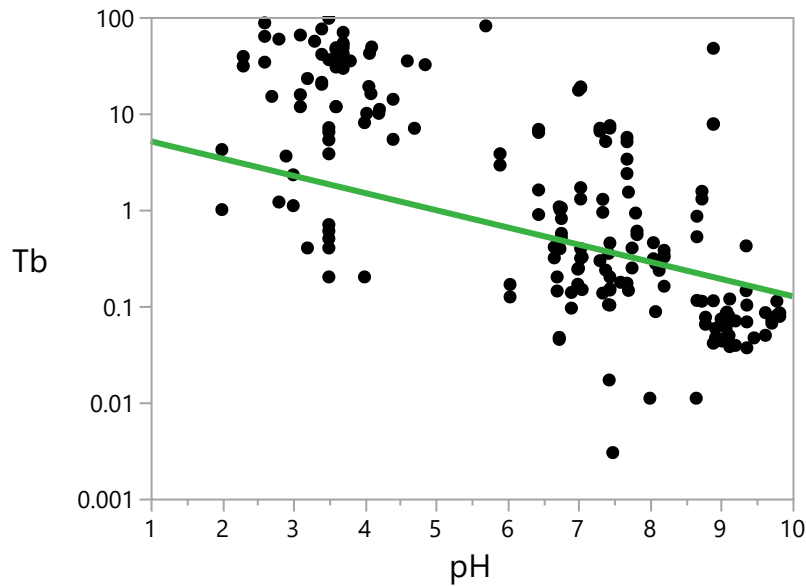
Transformed Fit Log

Transformed Fit Log

$Log(Tb) = 2.0469875 - 0.4118262 * pH$

Summary of Fit

RSquare	0.173087
RSquare Adj	0.167052
Root Mean Square Error	1.658485
Mean of Response	-0.98719
Observations (or Sum Wgts)	139

Analysis of Variance

Source	DF	Sum of Squares	Mean Square	F Ratio

Model	1	78.87679	78.8768	28.6765
Error	137	376.82823	2.7506	
C. Total	138	455.70502		<.0001*

Parameter Estimates

Term	Estimate	Std Error	t Ratio	Prob>|t|
Intercept	2.0469875	0.583803	3.51	0.0006*
pH	-0.411826	0.076904	-5.36	<.0001*

Fit Measured on Original Scale

Sum of Squared Error	4049.8126
Root Mean Square Error	5.436973
RSquare	-0.08665
Sum of Residuals	204.58312

Bivariate Fit of Th By pH
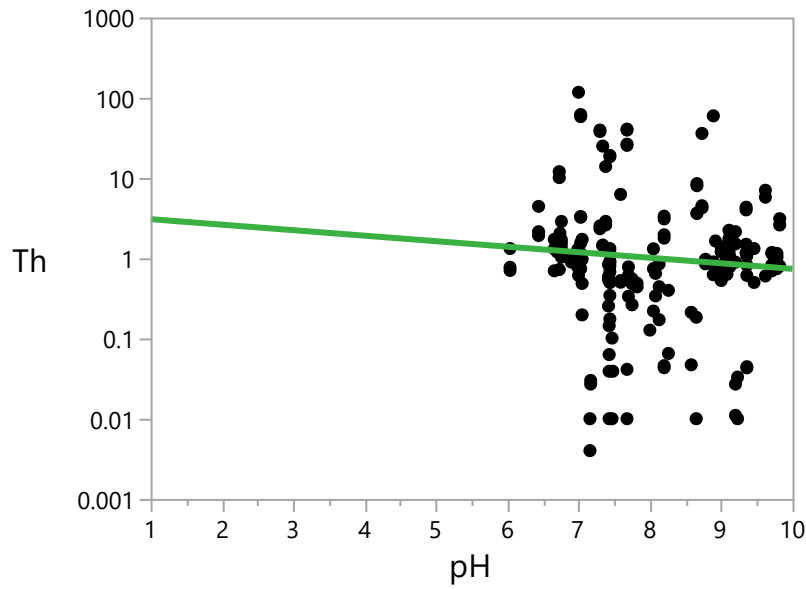
Transformed Fit Log
Log(Th) = 1.2811603 - 0.1584881*pH

Summary of Fit

RSquare	0.007323
RSquare Adj	0.002232
Root Mean Square Error	1.895752
Mean of Response	0.00974
Observations (or Sum Wgts)	197

Analysis of Variance

Source	DF	Sum of Squares	Mean Square	F Ratio
Model	1	5.16978	5.16978	1.4385
Error	195	700.80597	3.59388	
C. Total	196	705.97575		0.2318

Parameter Estimates

Term	Estimate	Std Error	t Ratio	Prob>|t|
Intercept	1.2811603	1.068641	1.20	0.2320
pH	-0.158488	0.132142	-1.20	0.2318

Fit Measured on Original Scale

Sum of Squared Error	52963.984
Root Mean Square Error	16.4806
RSquare	-0.085658
Sum of Residuals	919.30128

Bivariate Fit of Tm By pH

Transformed Fit Log
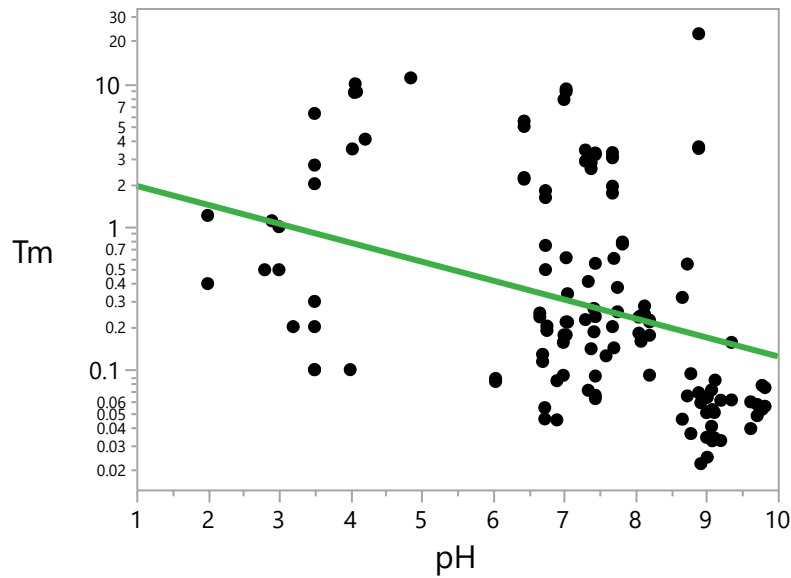
Transformed Fit Log
Log(Tm) = 0.9649478 - 0.3053295*pH

Summary of Fit

RSquare	0.117769
RSquare Adj	0.110417
Root Mean Square Error	1.538992
Mean of Response	-1.26611
Observations (or Sum Wgts)	122

Analysis of Variance

Source	DF	Sum of Squares	Mean Square	F Ratio
Model	1	37.94063	37.9406	16.0189
Error	120	284.21972	2.3685	
C. Total	121	322.16034		0.0001*

Parameter Estimates

Term	Estimate	Std Error	t Ratio	Prob>|t|
Intercept	0.9649478	0.574586	1.68	0.0957
pH	-0.30533	0.076287	-4.00	0.0001*

Fit Measured on Original Scale

Sum of Squared Error	953.44415
Root Mean Square Error	2.8187529
RSquare	-0.106724
Sum of Residuals	102.36032

Bivariate Fit of U By pH
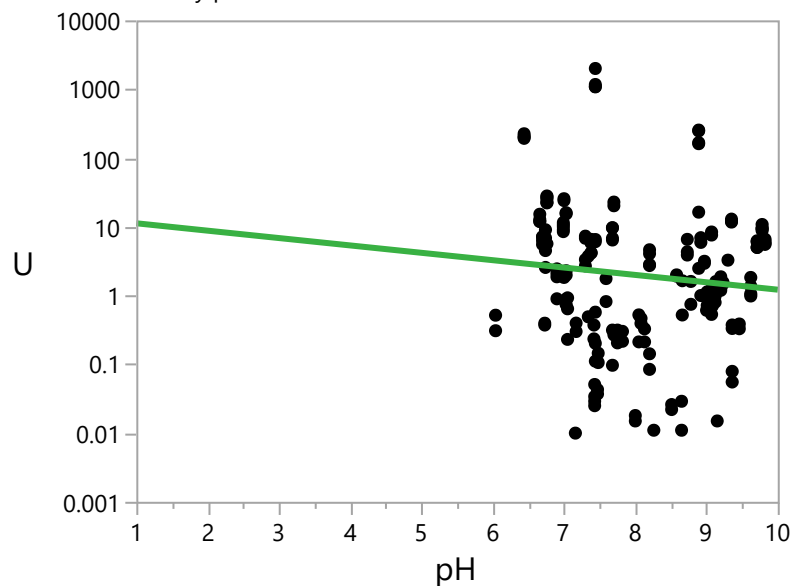
Transformed Fit Log

Transformed Fit Log
Log(U) = 2.662518 - 0.2465521*pH

Summary of Fit

RSquare	0.012214
RSquare Adj	0.007069
Root Mean Square Error	2.30443
Mean of Response	0.672792
Observations (or Sum Wgts)	194

Analysis of Variance

Source	DF	Sum of Squares	Mean Square	F Ratio
Model	1	12.6068	12.6068	2.3740
Error	192	1019.5963	5.3104	
C. Total	193	1032.2031		0.1250

Parameter Estimates

Term	Estimate	Std Error	t Ratio	Prob>|t|
Intercept	2.662518	1.301934	2.05	0.0422*
pH	-0.246552	0.160018	-1.54	0.1250

Fit Measured on Original Scale

Sum of Squared Error	8049684.7
Root Mean Square Error	204.75703
RSquare	-0.035957
Sum of Residuals	7412.4968

Bivariate Fit of Y By pH
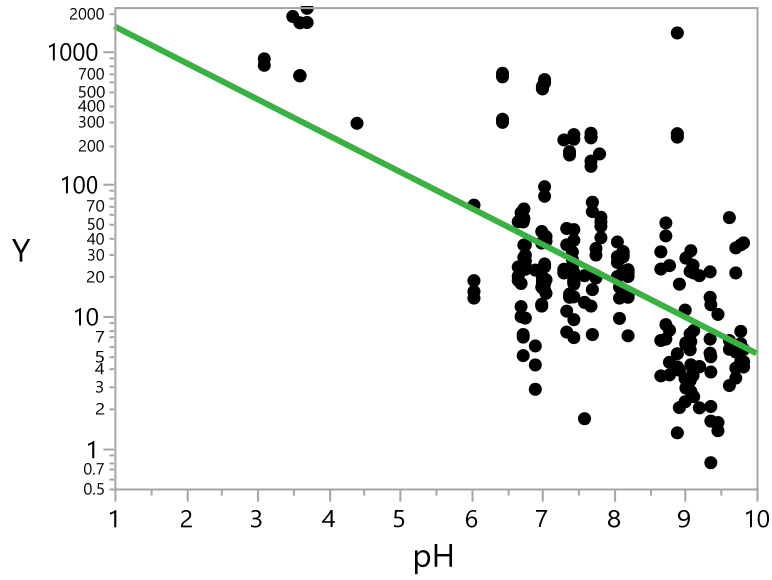
Transformed Fit Log

Log(Y) = 7.990899 - 0.6328696*pH

Summary of Fit

RSquare	0.230902
RSquare Adj	0.227018
Root Mean Square Error	1.217446
Mean of Response	2.910538
Observations (or Sum Wgts)	200

Analysis of Variance

Source	DF	Sum of Squares	Mean Square	F Ratio
Model	1	88.10724	88.1072	59.4446
Error	198	293.47056	1.4822	
C. Total	199	381.57780		<.0001*

Parameter Estimates

Term	Estimate	Std Error	t Ratio	Prob>|t|
Intercept	7.990899	0.664528	12.02	<.0001*
pH	-0.63287	0.082084	-7.71	<.0001*

Fit Measured on Original Scale

Sum of Squared Error   4504030.9
Root Mean Square Error   150.82318
RSquare   -0.034068
Sum of Residuals   7325.9568

Bivariate Fit of Yb By pH
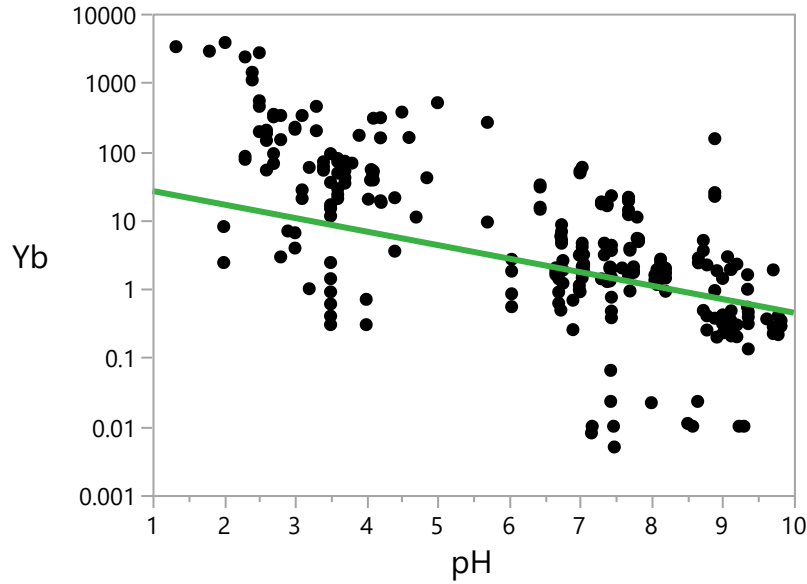
—— Transformed Fit Log

Transformed Fit Log
Log(Yb) = 3.7245479 - 0.4525556*pH

Summary of Fit
RSquare   0.146638
RSquare Adj   0.141844
Root Mean Square Error   2.00475
Mean of Response   0.413877
Observations (or Sum Wgts)   180

Analysis of Variance

Source	DF	Sum of Squares	Mean Square	F Ratio
Model	1	122.92920	122.929	30.5868
Error	178	715.38581	4.019	
C. Total	179	838.31501		<.0001*

Parameter Estimates

Term	Estimate	Std Error	t Ratio	Prob>|t|
Intercept	3.7245479	0.616984	6.04	<.0001*
pH	-0.452556	0.081829	-5.53	<.0001*

Fit Measured on Original Scale

|	
Sum of Squared Error	32313957
Root Mean Square Error	426.07404
RSquare	-0.009385
Sum of Residuals	10380.542

Appendix B

Preliminary Analysis of Data from Quillinan, et al. 2018. Assessing rare earth element concentrations in geothermal and oil and gas produced waters: A potential domestic source of strategic mineral commodities (DE-EE0007603).

William Stringfellow & Patrick Dobson, Lawrence Berkeley National Laboratory

May 21, 2020

Fit Group

Bivariate Fit of Ce_ppt By ph_Field

Transformed Fit Log
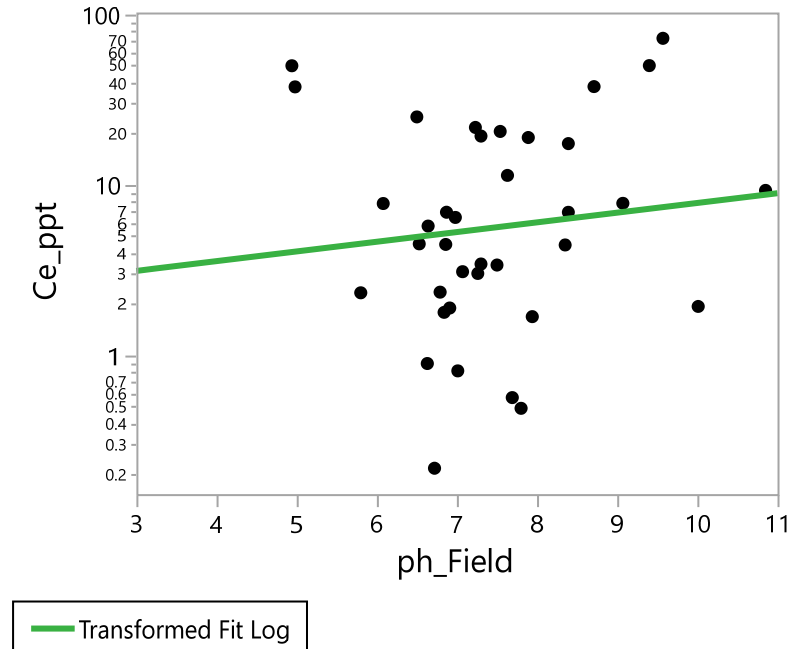
Transformed Fit Log
Log(Ce_ppt) = 0.742605 + 0.1311869*ph_Field

Summary of Fit

RSquare	0.013728
RSquare Adj	-0.01445
Root Mean Square Error	1.418213
Mean of Response	1.721082
Observations (or Sum Wgts)	37

Analysis of Variance

Source	DF	Sum of Squares	Mean Square	F Ratio
Model	1	0.979880	0.97988	0.4872
Error	35	70.396494	2.01133	
C. Total	36	71.376374		0.4898

Parameter Estimates

Term	Estimate	Std Error	t Ratio	Prob>|t|
Intercept	0.742605	1.42112	0.52	0.6046
ph_Field	0.1311869	0.187951	0.70	0.4898

Fit Measured on Original Scale

Sum of Squared Error	11812.355
Root Mean Square Error	18.37106
RSquare	-0.168478
Sum of Residuals	262.63559

Bivariate Fit of Dy_ppt By ph_Field
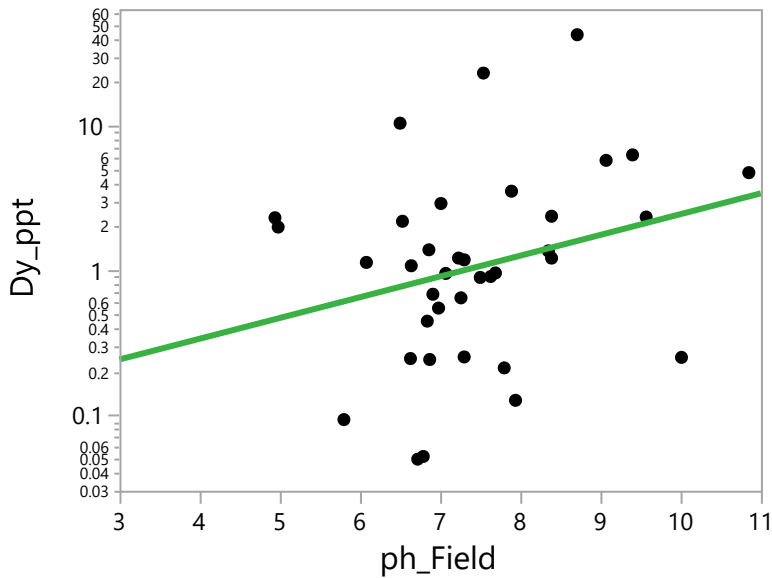
Transformed Fit Log

Log(Dy_ppt) = -2.408803 + 0.3304775*ph_Field

Summary of Fit

RSquare	0.074227
RSquare Adj	0.047776

Root Mean Square Error	1.488595
Mean of Response	0.056113
Observations (or Sum Wgts)	37

Analysis of Variance

Source	DF	Sum of Squares	Mean Square	F Ratio
Model	1	6.218356	6.21836	2.8062
Error	35	77.557041	2.21592	
C. Total	36	83.775397		0.1028

Parameter Estimates

Term	Estimate	Std Error	t Ratio	Prob>|t|
Intercept	-2.408803	1.491646	-1.61	0.1153
ph_Field	0.3304775	0.197279	1.68	0.1028

Fit Measured on Original Scale

Sum of Squared Error	2327.0451
Root Mean Square Error	8.1539562
RSquare	-0.065989
Sum of Residuals	83.893608

Bivariate Fit of Er_ppt By ph_Field

Transformed Fit Log
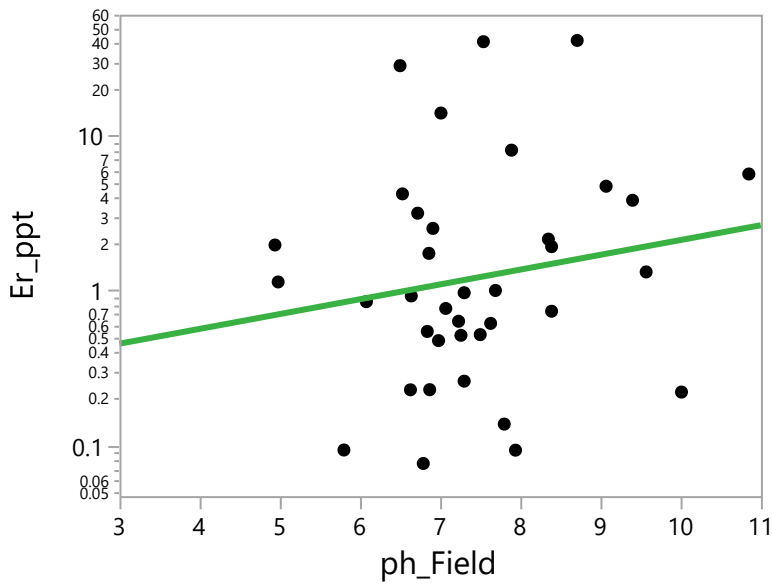
Transformed Fit Log
Log(Er_ppt) = -1.452045 + 0.2204124*ph_Field

Summary of Fit

RSquare	0.029143
RSquare Adj	0.001404
Root Mean Square Error	1.622594
Mean of Response	0.191933
Observations (or Sum Wgts)	37

Analysis of Variance

Source	DF	Sum of Squares	Mean Square	F Ratio
Model	1	2.766075	2.76607	1.0506
Error	35	92.148404	2.63281	
C. Total	36	94.914479		0.3124

Parameter Estimates

Term	Estimate	Std Error	t Ratio	Prob>|t|
Intercept	-1.452045	1.62592	-0.89	0.3779
ph_Field	0.2204124	0.215037	1.02	0.3124

Fit Measured on Original Scale

Sum of Squared Error	4159.3822
Root Mean Square Error	10.901353
RSquare	-0.118414
Sum of Residuals	130.19186

Bivariate Fit of Eu_ppt By ph_Field
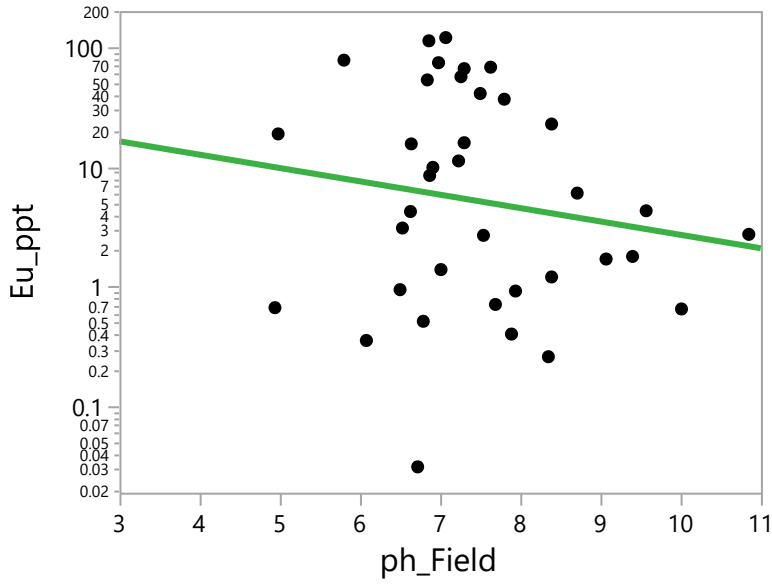
Transformed Fit Log
Log(Eu_ppt) = 3.5673074 - 0.2566329*ph_Field

Summary of Fit

RSquare	0.024445
RSquare Adj	-0.00343
Root Mean Square Error	2.067773
Mean of Response	1.653173
Observations (or Sum Wgts)	37

Analysis of Variance

Source	DF	Sum of Squares	Mean Square	F Ratio
Model	1	3.74987	3.74987	0.8770
Error	35	149.64894	4.27568	
C. Total	36	153.39882		0.3554

Parameter Estimates

Term	Estimate	Std Error	t Ratio	Prob>|t|
Intercept	3.5673074	2.072011	1.72	0.0940
ph_Field	-0.256633	0.274036	-0.94	0.3554

Fit Measured on Original Scale

Sum of Squared Error	49947.478
Root Mean Square Error	37.776591
RSquare	-0.268567
Sum of Residuals	642.33329

Bivariate Fit of Gd_ppt By ph_Field
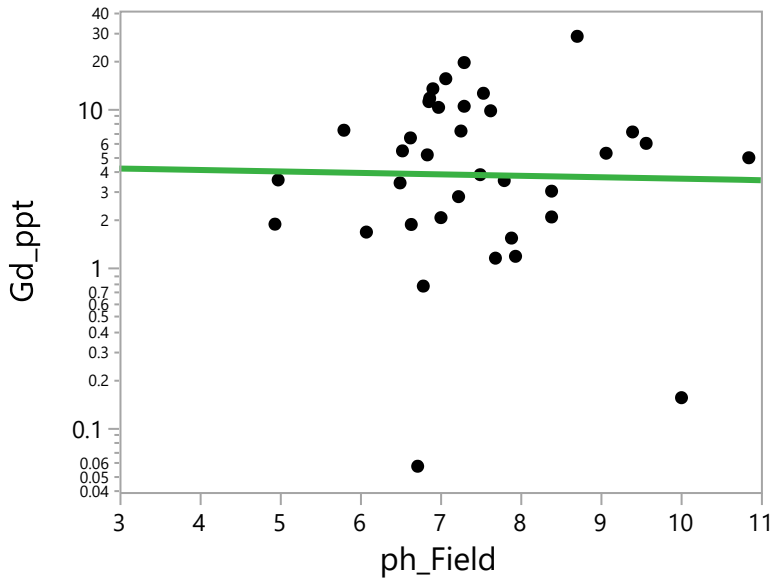
Transformed Fit Log

Transformed Fit Log
Log(Gd_ppt) = 1.4956682 - 0.0210637*ph_Field

Summary of Fit

RSquare	0.000448
RSquare Adj	-0.02895
Root Mean Square Error	1.278541
Mean of Response	1.339083
Observations (or Sum Wgts)	36

Analysis of Variance

Source	DF	Sum of Squares	Mean Square	F Ratio
Model	1	0.024899	0.02490	0.0152
Error	34	55.578666	1.63467	
C. Total	35	55.603565		0.9025

Parameter Estimates

Term	Estimate	Std Error	t Ratio	Prob>|t|
Intercept	1.4956682	1.286507	1.16	0.2531
ph_Field	-0.021064	0.170669	-0.12	0.9025

Fit Measured on Original Scale

Sum of Squared Error	1493.1364
Root Mean Square Error	6.6268979
RSquare	-0.194924
Sum of Residuals	93.00683

Bivariate Fit of Ho_ppt By ph_Field
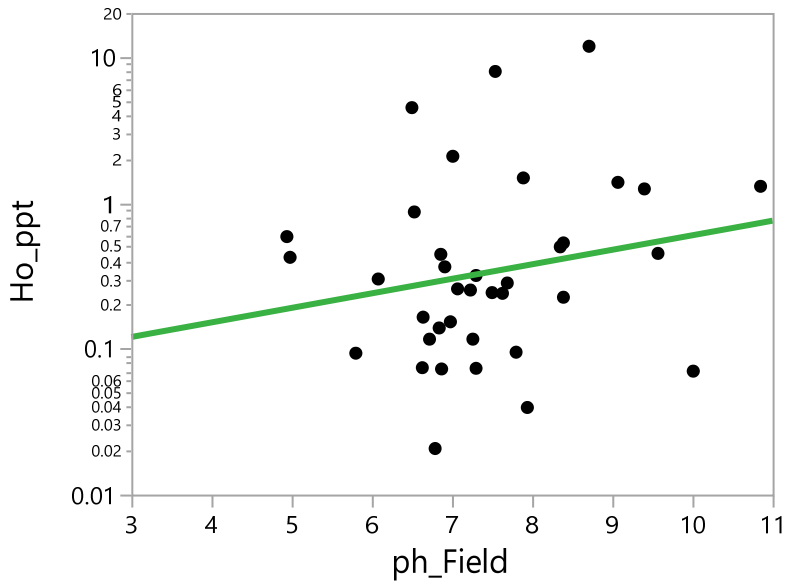
———— Transformed Fit Log

Transformed Fit Log
Log(Ho_ppt) = -2.806881 + 0.2295066*ph_Field

Summary of Fit

RSquare	0.041622
RSquare Adj	0.01424
Root Mean Square Error	1.404641
Mean of Response	-1.09507
Observations (or Sum Wgts)	37

Analysis of Variance

Source	DF	Sum of Squares	Mean Square	F Ratio

Model	1	2.999039	2.99904	1.5200
Error	35	69.055603	1.97302	
C. Total	36	72.054642		0.2258

Parameter Estimates

Term	Estimate	Std Error	t Ratio	Prob>|t|
Intercept	-2.806881	1.40752	-1.99	0.0540
ph_Field	0.2295066	0.186153	1.23	0.2258

Fit Measured on Original Scale

Sum of Squared Error	212.86879
Root Mean Square Error	2.4661641
RSquare	-0.084279
Sum of Residuals	26.342173

Bivariate Fit of La_ppt By ph_Field

Transformed Fit Log
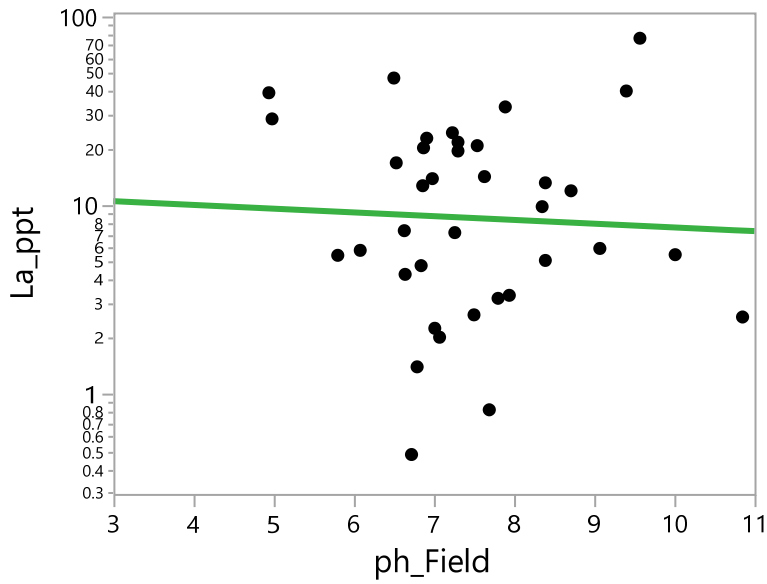
Transformed Fit Log
Log(La_ppt) = 2.4869047 - 0.045638*ph_Field

Summary of Fit

RSquare	0.002387
RSquare Adj	-0.02612
Root Mean Square Error	1.190093
Mean of Response	2.146507
Observations (or Sum Wgts)	37

Analysis of Variance

Source	DF	Sum of Squares	Mean Square	F Ratio
Model	1	0.118589	0.11859	0.0837
Error	35	49.571208	1.41632	
C. Total	36	49.689797		0.7740

Parameter Estimates

Term	Estimate	Std Error	t Ratio	Prob>|t|
Intercept	2.4869047	1.192532	2.09	0.0444*
ph_Field	-0.045638	0.157719	-0.29	0.7740

Fit Measured on Original Scale

Sum of Squared Error	10688.851
Root Mean Square Error	17.475576
RSquare	-0.16918
Sum of Residuals	237.88606

Bivariate Fit of Lu_ppt By ph_Field

Transformed Fit Log
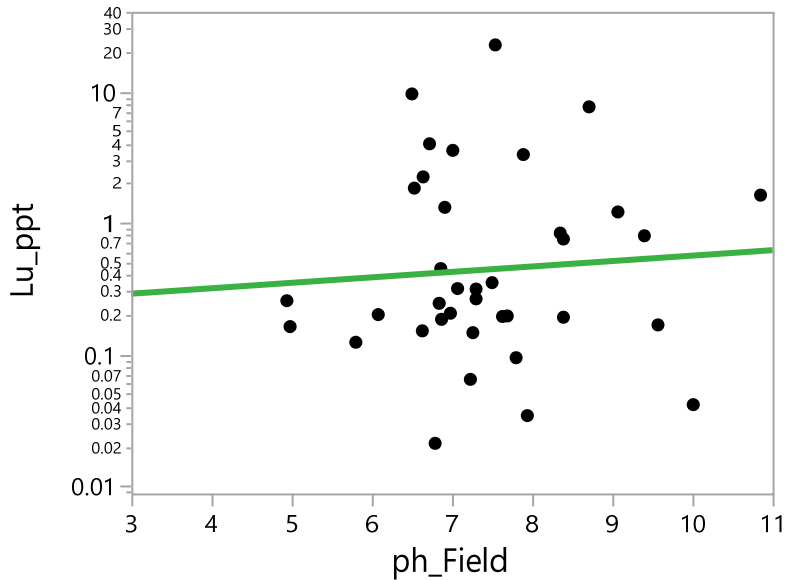
Transformed Fit Log
Log(Lu_ppt) = -1.525043 + 0.0952146*ph_Field

Summary of Fit

RSquare	0.005475
RSquare Adj	-0.02294
Root Mean Square Error	1.636717
Mean of Response	-0.81487
Observations (or Sum Wgts)	37

Analysis of Variance

Source	DF	Sum of Squares	Mean Square	F Ratio
Model	1	0.516177	0.51618	0.1927
Error	35	93.759528	2.67884	
C. Total	36	94.275705		0.6634

Parameter Estimates

Term	Estimate	Std Error	t Ratio	Prob>|t|
Intercept	-1.525043	1.640072	-0.93	0.3588
ph_Field	0.0952146	0.216909	0.44	0.6634

Fit Measured on Original Scale

Sum of Squared Error	657.56136
Root Mean Square Error	4.3344512
RSquare	-0.108841
Sum of Residuals	48.875514

Bivariate Fit of Nd_ppt By ph_Field
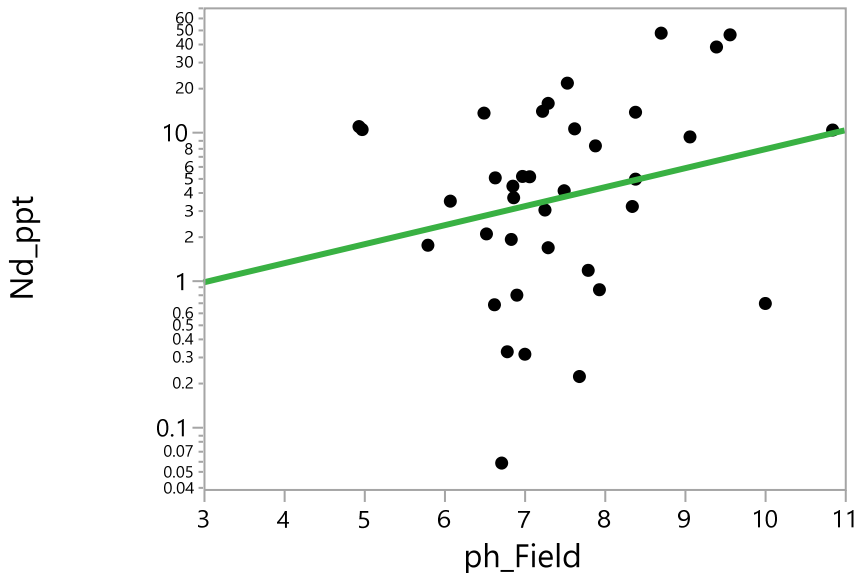
Transformed Fit Log
Log(Nd_ppt) = -0.928844 + 0.2969389*ph_Field

Summary of Fit

RSquare	0.058377
RSquare Adj	0.031474
Root Mean Square Error	1.521057
Mean of Response	1.285919
Observations (or Sum Wgts)	37

Analysis of Variance

Source	DF	Sum of Squares	Mean Square	F Ratio
Model	1	5.020257	5.02026	2.1699
Error	35	80.976521	2.31361	
C. Total	36	85.996778		0.1497

Parameter Estimates

Term	Estimate	Std Error	t Ratio	Prob>|t|
Intercept	-0.928844	1.524175	-0.61	0.5462
ph_Field	0.2969389	0.201581	1.47	0.1497

Fit Measured on Original Scale

Sum of Squared Error	5483.3376
Root Mean Square Error	12.51666
RSquare	-0.081738
Sum of Residuals	180.1028

Bivariate Fit of Pr_ppt By ph_Field
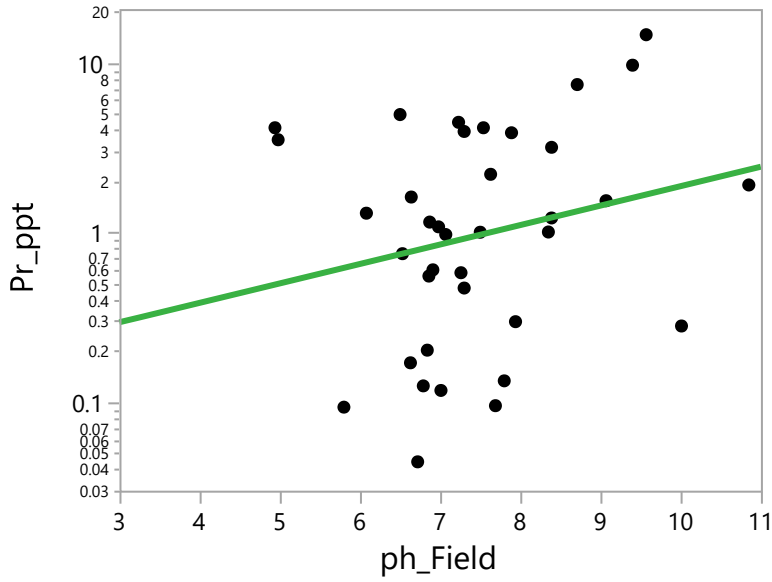
Transformed Fit Log
Log(Pr_ppt) = -2.014302 + 0.2639615*ph_Field

Summary of Fit

RSquare	0.05118
RSquare Adj	0.024071
Root Mean Square Error	1.449591
Mean of Response	-0.04551
Observations (or Sum Wgts)	37

Analysis of Variance

Source	DF	Sum of Squares	Mean Square	F Ratio
Model	1	3.967097	3.96710	1.8879
Error	35	73.546039	2.10132	
C. Total	36	77.513136		0.1782

Parameter Estimates

Term	Estimate	Std Error	t Ratio	Prob>|t|
Intercept	-2.014302	1.452563	-1.39	0.1743
ph_Field	0.2639615	0.19211	1.37	0.1782

Fit Measured on Original Scale

Sum of Squared Error	362.9412
Root Mean Square Error	3.2202094
RSquare	-0.103117
Sum of Residuals	45.789125

Bivariate Fit of Sc_ppt By ph_Field
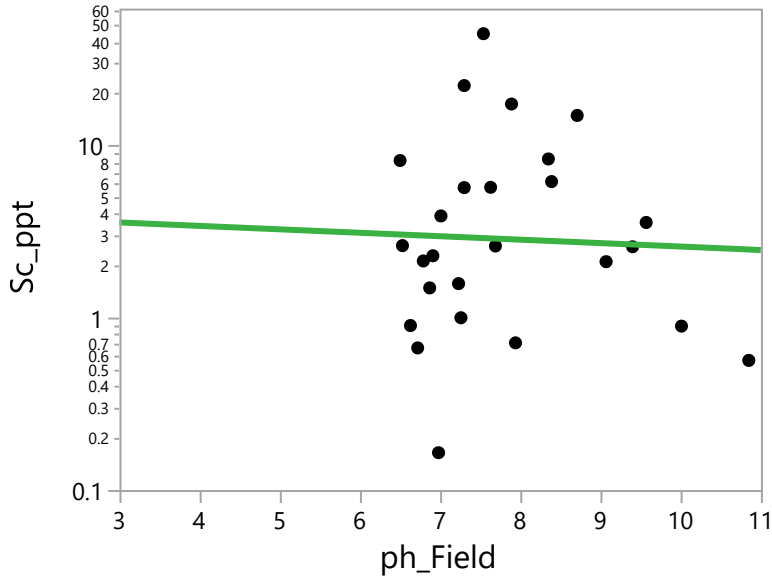
Transformed Fit Log
Log(Sc_ppt) = 1.4126262 - 0.0462029*ph_Field

Summary of Fit

RSquare	0.00176
RSquare Adj	-0.03983
Root Mean Square Error	1.310477
Mean of Response	1.051764
Observations (or Sum Wgts)	26

Analysis of Variance

Source	DF	Sum of Squares	Mean Square	F Ratio
Model	1	0.072650	0.07265	0.0423
Error	24	41.216381	1.71735	
C. Total	25	41.289031		0.8388

Parameter Estimates

Term	Estimate	Std Error	t Ratio	Prob>|t|
Intercept	1.4126262	1.773219	0.80	0.4335
ph_Field	-0.046203	0.224636	-0.21	0.8388

Fit Measured on Original Scale

Sum of Squared Error	2587.1053
Root Mean Square Error	10.382488
RSquare	-0.130222
Sum of Residuals	88.391582

Bivariate Fit of Sm_ppt By ph_Field
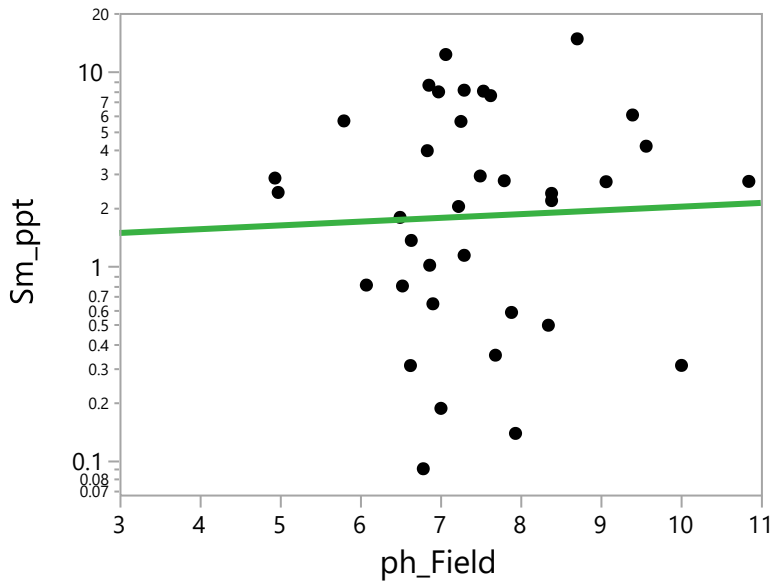
Transformed Fit Log

Transformed Fit Log
Log(Sm_ppt) = 0.2604962 + 0.0445685*ph_Field

Summary of Fit

RSquare	0.001821
RSquare Adj	-0.02754
Root Mean Square Error	1.343577
Mean of Response	0.593831
Observations (or Sum Wgts)	36

Analysis of Variance

Source	DF	Sum of Squares	Mean Square	F Ratio

Model	1	0.111982	0.11198	0.0620
Error	34	61.376770	1.80520	
C. Total	35	61.488752		0.8048

Parameter Estimates

Term	Estimate	Std Error	t Ratio	Prob>|t|
Intercept	0.2604962	1.356953	0.19	0.8489
ph_Field	0.0445685	0.178943	0.25	0.8048

Fit Measured on Original Scale

Sum of Squared Error	556.89247
Root Mean Square Error	4.0471212
RSquare	-0.216586
Sum of Residuals	60.154595

Bivariate Fit of Tb_ppt By ph_Field

Transformed Fit Log
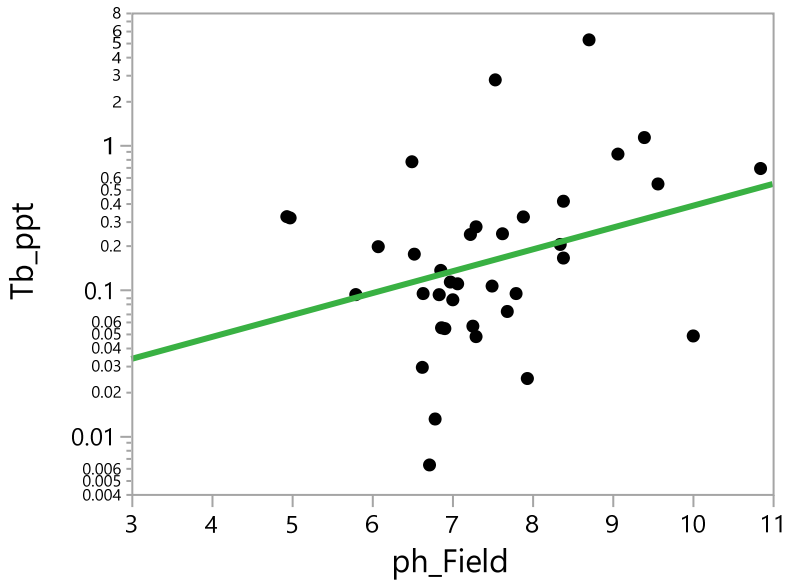
Transformed Fit Log

$$\text{Log}(Tb\_ppt) = -4.424571 + 0.3451357 \times ph\_Field$$

Summary of Fit

RSquare	0.100209
RSquare Adj	0.074501
Root Mean Square Error	1.319072
Mean of Response	-1.85032
Observations (or Sum Wgts)	37

Analysis of Variance

Source	DF	Sum of Squares	Mean Square	F Ratio
Model	1	6.782215	6.78222	3.8979
Error	35	60.898250	1.73995	
C. Total	36	67.680465		0.0563

Parameter Estimates

Term	Estimate	Std Error	t Ratio	Prob>|t|
Intercept	-4.424571	1.321775	-3.35	0.0020*
ph_Field	0.3451357	0.174813	1.97	0.0563

Fit Measured on Original Scale

Sum of Squared Error	33.147724
Root Mean Square Error	0.9731792
RSquare	-0.043595
Sum of Residuals	9.6539991

Bivariate Fit of Tm_ppt By ph_Field
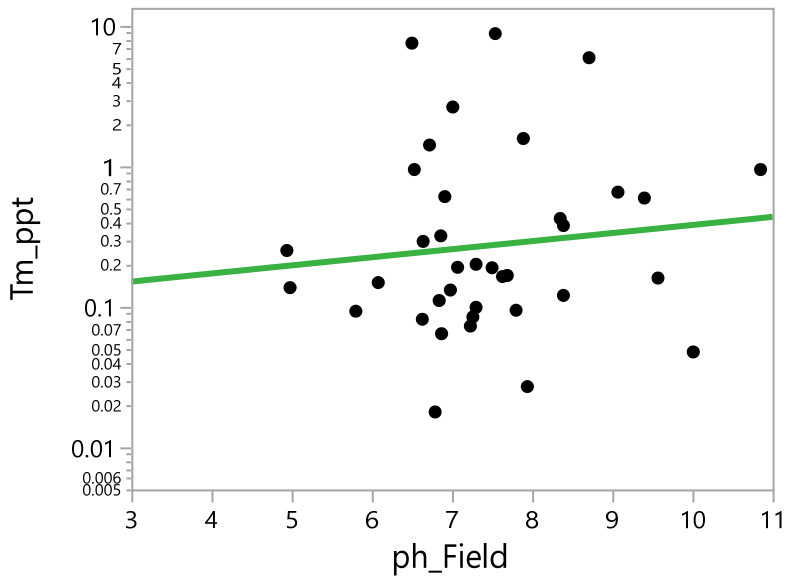
Transformed Fit Log

Transformed Fit Log
Log(Tm_ppt) = -2.286223 + 0.1327808*ph_Field

Summary of Fit

RSquare	0.012721
RSquare Adj	-0.01549
Root Mean Square Error	1.491966
Mean of Response	-1.29586
Observations (or Sum Wgts)	37

Analysis of Variance

Source	DF	Sum of Squares	Mean Square	F Ratio
Model	1	1.003834	1.00383	0.4510
Error	35	77.908665	2.22596	
C. Total	36	78.912500		0.5063

Parameter Estimates

Term	Estimate	Std Error	t Ratio	Prob>|t|
Intercept	-2.286223	1.495024	-1.53	0.1352
ph_Field	0.1327808	0.197726	0.67	0.5063

Fit Measured on Original Scale

Sum of Squared Error	169.5772
Root Mean Square Error	2.2011504
RSquare	-0.116549
Sum of Residuals	25.623203

Bivariate Fit of Yb_ppt By ph_Field
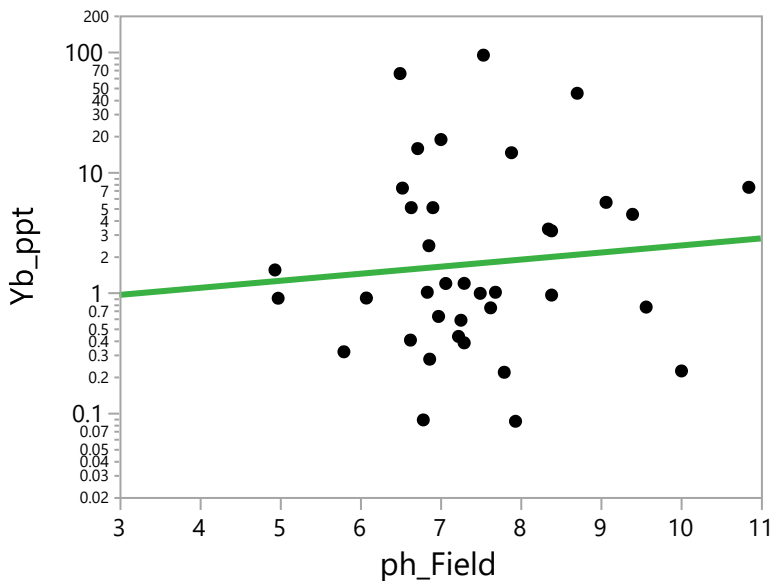
Transformed Fit Log
Log(Yb_ppt) = -0.45606 + 0.1352281*ph_Field

Summary of Fit

RSquare	0.0095
RSquare Adj	-0.0188
Root Mean Square Error	1.761159
Mean of Response	0.552559
Observations (or Sum Wgts)	37

Analysis of Variance

Source	DF	Sum of Squares	Mean Square	F Ratio
Model	1	1.04118	1.04118	0.3357
Error	35	108.55882	3.10168	
C. Total	36	109.60000		0.5660

Parameter Estimates

Term	Estimate	Std Error	t Ratio	Prob>|t|
Intercept	-0.45606	1.764769	-0.26	0.7976
ph_Field	0.1352281	0.233401	0.58	0.5660

Fit Measured on Original Scale

Sum of Squared Error	15130.147
Root Mean Square Error	20.791583
RSquare	-0.121735
Sum of Residuals	246.30115